CHEMICAL LASER REACTIONS CROSS-SECTION MEASUREMENTS

J. F. Friichtenicht

TRW Systems Group

Prepared for:

Air Force Weapons Laboratory

April 1974

UNCLASSIFIED
Security Classification

DOCUMENT CONTROL DATA - R & D

(Security classification of title, body of abstract and indexing annotation must be entered when the overall report is classified)

1. ORIGINATING ACTIVITY (Corporate author)	2a. REPORT SECURITY CLASSIFICATION
TRW Systems Group One Space Park Redondo Beach, CA 90278	UNCLASSIFIED
	2b. GROUP AD-779 716

3. REPORT TITLE

CHEMICAL LASER REACTIONS CROSS-SECTION MEASUREMENTS

4. DESCRIPTIVE NOTES (Type of report and inclusive dates)

Final Report for Period 1 January 1972 - 1 October 1973

5. AUTHOR(S) (First name, middle initial, last name)

J. F. Friichtenicht

6. REPORT DATE	7a. TOTAL NO. OF PAGES	7b. NO. OF REFS
April 1974	112	3

8a. CONTRACT OR GRANT NO.	9a. ORIGINATOR'S REPORT NUMBER(S)
F29601-72-C-0039	AFWL-TR-73-236
b. PROJECT NO. 1256	
c. Task 06	9b. OTHER REPORT NO(S) (Any other numbers that may be assigned this report)
d.	

10. DISTRIBUTION STATEMENT

Approved for public release; distribution unlimited.

11. SUPPLEMENTARY NOTES	12. SPONSORING MILITARY ACTIVITY
	AFWL (ALD) Kirtland AFB, NM 87117

13. ABSTRACT

(Distribution Limitation Statement A)

The objective of this program was the measurement of energy-dependent cross sections for each of the final vibrational states of the DF molecule resulting from the reaction $F + D_2 \rightarrow DF^* + D$. In pursuit of this objective, a powerful new technique for the detailed study of gas-phase chemical reactions was developed. The high-intensity atomic beam is produced by the irradiation of thin films of solid material with a Q-switched ruby laser pulse. For example, the flux of 4 eV fluorine atoms produced by the irradiation of a BiF_3 film with a 1/2 joule laser pulse has been estimated to be 10^{17} atoms cm^{-2} sec^{-1} at a point 60 cm from the laser target. The experiment utilizes a crossed beam configuration where the fluorine atom beam interacts with a deuterium gas beam obtained from a nozzle source. The method of detailed energy balance was to be used to determine the internal energy state of the product molecules. Two approaches to achieving the required energy discrimination were evaluated: One involving the use of a velocity-dependent product detector and the other using mechanical velocity selection of the incident beam. The mechanical velocity selection technique was shown to be better suited to the kinematics of the DF formation reaction. The several components were assembled into an integrated system which was thoroughly tested with satisfactory results. However, completion of the experimental measures was precluded by the budgetary constraints of the program.

DD FORM 1 NOV 68 1473

UNCLASSIFIED
Security Classification

14 KEY WORDS	LINK A		LINK B		LINK C	
	ROLE	WT	ROLE	WT	ROLE	WT
High flux pulsed atomic beams Reaction cross section measurements Chemical laser reactions						

AFWL-TR-73-236

CHEMICAL LASER REACTIONS CROSS-SECTION MEASUREMENTS

J. F. Friichtenicht

TRW Systems Group
Redondo Beach, CA 90278

Final Report for Period 1 January 1972 - 1 October 1973

FOREWORD

This report was prepared by TRW Systems Group, Redondo Beach, California, under Contract F29601-72-C-0039. The research was performed under Program Element 62301D, Project 1256, Task 06, and was funded by the Advanced Research Projects Agency under ARPA Order 1256.

Inclusive dates of research were 1 January 1972 through 1 October 1973. The report was submitted 5 February 1974 by the Air Force Weapons Laboratory Project Officer, Captain William E. Thompson (ALD).

The author wishes to acknowledge the efforts expended in behalf of this program by Dr. A. V. Haeff, D. O. Hansen, and N. L. Roy of TRW Systems and Captain William E. Thompson of the Air Force Weapons Laboratory.

This technical report has been reviewed and is approved.

William E. Thompson, III

WILLIAM E. THOMPSON III
Captain, USAF
Project Officer

Robert P Thompson for

JOHN C. RICH
Lt Colonel, USAF
Chief, Advanced Laser Technology Division

CONTENTS

Pages iii/iv are blank

ILLUSTRATIONS

ILLUSTRATIONS (Continued)

ILLUSTRATIONS (Continued)

SYMBOLS

D	Nozzle Diameter, Disc Diameter
e	Base of the natural logarithms
eV	Electron-Volt
E_x	Kinetic Energy of x
f	Focal length
H	Magnetic Field
k	Boltzmann's Constant
L	Unit of Length
m	Molecular Mass
n	Number density
n_o	Stagnation number density
n_x	Axial number density at distance x
N	Total number of atoms in a beam pulse
N'	Total number of reaction products
P_x	Momentum of x
Q	Reaction exothermicity
R	Rotational Speed
t	Time
T	Temperature, Rotational period
T_R	Reservoir temperature
u_x	Velocity of x
v	Vibrational quantum number
V	Volts
w	Slit width

SYMBOLS (Cont'd)

x	Unit of length
γ	Ratio of specific heats
θ	Scattering angle (Lab system)
θ'	Scattering angle (Center of mass sytem)
σ_i	Reaction Cross Section (ith state)
σ_T	Total Reaction Cross Section
$\sigma(E)$	Energy Dependent Reaction Cross Section
μ	Reduced mass of reactants

SECTION I
INTRODUCTION

The principal objective of this research program was the measurement of energy-dependent reaction cross sections for each of the final vibrational states of the DF molecule resulting from the reaction $F + D_2 \rightarrow DF^* + D$. This reaction has been used extensively in the high-power chemical laser technology program at TRW. The motivation behind the research program was the desire to obtain more detailed information on the reaction kinetics than was available from other sources for the purpose of increasing the capability of high power chemical laser systems.

In pursuit of this objective, a powerful new technique for the detailed study of chemical reactions has been developed. The key element in this technique has been the development of an intense pulsed atomic beam source. The high-intensity atomic beam is produced by the irradiation of thin films of solid material with a Q-switched ruby laser in a geometry conducive to the generation of neutral atoms as opposed to the highly ionized plasma normally observed. The laser irradiation converts the solid material into a high-temperature vapor cloud which subsequently expands into vacuum. The expansion process cools the vapor and orders the flow such that an observer positioned at some distance from the laser beam target sees a short duration burst of neutral atoms traveling in straight line trajectories. The burst of atoms may contain a broad range of energies, but the arrival time of a particular atom at the detector specifies its velocity and, therefore, its energy. The flux of 4 eV fluorine atoms produced by the irradiation of a BiF_3 target has been estimated to be 10^{17} atoms cm^{-2} sec^{-1} at a distance of 60 cm from the laser target - a value many orders of magnitude greater than that achieved by other techniques.

The experiment utilizes a crossed beam configuration wherein the primary (fluorine atom) beam interacts with a crossed beam of deuterium gas obtained from a pulsed nozzle source. The method of detailed energy balance is used to determine the internal energy state (i.e., the vibrational level) of the product molecules by the measurement of their kinetic energy subsequent to the reaction. In order to accomplish

this the allowable energy range in the incident beam pulse must be markedly reduced from its normal value. Two approaches to achieving the required energy discrimination were taken: one involving the use of a velocity-dependent product detector and the other utilizing a mechanical velocity selector on the incident fluorine atom beam. Although significant progress was made on the velocity-dependent detector concept, it was found to function adequately only for energies larger than of immediate interest in this program. Of the two techniques, mechanical energy selection is the best suited for the present application.

The several components have been assembled into a complete experimental system which has been thoroughly tested and evaluated with satisfactory results. However, completion of the experimental measurements has been precluded by the budgetary constraints of the program as presently constituted.

Section II of this report (and Appendix A) gives the rationale behind our approach to this problem and identifies the experimental requirements for measurements on the DF formation reaction. Section III (and Appendix B) describes the experimental system developed to meet these requirements and presents data demonstrating the results that have been obtained. The current status of the program is discussed briefly in Section IV.

SECTION II

EXPERIMENTAL REQUIREMENTS FOR REACTION CROSS-SECTION MEASUREMENTS

2.1 Fundamental Considerations

The principal objective of the program was the measurement of energy-dependent reaction cross sections for each of the final vibrational states of the DF-molecule resulting from the reaction $F + D_2 \rightarrow DF^* + D$. Much of the discussion that follows is general in nature. However, it is tacitly assumed that the experiment is to be done in a crossed beam configuration wherein relatively energetic fluorine atoms are incident on a crossed low-energy beam of deuterium gas. The dimensions of the interaction volume are assumed to be small compared to the distance from the interaction volume to the instruments used to detect and measure the reaction products.

With these considerations in mind, assume that a monoenergetic pulse of N fluorine atoms is incident on a small volume of D_2 target gas of known density. Some fraction of the F-atoms react chemically with the D_2 to produce a number N' of DF-molecules and, likewise, N' D-atoms. Because of the energetics of the reaction, the DF-molecules may be formed with varying degrees of internal energy (i.e., vibrational and rotational excitation). For reasons of clarity and fully realizing that the real case will not be as simple as this idealized model, it will be assumed that there is no rotational excitation and that the degree of internal energy is specified by the vibrational state only. Denoting the number of product molecules in the ground vibrational state (v = 0) by N_o, in the first vibrationally excited state (v = 1) by N_1, etc., it is seen that $N' = \Sigma_i N_i$.

The total reaction cross section (summed over all the internal energy states) is given by

$$\sigma_T = -\frac{1}{n} \ell n \frac{N'}{N} \qquad (1)$$

where n is the total number of D_2 molecules in the volume defined by the cross sectional area of the incident beam and the thickness of the D_2 target gas in the direction of the F-atom velocity vector. Similarly the cross section for formation of the product molecule in the ith vibrational state is given by

$$\sigma_i = -\frac{1}{n} \ln \frac{N_i}{N} \tag{2}$$

Thus, in order to determine the desired cross sections, the total number of product molecules in each of the vibrationally excited states must be specified. In practice, it would be sufficient to determine the relative number of product molecules in the several excited states and to perform an independent measurement of the total reaction cross section.

In gas phase chemical reactions, it is usually more convenient to work with reaction rate constants as opposed to cross sections. If the reaction cross section is determined over a range of collisional energies, it is usually possible to determine the rate constant for the reaction for any set of conditions providing the energy distribution of the reactants is known. For an equilibrium velocity distribution at temperature T, the rate constant is related to the energy dependent cross section $\sigma(E)$ by

$$K(T) = \left(\frac{1}{\pi\mu}\right)^{1/2}\left(\frac{2}{kT}\right)^{3/2}\int \sigma(E)Ee^{-\frac{E}{kT}}\,dE \tag{3}$$

where μ is the reduced mass of the reactants.

In order to perform reaction cross section measurements of the type described above, a means for identifying the internal energy states of the product molecules must be developed. In principle, this can be done by the method of detailed energy balance. Applying the conservation of energy to the reaction gives

$$E_F + E_{D_2} + Q = E_{DF} + E_D + E_{DF}^{int} \tag{4}$$

where Q is the reaction exothermicity, the E's are the kinetic energies of the indicated particles and E_{DF}^{int} is the internal energy of the DF molecule. At the same time, momentum must be conserved, i.e.,

$$\vec{P}_F + \vec{P}_{D_2} = \vec{P}_{DF} + \vec{P}_D \tag{5}$$

In a crossed beam experiment, the velocity of the target gas (D_2) is usually negligibly small compared to that of the primary beam with the consequence that $E_{D_2} \approx 0$ and $P_{D_2} \approx 0$. Therefore, the measurement of any two of the remaining quantities in Eq. (5)specifies the third and then Eq. (4) can be solved for E_{DF}^{int}. In other words for a given value of E_F, the internal energy state of a product molecule can be determined by the measurement of its kinetic energy.

The foregoing serves to illustrate the basic requirements. In practice, however, the situation is a bit more complicated. In the first place the pulse of F-atoms produced by the laser vaporization of a solid target contains a wide range of energies (up to several tens of electron volts). Secondly, the reaction products are scattered into a wide range of laboratory angles which means that the total number of products in a given state can be obtained only by summing over all scattering angles. There are, however, satisfactory solutions to these experimental complications as demonstrated by the discussion in the following sections.

2.2 Kinematics Of The DF Formation Reaction

The kinematics of the $F + D_2 \rightarrow DF^* + D$ reaction have been analyzed extensively for the primary purpose of specifying the optimum experimental configuration to be used in the measurement of reaction cross sections for the several energetically accessible vibrationally excited states resulting from the reaction. The reader is referred to Appendix A of this report for the complete analysis. Only the key findings will be presented here.

Expanding on the thesis advanced above, the DF formation reaction is one where two reactant species collide at some relative velocity and two product species emerge subsequent to the chemical reaction. In the process, the exothermicity of the reaction and the initial kinetic energy of the reactants is converted into kinetic energy of the products and possibly into internal energy of the resultant molecule. Since the total energy of the systems must be conserved throughout the process (Eq. (4) above), specification of the internal energy state of the product molecule specifies the combined kinetic energy of the reaction products.

But, as Eq. (5) points out, momentum must also be conserved with the consequence that the measurement of the kinetic energy of one of the reaction products specifies the kinetic energy of the other. Thus, experimentally, one has a choice of detecting either the D-atom or DF-molecule resulting from the reaction. Because of the large mass difference between D-atoms and DF-molecules, however, their trajectories in the laboratory reference frame are substantially different. This difference is illustrated graphically in Figures 1 and 2 where curves giving the scattering angle of the product species as a function of velocity are shown for each of the possible internal energy states (vibrational only) of the DF-molecule. These curves were generated for an assumed F-atom velocity of 2×10^5 cm sec^{-1} and the laboratory observation angle is referenced from the direction of the F-atom beam. These curves show that all of the DF-molecules are emitted in the forward hemisphere. In contrast, the D-atoms may be scattered into all laboratory angles.

It should be noted that these curves were generated strictly on the basis of conservation of energy and momentum and are arrived at on the assumption that all scattering angles in the center mass reference frame are accessible. It doesn't follow that all scattering angles are equally significant. In the general case, the angular distribution of reaction products must be determined experimentally. The curves of Figures 1 and 2 identify the angular range that must be covered.

It should be noted for future reference that the laboratory velocity of the DF-molecule is comparable to that of the incident F-atom. In contrast, the velocity of the D-atom is significantly larger except for those D-atoms scattered in the backward direction for large values of internal excitation of the corresponding DF-molecule.

Another significant feature of the reaction is illustrated by an examination of Figures 3 and 4. In these two figures the velocities of the reaction products are plotted as a function of the incident F-atom velocity for a fixed laboratory observation angle of 0°. As noted on the figures, there is a family of curves corresponding to the possible final internal energy states of the DF-molecule. In Figure 3, it can be seen that there are two possible values for the velocity of

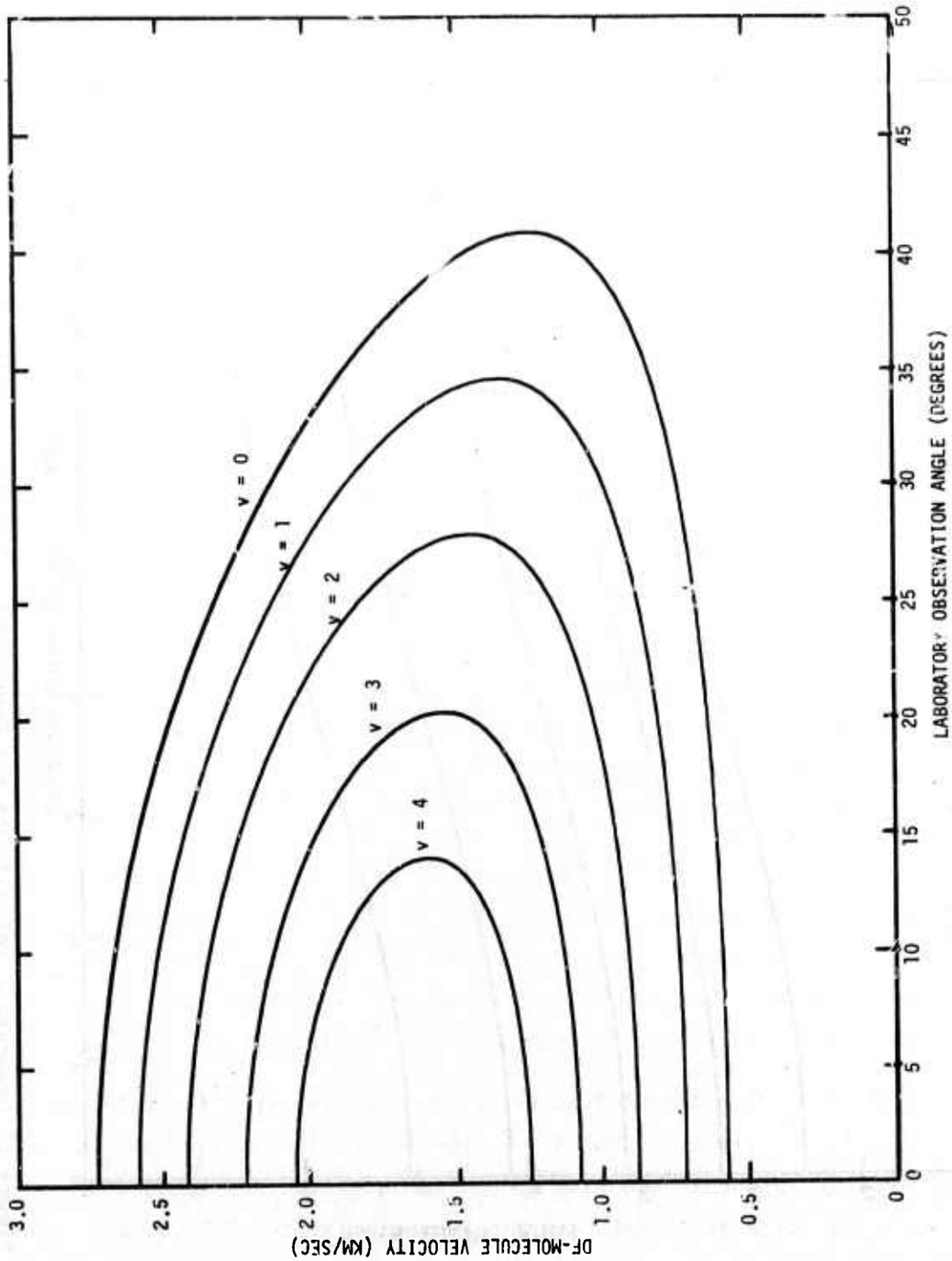

Figure 1. Laboratory velocity of the DF-molecule as a function of laboratory scattering angle for the reaction $F + D_2 \rightarrow DF + D$.

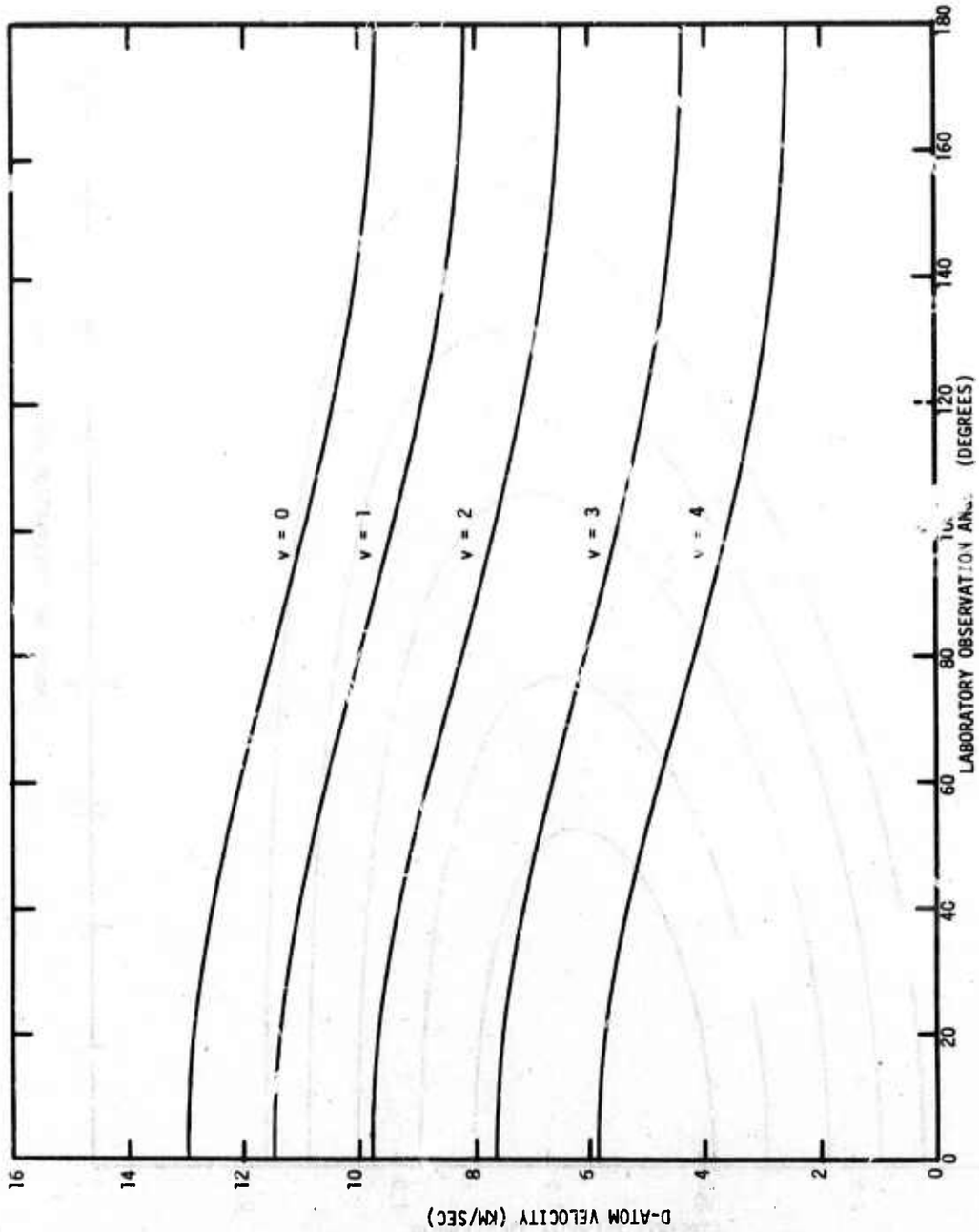

Figure 2. Laboratory velocity of the D-atom as a function of laboratory scattering angle for the reaction $F + D_2 \rightarrow DF + D$.

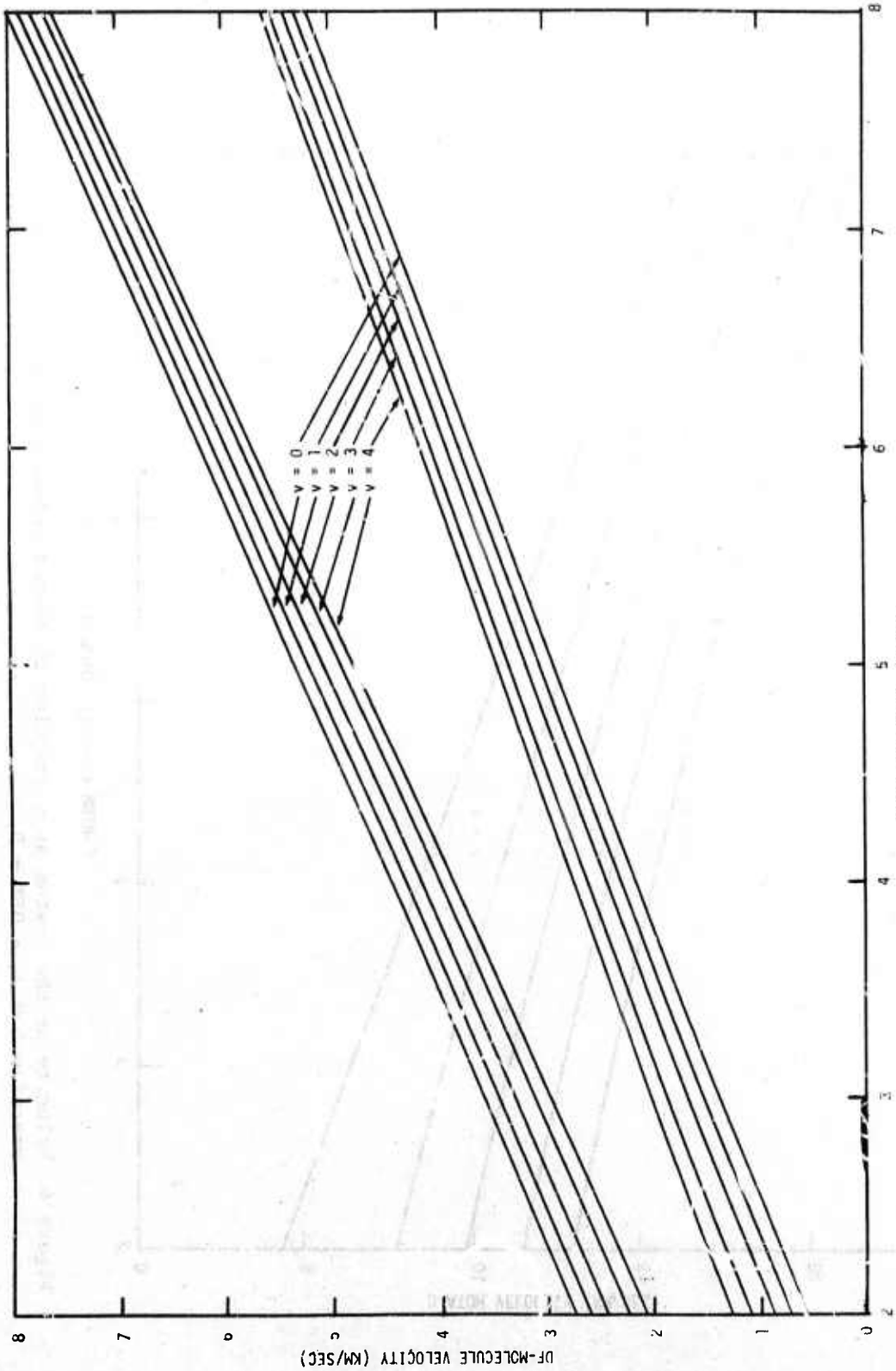

Figure 3. Velocity of the DF-molecule as a function of F-atom velocity at $\theta = 0°$ for the reaction $F + D_2 \rightarrow DF^* + D$.

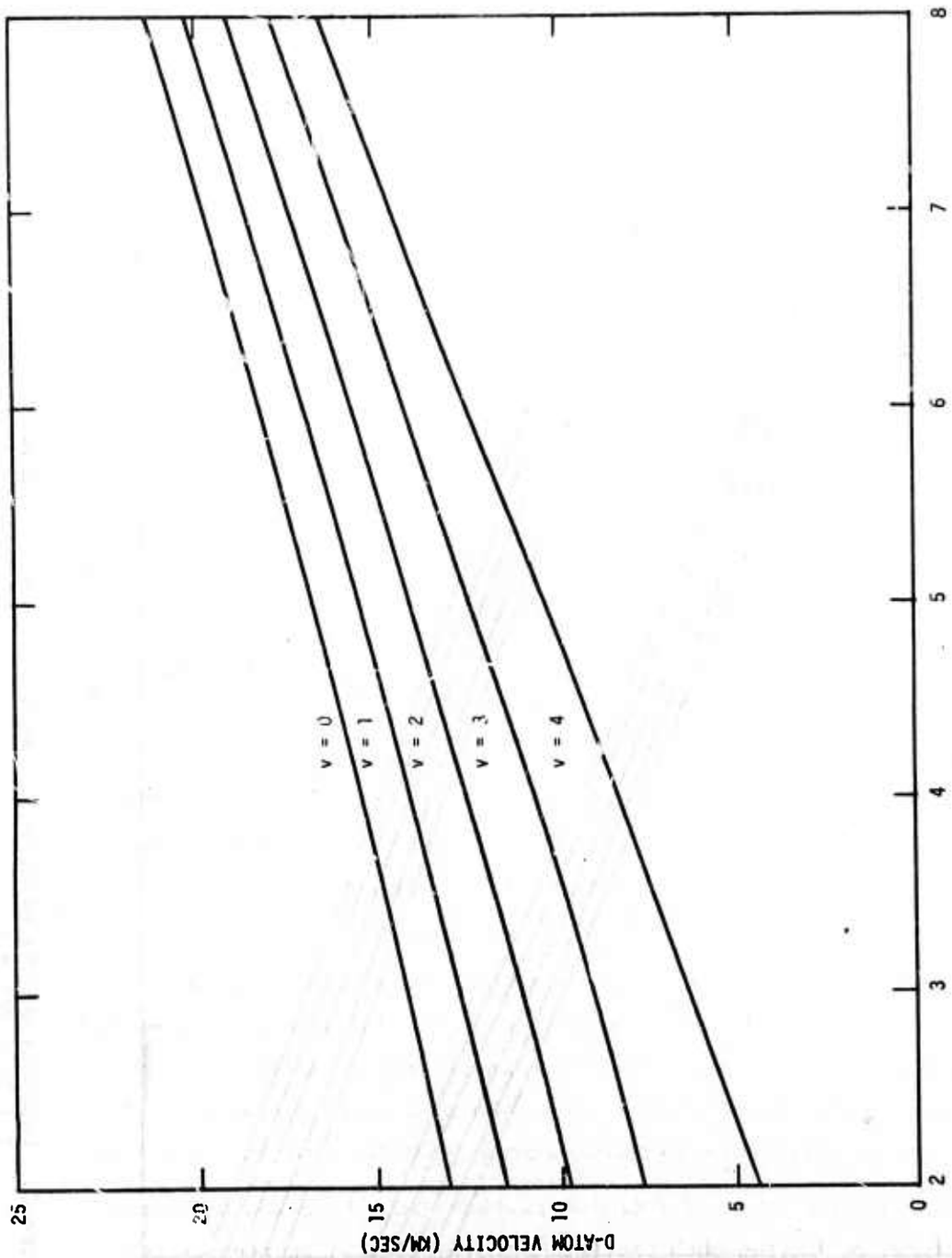

Figure 4. Velocity of the D-atom as a function of F-atom velocity at $\theta = 0°$ for the reaction $F + D_2 \rightarrow DF^* + D$.

the DF-molecule with a given internal energy state. These correspond to scattering at 0° and 180° in the center of mass reference frame, but both of these angles transform to 0° in the laboratory reference frame. Since, as was mentioned previously, the velocity of the D-atom is greater than that of the F-atom, scattering of the D-atom at 180° in the center of mass transforms to scattering at 180° in the laboratory also. Hence, the velocity of the D-atom is single valued in F-atom velocity as shown in Figure 4.

For a given discrete value of F-atom velocity, a unique set of DF-atom velocities exist determined by the internal energy state of the DF-molecule. Because of the double-valued nature of the DF scattering function there are, in fact, two DF-molecule velocities for each vibrational state, but this poses no fundamental difficulty because they are inherently different. Likewise, there is a unique set of D-atom velocities for a given value of F-atom velocity.

Suppose, however, that the incident F-atom pulse contains a range in velocity. Clearly, there will be a corresponding range in the velocity spectra of the reaction products with the consequence that specification of the velocity of the reaction products alone is insufficient to specify the internal energy state of the product molecule. Two means of solving this problem were evaluated during this program and they are discussed below.

2.3 Energy Selection Techniques

Two distinctly different means of achieving energy selectivity were pursued during the course of this program. In this sub-section the rationale behind the two approaches will be developed.

2.3.1 Energy Selection of the Incident Beam

Mechanical chopping of the incident beam pulse is perhaps the easier of the two approaches to visualize. As discussed in Section 3.1 and Appendix E, the fluorine atoms originate from an effective point source over a time interval that is so short as to be virtually instantaneous. At a point some distance removed from the source, a burst of atoms containing a range of energies is observed. However, the motion of the atoms is ordered such that the arrival time of an atom at the observation point specifies its velocity. Now suppose a normally closed shutter is opened for a brief time interval Δt at a time t after the

laser is Q-switched. All of the atoms arriving at the plane of the shutter during Δt will pass through the shutter and proceed onward to the crossed target gas beam. The transmitted pulse of atoms will contain a range of velocities bounded by $u_{F(max)} = L/t$ and $u_{F(min)} = L/(t + \Delta t)$ where L is the distance from the source to the shutter.

The maximum acceptable range in F-atom velocities for the DF formation reaction is as specified in Figure 5. The curves of Figure 5 were generated on the basis of the requirement that the laboratory velocity of the most energetic DF-molecule (or D-atom) in the v = 1 state be less than that of the least energetic DF-molecule (or D-atom) in the v = 0 state. If this condition is not met as a minimum the product molecules cannot be separated according to their time of flight to a product detector.

It can be seen by inspection of Figure 5 that velocity selection requirements to meet this minimum condition are more severe for detection of the DF-molecules than for detection of the corresponding D-atoms, which would lead to the seemingly obvious conclusion that one should detect the D-atoms from the reaction. In point of fact, the practical situation places additional constraints on the velocity selection process. Consider the consequences of the fact that the target gas beam has a finite thickness ΔL and the ionizer also has a finite distance ΔL_1 over which the incident atoms (or molecules) are converted to ions. We will assume that the post-ionization velocity of the reaction products is much larger than before ionization with the result that the balance of the transit time to the final detector is negligibly small. The on-axis forward-scattered case where $u_{DF}(0) > u_{DF}(1) > u_{F(max)}$ is illustrated in the x-t diagram of Figure 6. It can be seen that the total transit time of the latest arriving DF-molecule in the v = 0 state is given by

$$t_{max}(v = 0) = \frac{L + \Delta L}{u_{F(min)}} + \frac{L_1 - \Delta L + \Delta L_1}{u_{DF}(0)} \qquad (6)$$

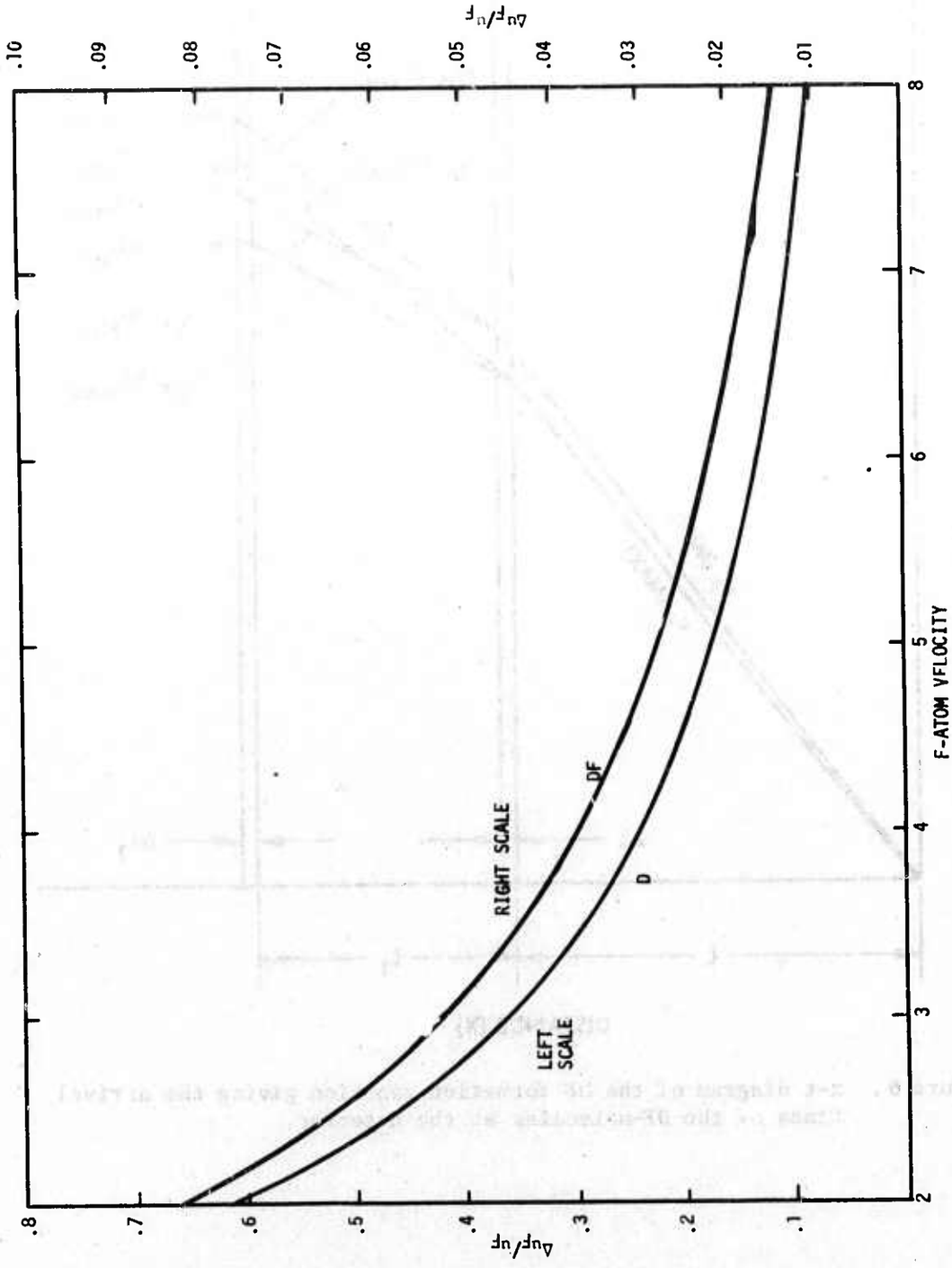

Figure 5. Maximum permissible velocity spread in the incident F-atom beam pulse as a function of u_F that results in velocity separation of DF-molecules in the v = 0 and v = 1 states and in velocity separation of D-atoms corresponding to the v = 0 and v = 1 states for $\theta = 0°$.

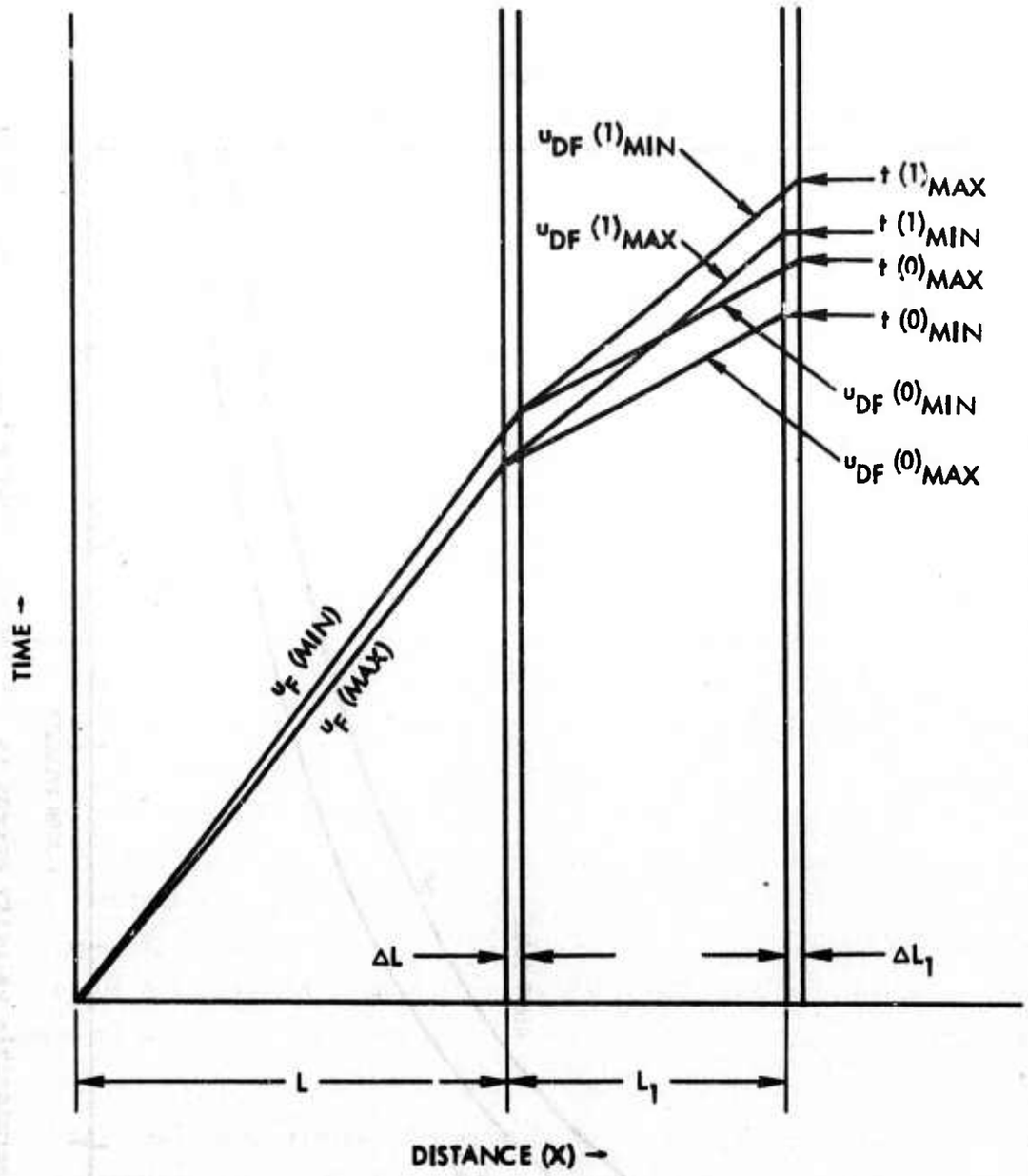

Figure 6. x-t diagram of the DF formation reaction giving the arrival times of the DF-molecules at the detector.

Similarly, the earliest arriving DF-molecule in the v = 1 state is

$$t_{min}(v = 1) = \frac{L}{u_{F(max)}} + \frac{L_1 + \Delta L}{u_{DF}(1)} \tag{7}$$

In order for the two types of DF-molecules to be resolved, we require that

$$t_{max}(v = 0) \leq t_{min}(v = 1) \tag{8}$$

It can be seen by inspection of Eqs. (6) and (7) that the condition imposed by Eq. (8) is more severe than simply requiring that $u_{DF}(v = 0) > u_{DF}(v = 1)$.

The same considerations apply to the resolution of the two D-atom groups associated with the internal energy states of the corresponding DF-molecules. However, as noted above, the velocity of the D-atoms is much larger than that of the DF-molecules with the result shown qualitatively in Figure 7. Because of the generally higher velocity of the D-atoms compared to the DF-molecules, the transit time from the gas target region to the detection region is less and so is the difference in arrival times of the two D-atom groups. In the illustration of Figure 7, the two groups are not resolved which is more or less representative of the real case. If the condition that $u_D(0) > u_D(1)$ is met, the distance L_1 can be increased so as to ultimately resolve the two groups. However, increasing the distance to the detector decreases the detection solid angle by the square of the distance with an attendant reduction in signal level.

Because of the number of independent quantities in Eqs. (6) and (7), it is impractical to develop a general analytical expression that can be used to illustrate the dependence of time-of-flight resolution on the several quantities. However, an example serves to illustrate that mechanical energy selection is a practical solution to the problem for small values of F-atom energy. A sample calculation was made for assumed conditions where the distance from the laser beam target to the gas target was 1 meter, the distance from the gas target to the product detector was 30 cm and the laboratory scattering angle was 20°. It was further assumed

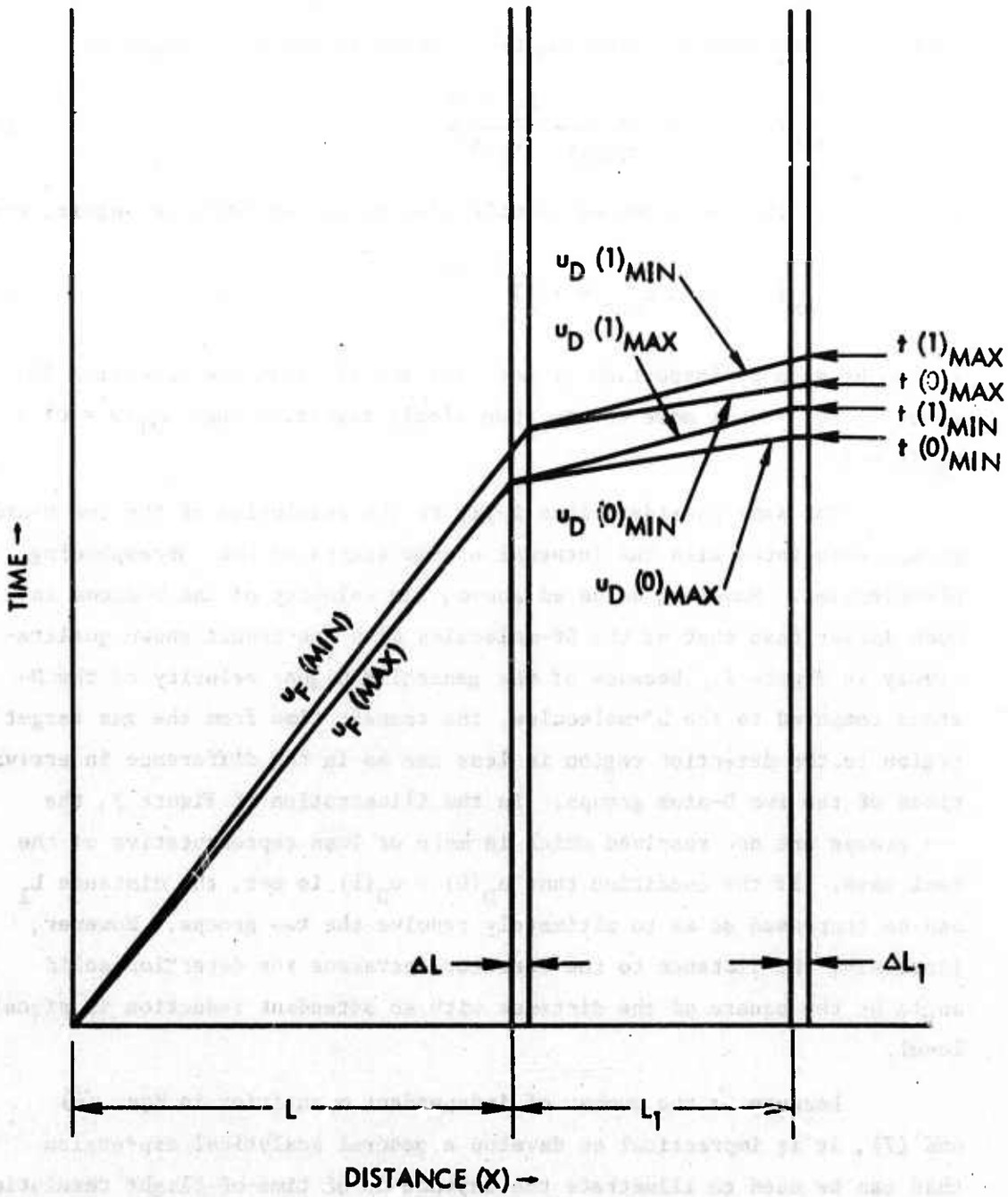

Figure 7. x-t diagram of the DF formation reaction giving the arrival times of the D-atoms at the detector.

that a shutter between the laser target and the gas target was opened for a time interval such that the time width of the F-atom pulse at the gas target was 10 microseconds and that the opening of the shutter was delayed from the time of the Q-switch pulse such that the velocity range of the incident F-atoms was from 3.00×10^5 to 3.10×10^5 cm/sec. The shutter assembly is presumed to consist of a stationary slit traversed by a high velocity slit. This arrangement gives a triangular shaped pulse with a peak when the two slits overlap as shown in Figure 8 where the incident beam pulse as observed at the plane of the gas target is represented. The incident beam pulse produces a number of reaction products and they would be observed at the detection station in the time sequence shown. For clarity we show only the v = 0 and v = 1 state molecules. Since forward and backward scattering in the center of mass system both translate to forward scattering in the laboratory reference frame, four peaks are observed. For the stated conditions, the forward scattered molecules are nearly resolved while the backward scattered molecules are completely resolved. The amplitudes of the peaks shown in Figure 8 have been arbitrarily set at unity which will most certainly not be the case in the real situation. The resolution demands placed on the velocity filter have been met as discussed in sub-section 3.3.

2.3.2 Energy Selectivity By A Velocity-Dependent Product Detector

Prompted by the large differences in the velocities of deuterium atoms resulting from the DF formation reaction, the concept of utilizing a velocity dependent D-atom detector was thoroughly explored. The concept is understood with the assistance of the vector diagram in Figure 9. The velocity of a deuterium atom in the lab reference frame u_{DL} is the vector sum of the velocity of the center of mass in the lab frame u_{cm} and the velocity of the D-atom relative to the center of mass u_D. The vector diagram shows two cases that yield the same D-atom velocity, i.e.,

$$\vec{u}_{cm} + \vec{u}_D = \vec{u}_{cm} + \vec{u}'_D = \vec{u}_{DL} \tag{9}$$

where the primed symbols refer to one internal energy state of the

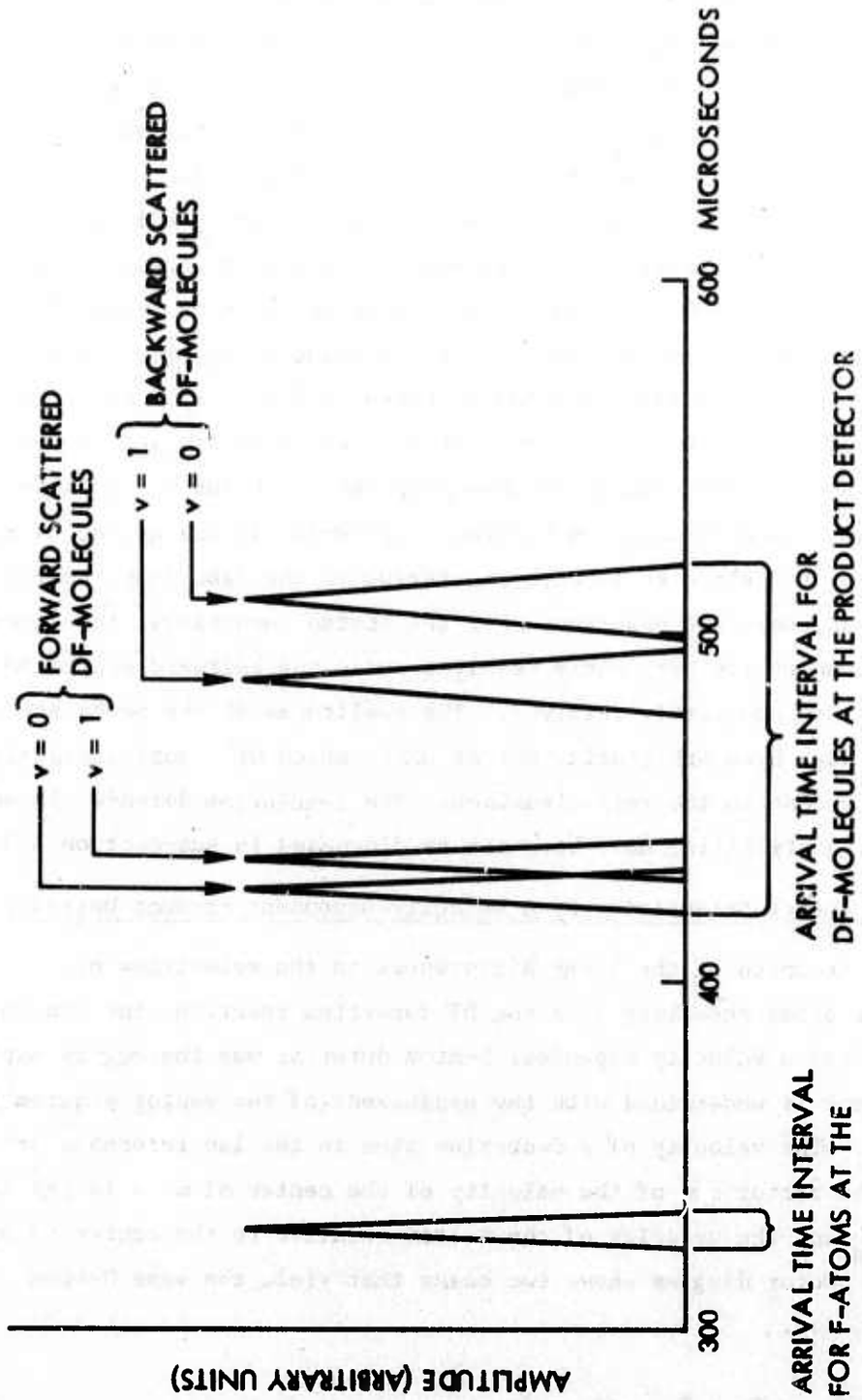

Figure 5. Diagram giving the arrival times of DF-molecules as a function of internal energy state for a velocity selected F-atom pulse.

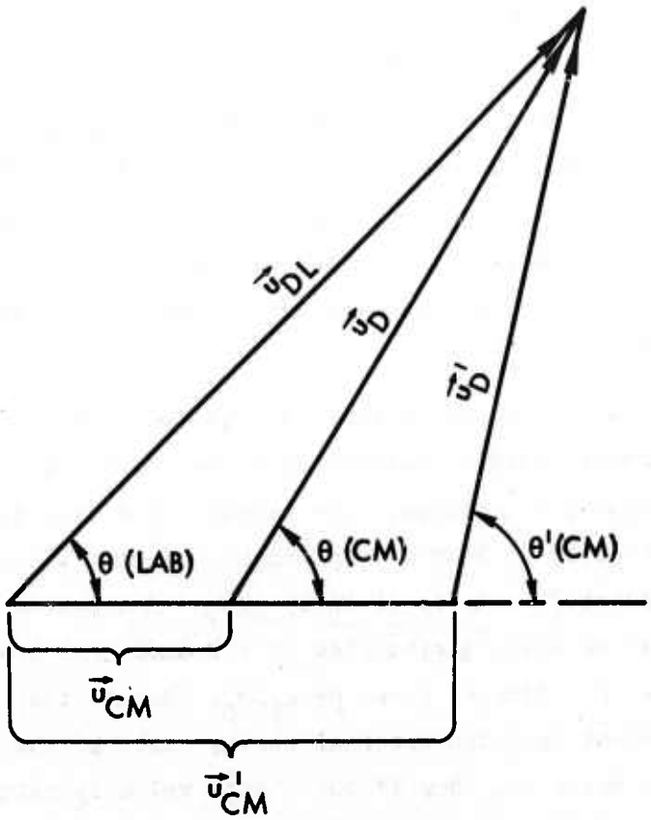

Figure 9. Velocity vector diagram illustrating the equality $\vec{u}_{cm} + \vec{u}_D = \vec{u}'_{cm} + \vec{u}'_D$.

corresponding DF-molecule and the unprimed symbols to another. In the DF formation reaction as many as five combinations of $\vec{u}_{cm}$ and $\vec{u}_D$ can result in the same $\vec{u}_{DL}$. However, as developed below, the time of arrival at the D-atom detector is different for each of the combinations.

Assume that a fluorine rich laser target material is located at a distance L from a crossed thermal D_2 beam and that a D-atom detector is located at a distance L_1 from the D_2 beam. Assume further that the D-atom detector includes a velocity filter set to pass only D-atoms with a given velocity u_D. (Ignore for a moment the pass band of the filter)

At t = 0 the laser is Q-switched generating a swarm of F-atoms that travels radially outward from the target with a wide range of translational velocities. The transit time from the fluorine target to the crossed D_2 beam of a particular F-atom within the expanding cloud (denoted by t) is given by L/u_F. Now assume that this atom reacts with a D_2 molecule giving rise to a D-atom that travels to the D-atom detector in a time t_1 given by L_1/u_D. Recall that the magnitude of u_D is dependent upon the internal energy state of the DF-molecule resulting from the reaction. Now if the D-atom velocity matches the acceptance velocity of the filter, the D-atom will be detected at a time t_2 (referenced from the laser firing) which is the sum of the quantities t and t_1 i.e.,

$$t_2 = t + t_1 = \frac{L}{u_F} + \frac{L_1}{u_D} \tag{10}$$

Rearrangement gives

$$u_F = \frac{L\, u_D}{t_2\, u_D - L_1} \tag{11}$$

In this expression u_D is specified by the velocity filter, L and L_1 are known, and t_2 can be measured, thereby providing sufficient information to determine u_F.

Although there are several sets of conditions that will produce a reaction product with the same velocity vector, simultaneously determining the elapsed time between laser firing and detection of the product uniquely defines the velocity (or energy) of the F-atom participating in the reaction and the internal energy state of the product molecule can be calculated unambiguously.

In practice, the velocity filter must have a finite velocity pass band Δu_D. For products in a given energy state this gives rise to a range of F-atom velocities Δu_F capable of producing products within Δu_D. The effect of a finite velocity band pass on the D-atom detector is illustrated in Figure 10. The minimum condition for maintaining the uniqueness of the measurement is that $\vec{u}_{cm} + \Delta\vec{u}_{cm} < \vec{u}'_{cm}$ which is essentially the same condition imposed in developing the data presented in Figure 5 of Appendix A. The same result can be obtained analytically. Starting with the preceding equation it can be shown that

$$\frac{\Delta u_F}{u_F} = \left| \frac{\Delta u_D}{u_D} \cdot \frac{L_1}{u_D} \cdot \frac{u_F}{L} \right| = \left| \frac{\Delta u_D}{u_D} \cdot \frac{t_1}{t} \right| \qquad (12)$$

Data shown in Figure 5 of Appendix A gives the maximum permissible velocity range in the incident beam that results in velocity separation of D-atom corresponding to adjacent vibrational levels. The maximum values of $\Delta u_F/u_F$ range from about 0.6 at u_F = 2 km/sec to 0.1 at u_F = 8 km/sec. However, this criterion permits a large uncertainty in the final measurement of the energy-dependent reaction cross section, particularly at low energies. A more realistic requirement is that the quantity $\Delta u_F/u_F$ be specified to about 0.1 throughout the entire energy range.

In the DF formation reaction, u_D is always larger than u_F for the lower v-levels and u_D is comparable in magntiude to u_F for high states of excitation scattered in the backward direction. In a practical situation the ratio of L_1 to L can be less than unity with the result that the quantity t_1/t in Eq. (12) is always less than unity. Assuming t_1/t = 0.5

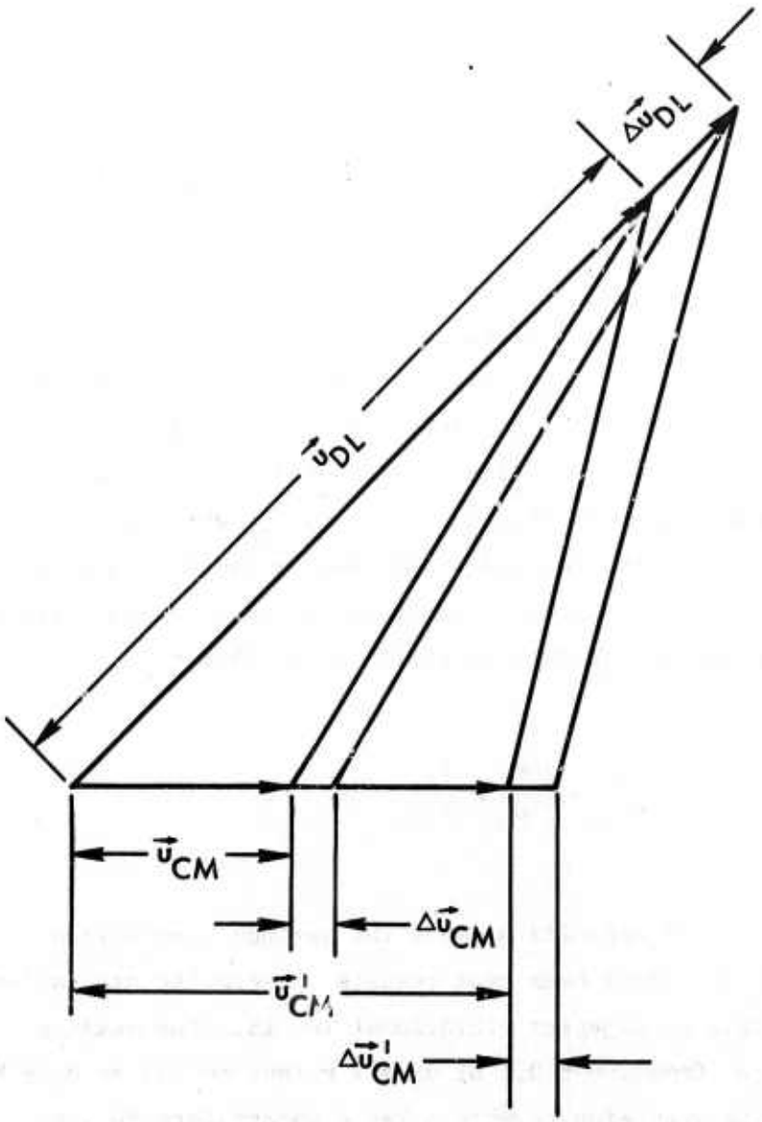

Figure 10. Velocity vector diagram illustrating the effect of a velocity dependent detector with a finite velocity band pass.

and requiring that $\Delta u_F/u_F = 0.1$ places a resolution requirement on the velocity filter of

$$\frac{\Delta u_D}{u_D} \leq 0.2 \tag{13}$$

Since the use of a velocity-dependent D-atom detector appeared to be applicable across the energy range of interest, a concentrated effort to develop such a system was undertaken. Unfortunately, this effort met with only partial success and the decision was finally made to abandon this approach in favor of the mechanical velocity selector. This had a large impact on the program because the design of the cross section measurement system was predicated on the use of a velocity dependent detector. In fact, the system was completely assembled and was being tested before it was finally confirmed that the characteristics of the velocity-dependent detector were unacceptable.

The requirement for the measurement of reaction cross sections for different vibrational states of the product molecule imposes a severe limitation on the allowable ion energy spread within the ionizer and on the velocity selectivity of the filter. However, the velocity filter approach still appeared sufficiently promising to justify the development of two essential components: The ionizer and the filter proper.

Conventional ionizers in addition to low ionization efficiency (usually less than 10^{-3}) introduce an ion energy spread of many volts (20-30 V) which is unacceptably high for the present application where the maximum allowable spread must be less than a fraction of a volt (1/4 to 1/2). A novel ionizer design was conceived in which the electric field in the ionization region in the direction of molecular and ion flow was minimized by confining the ionizing electron flow by a uniform axial magnetic field produced by a special arrangement of a number of permanent magnets. At the same time the transverse electric field due to the electron space charge was utilized to collimate the ions as they move from the point of generation toward the exit aperture

of the ionizer. Since there are no axial electric fields over the major part of the ionizer, the ions move in the axial direction at the same speed as the neutral molecules so that the ion arrival time at the detector is independent of the position where the ion is generated within the ionizer. This characteristic makes it possible to make the ionizing region considerably longer than in conventional designs. As a result, much higher ionization efficiency, of the order of several percent (about 1 ampere per Torr) was achieved which is an improvement of at least two orders of magnitude over the conventional design. Since this improvement in efficiency was realized together with minimal ion energy spread, it was believed that the ionizer performance was adequate for the proposed differential reaction cross section measurements.

The primary considerations for the final design of the velocity filter were the achievement of high transmission efficiency and adequate velocity discrimination. The use was made of the uniform magnetic field generated by an electromagnet into which the ions are injected from the ionizer. Ions of specified mass and velocity are focused by the magnetic field on the exit aperture leading to the detector (quadrupole mass spectrometer with electron multiplier detector was used in preliminary measurements of ionizer and velocity filter performance). Since the ions of interest in the DF formation reaction are deuterium, the required intensity of the magnetic field (several hundred gauss) and its extent (15 cm) are quite practical.

The ionizer-velocity filter assembly was tested extensively using residual gas at pressure of the order of 10^{-6} Torr as a source of hydrogen atoms and molecules. It was found that when the ion energy in the filter was higher than about 30 volts the filter transmission was very good, approaching 100%. The effective velocity resolution which included the effects of residual ion energy spread in the ionizer and focusing apertures also appeared reasonable (10-15%). Figure 11 shows the relative currents of atomic and molecular hydrogen through the velocity filter as a function of magnetic field for the ion energy of about 25 volts. The operation of the filter at this energy was quite reproducible. However, when the ion energy was reduced

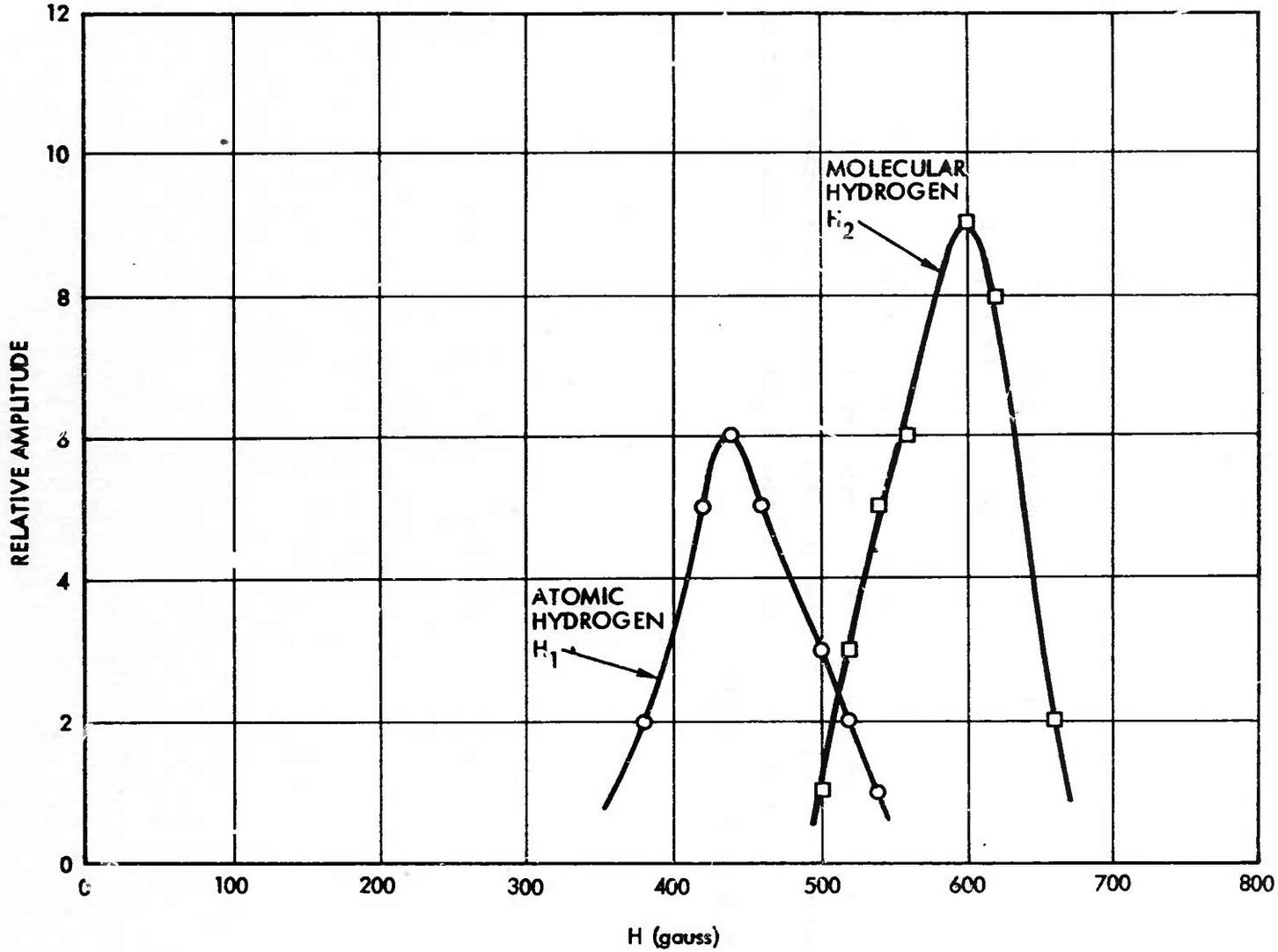

Figure 11. Mass Resolution of the Magnetic Velocity Filter

towards 10 volts the transmission of the filter decreased very rapidly. In addition, the ion current tended to drop significantly with time and there appeared a large "hysteresis" effect which made it difficult to reproduce results at low ion energies. These effects were interpreted as due to charging of the filter chamber surfaces by impinging ions. Several attempts were made to clean the surfaces to get rid of formation of insulating films responsible for surface charging but the results were not at all encouraging.

In view of the requirement for the operation of the filter with relatively high resolution at ion energies of only a few volts, further attempts to improve the velocity filter performance were abandoned in favor of the use of mechanical chopper technique which appears effective at low F-atom energies.

SECTION III

CROSSED MOLECULAR BEAM APPARATUS

3.1 Atomic Beam Source

One of the significant achievements of the program was the development of a new type of atomic beam source. As originally conceived, the DF formation reaction was to be studied in a crossed molecular beam configuration wherein the primary (i.e., fluorine atom) beam was to be produced by the laser vaporization of high velocity microparticles composed of a fluorine-rich compound material. It had been expected that the intensity of a short-duration, Q-switched laser pulse could be adjusted so that the amount of energy absorbed by the particles would just be sufficient to completely vaporize the particles. If this were the case, the end result of the laser irradiation would be the formation of a slowly expanding cloud of vapor traveling with a translational velocity equal to that of the particle prior to irradiation. An observer stationed downstream would see a high-intensity, short-duration burst of nearly monoenergetic neutral atoms and molecules.

A 2-year effort to develop this concept preceded the commencement of the present program. It was found that the approach was unacceptable due primarily to excessive heating of the vapor cloud by the absorption of radiant energy from the laser beam. This resulted in a rapidly expanding vapor cloud which destroyed the monoenergetic characteristic of the pulse and, at the same time, drastically reduced the instantaneous beam intensity as observed at a downstream station. A model consistent with the experimental observations has been developed. For values of laser beam intensity resulting in absorbed energy less than that required for appreciable vaporization to occur, the particle remains intact and continues on its original trajectory. Once vaporization begins, the effective absorption cross section of the particle increases due to absorption of the laser light by the expanding vapor. More than likely, it is the free electrons in the vapor cloud that are the most efficient absorbers of radiant energy. The electrons transfer their energy to the atoms and molecules in the vapor cloud thereby increasing the temperature and, therefore, the rate of expansion. This further increases the absorption cross section leading to a situation

where the temperature of the cloud is much larger than desired. The end result is the aforementioned rapidly expanding vapor cloud. There appeared to be no solution to this problem consistent with other constraints and this approach to the generation of a monoenergetic pulsed atomic beam was abandoned.

A viable alternative approach, developed in large measure under the auspices of the present program, involves the laser vaporization and heating of thin films of solid material. The technique is described in some detail in Appendix B which consists of a technical paper that has been accepted for publication in the Review of Scientific Instruments. The discussion here will be limited to a brief description of the technique and a summary of its features.

In principle, the method of producing the primary atomic beam is straightforward enough. The beam from a Q-switched ruby laser is brought to a partial focus on the surface of a solid sheet of material. The absorption of radiant energy volatilizes a small volume of the target and raises the temperature of the vapor. The subsequent expansion of the hot vapor cloud into vacuum orders the random motion into a laminar flow. At a point removed from the laser target, a "burst" of atoms is observed traveling in straight line trajectories. The burst of atoms contains a broad distribution (generally Maxwellian) of energies. However, if the distance from the target to the point of observation is large compared to the distance over which the gas cloud remains collisional, the energy of a particular atom is specified by its arrival time (i.e. the time of transit from the target to the observation point). Thus, even though the pulse contains a wide atom energy range, all of the atoms arriving at a particular instant of time have the same energy. This consideration requires that the laser pulse duration be short compared to the atom transit time. The laser pulse length used in our work was always 100 nsec or less which more than satisfies this requirement. A short duration laser pulse is also a requirement in order to achieve the high temperature. Otherwise, conduction and other loss mechanisms lessen the efficiency of utilization of the laser energy.

In practice, several subtle effects alter this simple picture to a certain extent, but the end result is essentially as stated. For example, it was originally assumed that a neutral atom beam could be produced as described above, i.e., the laser light could be focused on a solid block of material. It was recognized that the high temperature vapor cloud would be partially ionized. This appeared to pose no particular problem since the ions could be extracted from the cloud by an applied electric field leaving only neutral atomic species. For some materials, this was the case but for others (e.g., aluminum) the cloud was almost completely ionized. It was concluded that the direct irradiation of solid material resulted in raising the temperature of a small quantity of material to a very high value. This problem was solved by using thin film targets bonded to transparent substrates. The laser beam is directed through the substrate and focused on the "rear" side of the thin film target. In this configuration, the hot plasma is physically constrained from expanding until it has been cooled by conduction to the surrounding medium. This process ingests additional material into the constrained vapor cloud and continues until the free surface is reached. At this time the "moderate" temperature cloud is free to expand into vacuum with a result as described above.

The salient features of the pulsed atomic beam system as determined by the measurements described in Appendix B are listed below:

1. Atomic Species: The approach appears to be compatible with virtually any atomic and some molecular species with the possible exception of noble gases. Species that are stable in elemental form (e.g., metals) are most easily handled since they can be deposited in thin film form. Other species (e.g., fluorine) can be obtained by bombardment of thin films of a compound bearing the desired element (e.g., BiF_3). A requirement for the use of compounds is that the bond strength not be unduly large. Because of different physical properties of compound materials, experimentation to find the best set of laser bombardment conditions to achieve the desired result may be required. Some molecular species (e.g., HF, CF) have been observed under various conditions. As a general rule, it appears that only tightly bound molecules can survive the high-temperature environment without dissociating.

2. Atomic Beam Intensity: Perhaps the most significant feature of the pulsed atomic beam source insofar as the present application is concerned is the high beam intensity available. Data presented in Appendix A show that fluxes on the order of 10^{17} atoms/cm^2/sec at a distance of 60 cm from the laser target are obtained in the few electron volt energy range. This value is six to seven orders of magnitude greater than generally obtained with "conventional" beam sources (which, by the way, are often restricted to normally gaseous species). The total number of atoms in a pulse (i.e., the total number incident on a one square centimeter aperture at a distance of 60 cm from the source) is on the order of 10^{13}. For a pulse repetition rate of one pulse per 10 seconds, the "average" flux is reduced to about 10^{12} atoms/cm^2/sec, an apparently less dramatic increase over conventional techniques. However, in molecular beam experiments, the sensitivity of a measurement or the detectability of an event is often determined by signal-to-noise considerations. Usually, noise can be characterized as steady state. For a fixed number of detectable events, the signal-to-noise ratio is inversely proportional to the time interval over which the events occur. Thus, the pulsed character of the laser bombardment produced atomic beam is distinctly advantageous in most situations. Often, users of more conventional sources artificially modulate the normally steady state beam to take advantage of the noise suppression characteristics available from synchronous detection - an inherent feature of the pulsed beam source. The high beam intensities available have the added virtue of reducing instrumental requirements. For example, in mass spectrometric measurements, atoms are detected by first ionizing them and then detecting the ion current. If flux values are high, the resultant ion current can be measured directly, whereas very small currents can be detected only by ion counting techniques. Although the detection of single ions is a well developed art, it still imposes a degree of complexity better avoided if possible.

3. Atom Energy: As noted earlier, each atom pulse contains a broad spectrum of energies; however, each such pulse can be characterized by a "mean" value corresponding to the peak of a Maxwellian distribution specified by the temperature. Figure B5 of Appendix B shows that this

mean value can be varied over a rather wide range by selection of laser bombardment conditions. There are both upper and lower limits to the achievable mean energy range. The minimum temperature must exceed the vaporizati n temperature of the target material which for most common metals is several thousand degrees Kelvin. The maximum temperature is limited by excessive ionization of the vapor. This effect is shown indirectly in Figure B6 of Appendix B for aluminum where the total number of atoms in the pulse is seen to diminish as the average energy increases, due in part to loss by ionization. The severity of this limitation depends upon the ionization potential of the material.

4. Versatility: The ability to rapidly change from one atomic species to another is inherent in the pulsed atomic beam approach since it involves only substitution of the laser target. Different materials may have different properties with respect to the absorption of optical radiation and a few materials have been found to be incompatible with this approach. These can generally be classified as colorless compounds that tend to transmit the laser light. Fortunately, most elements are available in a variety of compounds with differing physical characteristics and chances are good that at least one of them would be satisfactory. Particularly good results have been obtained with metals where homogeneous films can be obtained by vapor deposition. The laser bombardment conditions required to achieve a given energy distribution in the beam cannot necessarily be determined in advance for an arbitrary material. Usually, however, only a few test shots are required to achieve the desired parameters.

Insofar as the present application is concerned, the broad energy range contained in the atom beam pulse imposes a requirement for post-burst energy discrimination. This would not have been the case if the particle vaporization approach had met with more success. Two different methods of energy discrimination were undertaken as discussed in Section II of this report.

3.2 Deuterium Target Gas Assembly

In selecting a target gas assembly configuration, the principal requirement was to achieve a reaction probability for the incident

fluorine atoms of about one-tenth. This condition essentially maximizes the reaction rate consistent with maintaining an adequately low probability of secondary reactions within the target volume. This requirement together with the length of the target volume along the incident beam axis determines the required molecular number density of the target gas. Assuming a 1.0 cm axial length for the gas target and a typical reaction cross section of 3×10^{-16} cm^2, the desired number density in the target volume is approximately 3×10^{14} molecules/cm^3. (The number density n is found from $n = 0.1/\sigma_R x$ where σ_R is the reaction cross section and $x = 1.0$ cm)

The required target gas density may be generated by a simple nozzle source. The axial number density n_x in a jet from a nozzle source is given approximately by the following relationship:

$$n_x \cong 0.16\, n_o \left(\frac{D}{X}\right)^2 \tag{14}$$

where n_o is the stagnation density in the source reservoir, D is the exit nozzle diameter, and x is the distance downstream along the jet axis. The above expression predicts an axial number density of $\approx 3 \times 10^{14}$ molecules/cm^3 at a distance x = 1.0 cm if D = 0.025 cm and the reservoir pressure = 100 Torr. For reaction cross sections larger than the value assumed above, the target gas density may be reduced by lowering the reservoir pressure or moving the interaction zone further downstream in the jet.

A nozzle source with the parameters discussed above is currently in use. The gas throughput from the nozzle is 2.7 Torr-liters sec^{-1}. Since a steady-state throughput of this magnitude would require an exorbitant pumping speed. The gas jet is pulsed on just prior to the arrival of the pulsed incident atom beam. A solenoid actuated valve has been constructed which has open and close times of less than 10^{-3} sec. This valve permits a gas pulse duration of 3×10^{-3} sec or less to be realized.

After passing through the interaction region, the gas jet from the nozzle is directed into a pumping chamber with a capacity of approximately 2000 liters sec^{-1}. The throughput of the pumps used is sufficient to return the system to a base pressure less than 10^{-5} Torr in less than 0.1 sec. The gas pulse time duration and relative amplitude are monitored by a nude structure ionization gauge of the Bayard-Alpert type which is located on the jet axis downstream from the target volume. The gauge collecting wire is placed normal to the axis and has a buffered amplifier output to provide fast time response.

It seems appropriate at this point to comment on the mean energy of the atoms in an expanded beam from a nozzle source. The final energy attained is higher than the mean thermal energy in the reservoir as a result of conversion of total enthalpy into beam translational energy by the expansion process. Above a Mach number of about 4 the factor is approximately $2\gamma[3(\gamma-1)]^{-1}$ where γ is the ratio of specific heats. Thus, for a diatomic gas with $\gamma = 7/5$, the final mean velocity attained is given approximately by:

$$v \cong \left[\frac{2\gamma}{3(\gamma-1)}\right]^{1/2}\left[\frac{3kT_R}{m}\right]^{1/2} \cong \left[\frac{7kT_R}{m}\right]^{1/2} \qquad (15)$$

where k is Boltzmann's Constant, T_R is the reservoir temperature and m is the mass of the gas molecule. The momentum of the D_2 gas molecules is thus generally much smaller than that of the incident fluorine atoms. Hence, the assumption that the target gas molecules are at rest is valid.

3.3 Detection Apparatus

Detection of the incident F-atom beam pulse and reaction products is accomplished with more or less standard instrumentation. A basic detector unit consists of an electron impact ionizer, a quadrupole mass filter and an electron multiplier tube ion detector. The ionizer and quadrupole are commerical units obtained from Extranuclear Laboratories, Inc. (Ionizer-high efficiency Type II, Quadrupole Model No. 324-9 used with either the Extranuclear C or E high-Q heads). The ion detector is

an EMI 11-stage venetian blind electron multiplier with beryllium-copper dynodes.

The electron impact ionizer ionizes some small fraction (estimated to be in the 10^{-4} to 10^{-3} range) of the incident atoms or molecules and, by means of an integral electrostatic lens assembly, injects them into the quadrupole mass filter. The quadrupole has the characteristic of passing ions within a preset charge to mass range. The resolution of the quadrupole is variable over a very large range, but it was normally set at about one amu. The electron multiplier assembly was operated with the anode at ground potential and with the first dynode at negative high voltage (2 to 3 kV). Ions emerging from the quadrupole are attracted to the first dynode of the tube structure and impact the surface at an angle of incidence at about 45° with an energy determined by the potential applied to the dynode structure. Secondary electrons released by the ion impact proceed down the dynode chain undergoing multiplication at each step. The result is a large electron signal at the anode. Tests indicate that the ion-to-electron conversion efficiency at the first dynode is near unity in which case, the electron multiplier serves the function of high gain, low noise amplifier.

In many of the tests that were conducted, variations of the basic detector unit were used as circumstances dictated. The simplest detection system consisted of the basic ionizer and an ion current collector. This system has the virtue of providing an absolute measure of the ion current at the expense of ion species identification. Another variation used only the ionizer and electron multiplier assembly from the basic unit. Again, at the expense of ion species identification, this variation gave the largest signal in terms of absolute amplitude because transmission losses inherent in the quadrupole mass filter were avoided.

3.4 Velocity Selection System

The broad range of energies in the F-atom beam pulse imposes the requirement of velocity selection. For the reasons discussed earlier the decision to utilize a mechanical velocity selector on the incident F-atom beam was made. Since the arrival time of a fluorine atom at a

point some distance removed from the laser beam target uniquely defines its velocity, velocity selection can be accomplished by simply opening a mechanical shutter for a brief time interval subsequent to the laser burst. The maximum velocity contained in the transmitted pulse is given by L/t where L is the distance from the laser target and t is the delay time before the shutter opens. The minimum velocity is given by $L/(t + \Delta t)$ where Δt is the time interval over which the shutter is open. The factors which determine the maximum allowable velocity range in the transmitted beam pulse have already been discussed in Section II above and in Appendix A. Suffice it to say here that the quantity $\Delta u_F/u_F$ must be less than a few percent even for small values of u_F. It follows that $\Delta t/t$ must be of the same magnitude.

The mechanical shutter consists of a stationary slit aperture mounted in front of a rotating disc containing a similar slit extending radially inward from its periphery. Once each revolution, the slits overlap permitting F-atoms to pass through it. For slits of equal width w, the total time interval between the time the shutter first starts to open and the time it closes is given by

$$\Delta t = \frac{2w}{u_T} = \frac{2w}{R\pi D} \tag{16}$$

where u_T is the tangential velocity component of the disc at its periphery, R is the rotational speed of the disc, and D is its diameter. During Δt, the area of overlap of the two slits increases linearly as the leading edge of the moving slit sweeps across the stationary one, reaches a maximum when the two slits completely overlap, and decreases as the trailing edge of the moving slit traverses the stationary slit. This gives rise to the triangular shaped pulse assumed in Figure 8.

In principle, Δt can be made arbitrarily small by simple decreasing w. But this is done, of course, at the expense of beam intensity. Another point to note is that the slit assembly can be placed anywhere between the laser beam target and the crossed beam gas target with equal effectiveness. For fixed values of R and D the value of w required to attain a specified Δt at the plane of the target gas beam can be calculated from Eq. (16). The slit width required to meet this condition

is directly proportional to the distance from the laser beam target to the plane of the slit. Thus, if a slit width w is required at the gas target plane, a slit width of w/2 is required at a point halfway between the laser beam target and the gas target. The delay time between firing of the laser and opening of the slit must be halved accordingly. Halving the slit width and the distance does not decrease the beam intensity at the gas target plane.

The velocity selector consists of a 20-cm diameter aluminum disc driven by a 15 watt synchronous motor rated at 24,000 rpm (400 rps). The slit assembly has been positioned at a distance of approximately 50 cm from the laser beam. At its rated rotational speed the use of 1/2 mm slits gives a Δt of $\sim$4 μsec at the plane of the shutter which translates to a Δt of 8 μsec at a distance of 1 meter from the laser beam target. This is adequate for our purposes.

The principal practical problem is that of maintaining the integrity of the high-speed disc. The disc was sized such that the centrifugal force was less than the tensile strength of the material. However, any unbalance in the rotating system which displaces the center of mass from the axis of rotation could result in forces dangerously close to or exceeding the yield strength of the material. To minimize this problem, the shaft to which the disc was affixed was suspended at both ends in "floating" bearings. Actually, the bearing races were suspended from an outer fixed ring by a number of radial springs. In this arrangement any unbalance in the rotating mass is taken up by a lateral displacement of the shaft which is damped by the radial spring assembly. Viewed from end-on the displacement of the shaft precesses around the geometrical center of the system at the rotational speed of the shaft. Starting with a reasonably well balanced assembly, the magnitude of the displacement is small. Nevertheless, this approach appears to be necessary particularly during start up when the shaft system passes through certain mechanical resonances which cause vibrations. Since the shaft must be free to move laterally, a flexible coupling to the drive motor consisting simply of a small gauge wire is used.

The firing of the laser must precede the opening of the shutter by some predetermined time interval in order to select the velocity range transmitted by the shutter on any given shot. This synchronizing function is accomplished by means of a rotational position sensor and a timing and logic electronic assembly. The positional information sensor consists of a collimated light source and a photodiode mounted on opposite sides of the rotating disc. The sensor is located diametrically opposite the fixed slit in the shutter system and produces a short pulse each time one of the slits in the rotating disc passes the sensor. The disc has two slits for balance purposes and, therefore, two pulses are produced for each revolution of the disc.

At its maximum rated rotational speed of 400 rps the duration of a half-period is 1.25 milliseconds. This is precisely the time required for one of the slits to travel from the position sensor to the stationary slit. As discussed in the following paragraphs, the required timing functions can be accomplished within this time period. The sequence of events that must be controlled is as follows: First the laser capacitor bank must be charged. At this point the operator commences the series by closing a manual switch which places a long duration (greater than one-half of a rotational period) pulse on one branch of a coincidence circuit. The chain of pulses from the photodiode sensor is applied to the other branch. The first such pulse that appears subsequent to the switch closure produces a coincident output pulse at a time defined as $t = 0$. The $t = 0$ marker pulse is fed to a series of time delays. At time $t = t_1$ a pulse is generated that is used to discharge the capacitor bank through the laser flash lamps. At time $t = t_2$ a pulse is produced that Q-switches the laser. At time $t_3 = T/2$ where T is the rotational period, the shutter opens.

The time interval t_2-t_1 is a function only of the characteristics of the laser and to all intents and purposes may be considered to be a constant c. Typically, this time interval is on the order of 800 microseconds. The time interval t_3-t_2 defines the transit time of atoms from the source to the slit; hence $\bar{u} = L/(t_3-t_2)$ where L is the distance from the laser target to the slit and $\bar{u}$ is the average velocity of the atom

pulse transmitted by the shutter. It follows that the average velocity of the transmitted is preselected by setting $t_1 = T/2 - c - L/\bar{u}$, where T/2, c, and L are all fixed for a given set of conditions.

Since there are two slits in the disc, it can be seen that the next pulse in the chain of pulses from the position sensor appears coincident with the opening of the shutter. Generally, this pulse and a pulse coincident with the Q-switch pulse are both displayed on an oscilloscope trace to establish an active time base. Recall that the time interval between these two pulses specifies the average velocity of the transmitted beam pulse.

The electronic subassembly provides additional timing markers for use at the discretion of the operator. One of these pulses may be used to actuate the fast valve on the D_2 target gas assembly. Usually, however, this valve is activated at t = 0. One of the other pulses is usually used to trigger the recording oscilloscope at a predetermined time.

Figure 12 is a photograph of the shutter system in place in the experimental assembly. The 24,000 rpm drive motor is located within the cooling water jacket slightly below the center of the photograph. The rotating disc is slightly to the upper right of center. The atomic beam enters from the lower left and passes through the enclosure in a plane beneath the drive motor-assembly. The coil of fine wire is an electromagnet that aligns a small permanent magnet attached to the shaft in such a manner that the wide slit visible in the rotating disc is positioned in line with the atomic beam for static testing purposes. The top of the nozzle beam assembly can be seen at the upper right beyond the wall of the velocity selector enclosure.

The complete system has been thoroughly tested with the result that its performance characteristics have been shown to meet the design objectives. Typical results are illustrated in the oscillographs shown in Figure 13. In each of the three photographs the integrated pulse from the photodiode used to monitor the laser beam is displayed on the upper trace. The sweep speeds of the upper and lower traces are equal

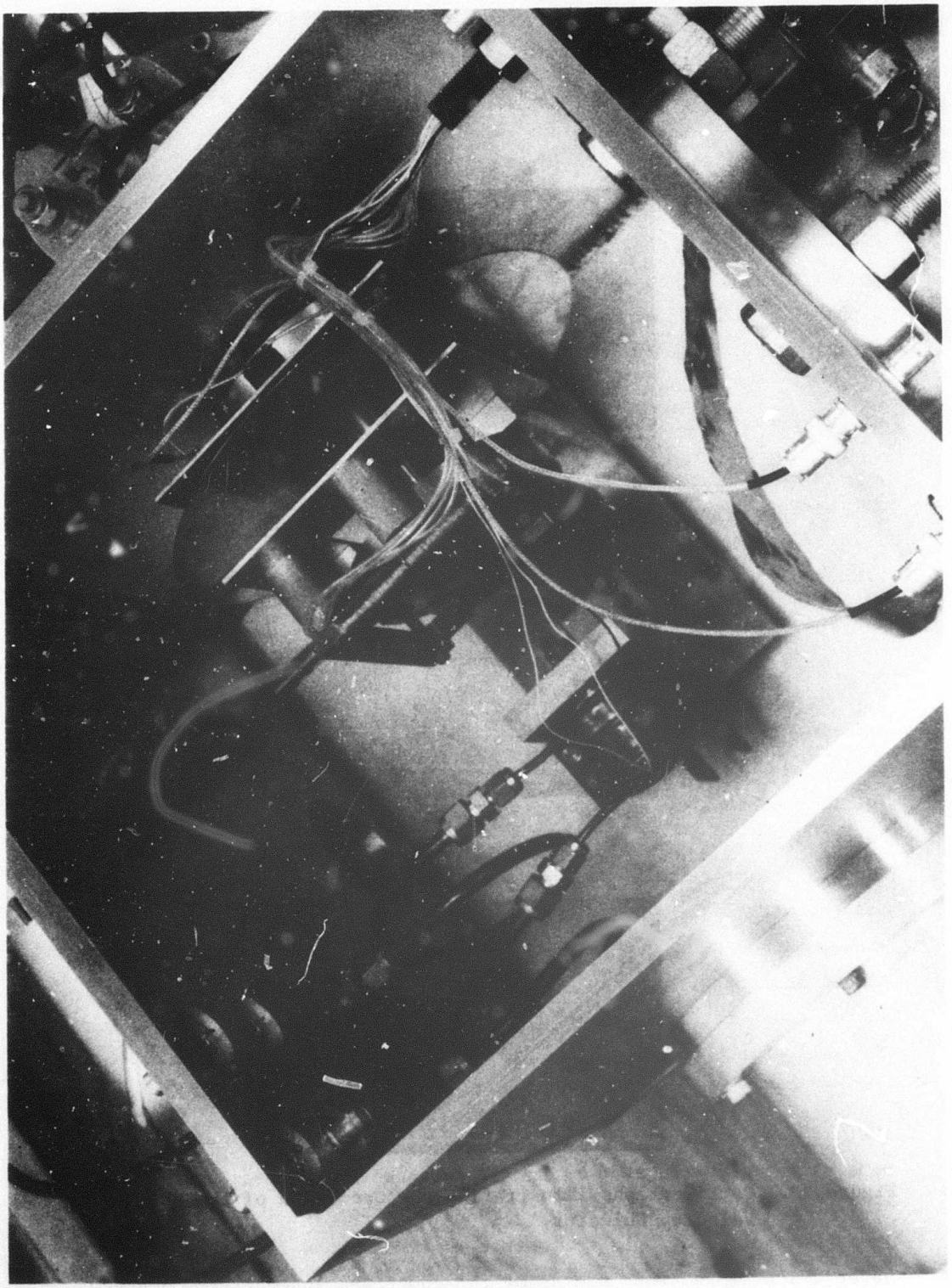

Figure 12. Mechanical Velocity Selector Assembly

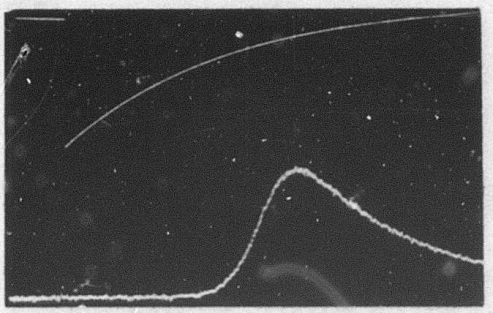

a.

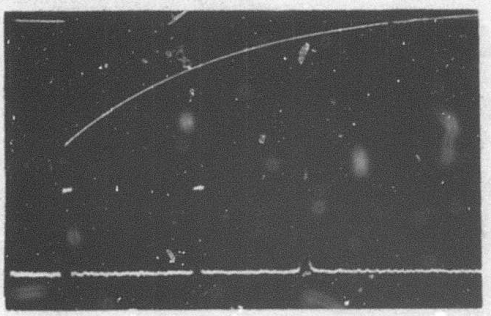

b.

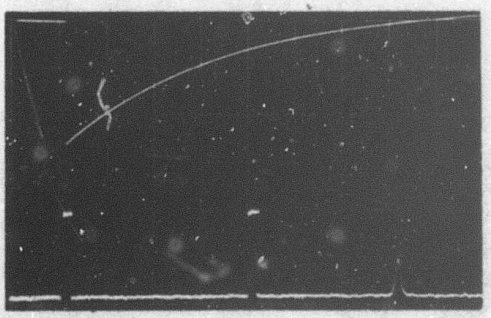

c.

Figure 13. Oscillographs Illustrating the Operation of the Mechanical Velocity Selector.

(50 μsec/division) and are synchronized. Both traces are triggered by an auxillary pulse that occurs approximately 55 microseconds before the laser is Q-switched. The lower trace of Figure 13-a shows an aluminum beam pulse as observed at a distance of 85 cm from the laser target with the velocity selector inoperative. In this trace the energy at the peak is 1.62 eV. Figure 13-b shows the chopped beam pulse with the timing synchronized to pass a narrow band near the peak of the distribution. The laser bombardment conditions were the same as in 13-a. The two flat-topped pulses on the bottom trace identify the time of the Q-switch and the time at which the shutter opens. The transmitted beam pulse has the triangular shape expected. The velocity of the peak of the beam pulse in 13-b is 3.27×10^5 cm/sec (1.5 eV) and $\Delta u/u$ is about .054. Figure 13-c shows another transmitted beam pulse at lower velocity. In 13-c the aluminum atom velocity at the peak is 2.38×10^5 cm/sec ($\sim$0.8 eV) and $\Delta u/u$ = .03. The vertical sensitivity was the same for all three pictures. Amplitude variations are within the shot-to-shot reproducibility of the beam pulse.

3.5 The Integrated System

Due in large measure to our initial decision to utilize a velocity-dependent detector on the D-atom products, the experimental apparatus was developed in a modular form with the capability of detecting products scattered at large angles. The latter requirement was eliminated when the switch was made to the mechanical velocity selection system. However, most of the components were retained when the change was made. The system contains four separate regions in which are performed the following four functions: (1) primary beam generation, (2) velocity selection, (3) crossed thermal beam generation, and (4) reaction product detection. The reaction volume is physically located within the enclosure occupied by the crossed beam assembly.

A photograph of the complete experimental system is shown in Figure 14. In this view, the primary atomic beam is generated in the assembly in the foreground of the picture. The laser beam target is attached to the rod extending vertically through the air lock assembly. The air lock assembly permits rapid changing of the target without

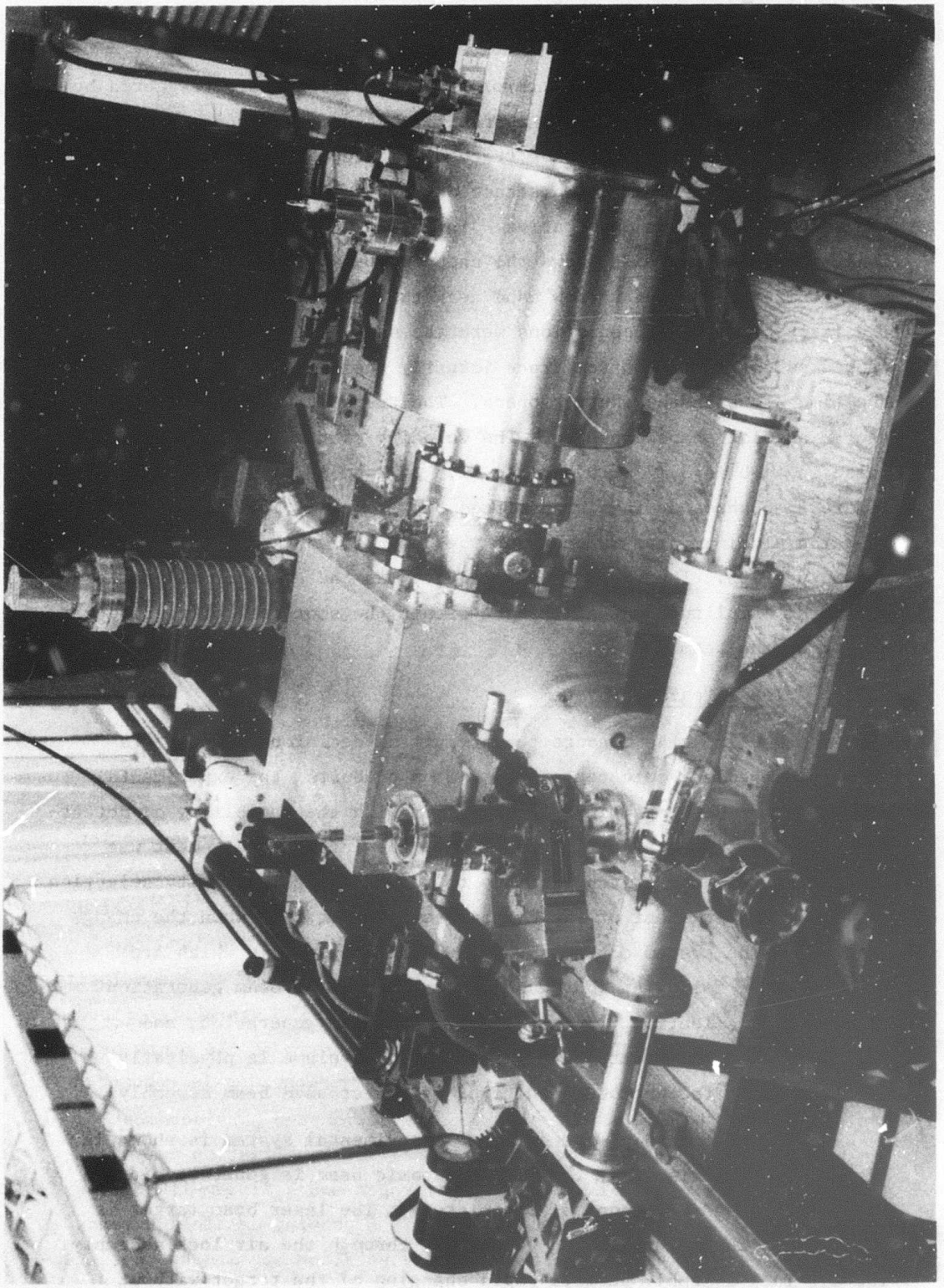

Figure 14. Photograph of the Crossed Molecular Beam Assembly

appreciably effecting the vacuum in the rest of the system. The arms extending to the left and right in the picture contain the focusing lens assembly and view ports. The laser beam is brought through a quartz window in the arm extending to the left. The ruby laser components are mounted on the I-beam at the left of the picture. Starting at the point nearest the entrance window the components on the rail are a prism for deflecting the laser beam by 90°, a piece of plain glass (not clearly visible in the picture) set at an angle of 45° for deflecting a small fraction of the laser light into the photodiode detector at the extreme left, an iris for collimation of the beam, the output mirror, the ruby rod housing, a polarizer, the kerr cell Q-switch, a quarter wave plate, and the end reflector. Not visible in the picture is a He-Ne laser used for alignment purposes. The cylindrical black object with the eye-piece is an auto-collimator used to align the laser cavity.

The primary beam flows toward the upper right in the picture. The cubical box contains the mechanical velocity selector previously shown in Figure 13. The large cylindrical object extended from the right side of the box is a combination ion-titanium sublimation pump used to evacuate the target and velocity selection sections of the system.

A small collimating aperture separates the velocity selection region from the target gas region. The target gas assembly cannot be seen in Figure 14 but was visible in Figure 13. The nozzle is located such that the crossed beam is injected vertically downward into the throat of a titanium sublimation pump similar to the one on the velocity selector housing. The target gas pressure monitoring system described in Section 3.2 is installed on the thermal beam axis at the mouth of the sublimation pump. A baffled 6-inch oil diffusion pump is connected in series with the sublimation pump. The diffusion pump provides most of the pumping speed under ambient conditions. The sublimation pump has a particularly high pumping speed for hydrogen and hydrogen-like gases and is used as a sink for the nozzle beam. A pumping manifold extends from the target gas region to the velocity selector box and to the detection section. This manifold "roughs down" these two sections to the point where the sublimation pumps and ion pumps can be started.

Part of the product detection system can be seen extending beyond the velocity selector section. This region is also isolated from the target gas region by a small aperture. The purpose of the aperture is to inhibit the flow of gas from the gas target nozzle into this region. Pumping in the region of the detector is supplied by the small 100 litre/second combination ion-titanium sublimation pump that can be seen extending vertically upward from the detector housing. The detector is comprised of the elements described in Section 3.3. The detection system can be installed at different angles with respect to the incident beam axis. It is shown at the 0° position. At any angular position, the detector axis and primary beam axis intersect on the axis of the nozzle beam.

Except for a few minor problems of a nuisance variety, the entire system performs satisfactorily. In the present configuration the detector can be set only at 0°, 30°, 60°, and 90° with respect to the incident beam axis. This gave adequate angular resolution for the detection of D-atoms, but smaller angular increments would be desirable for detecting the DF-molecules from the reaction. This change would require modification or replacement of only one part in the assembly. Another advantageous feature would be the addition of valves in the vacuum manifold to more thoroughly isolate the regions once reasonably good vacuum conditions are achieved. It has been found that the ultimate pressure in the detection region is limited by the influx of gas from the velocity selector region via the vacuum manifold. It would be desirable to provide a cold trap in the detection region to reduce the ultimate pressure and also to heat sink the ionizer. The extranuclear ionizer dissipates about 40 watts and radiative heating of the walls of the enclosure results in outgassing to the extent that continuous running time is limited to a period of about 20 minutes. As noted, these problems are of a minor nature and, on the whole, the system performs satisfactorily.

SECTION IV
CURRENT PROGRAM STATUS

As indicated in the preceding section of this report, the several subsystems of the experimental cross section measurement apparatus have been thoroughly tested and assembled into an operational system. The data presented in this report (including Appendix B particularly) indicate that the experimental problems have basically been solved and that the DF-formation reaction can, indeed, be studied by this technique with a reasonable assurance of success. However, the funds have been exhausted at this point in time and no possibility of completing the measurements remains, at least under the auspices of this program as it now stands. It is anticipated that additional results on the study of chemical reactions by this technique will accrue under other programs at TRW. New developments will be communicated to the sponsors of this program as they become available.

APPENDIX A

KINEMATICS OF THE $F + D_2 \rightarrow DF^* + D$ REACTION

The kinematics of the $F + D_2 \rightarrow DF^* + D$ reaction have been analyzed extensively for the primary purpose of specifying the optimum experimental configuration to be used in the measurement of reaction cross sections for the several energetically accessible vibrationally excited states resulting from the reaction. For simplicity and clarity of results, it is assumed that rotational excitation of the reaction product is nonexistent.

The DF formation reaction is of the general type where two particles m_1 and m_2 collide at some relative velocity, the chemical reaction occurs, and two products m_3 and m_4 emerge. Applying the conservation of energy principle yields (in the center-of-mass coordinate system)

$$E_1 + E_2 + Q = E_3 + E_4 \tag{1}$$

where Q is the exothermicity of the chemical reaction. We are concerned with the case where one of the products, say m_3, retains internal energy in the form of vibrational excitation subsequent to the reaction. We may define an "excess" energy $\varepsilon_1 = Q - \varepsilon_3(v = i)$ where $\varepsilon_3(v = i)$ is the internal energy of m_3 when it is in the ith vibrational state. It follows that

$$E_1 + E_2 + \varepsilon_i = E_3(v = i) + E_4 \tag{2}$$

where the subscript i implies that m_3 is in the ith state.

In the center-of-mass reference frame the momenta of m_3 and m_4 must be equal, i.e., $m_3 u_3 = m_4 u_4$. It follows that $E_4 = m_3 E_3/m_4$. For the special case of m_2 initially at rest in the laboratory frame, it can be shown from elementary considerations that $E_1 + E_2 = m_2 E_{1L}/(m_1 + m_2)$ where E_{1L} is the kinetic energy of m_1 measured in the lab system. Substitution of this quantity into Eq. (2) and making use of the

relationship between E_3 and E_4 yields

$$\frac{m_2}{m_1 + m_2} E_{1L} + \varepsilon_i = \frac{m_3 + m_4}{m_4} E_3 \tag{3}$$

This expression reduces to

$$u_3(v = i) = \left[\frac{2m_4}{m_3(m_3 + m_4)}\left(\frac{m_1 m_2}{2(m_1 + m_2)} u_{1L}^2 + \varepsilon_i\right)\right]^{1/2} \tag{4}$$

Similarly

$$u_4(v = i) = \left[\frac{2m_3}{m_4(m_3 + m_4)}\left(\frac{m_1 m_2}{2(m_1 + m_2)} u_{1L}^2 + \varepsilon_i\right)\right]^{1/2} \tag{5}$$

where i continues to refer to the vibrational excitation state of m_3.

The velocity of m_3 (or m_4) in the laboratory system is given by the vector sum of u_3 (or u_4) and the velocity of the center-of-mass in the lab system where $u_{cm} = m_1 u_{iL}/(m_1 + m_2)$. As shown in Figure A1, for a given value of u_{cm} (or equivalently, u_{1L}), u_{3L} (or u_{4L}) is dependent upon the center-of-mass scattering angle θ_o. Lacking a priori information it must be assumed that all values of θ_o are permissible; however, it doesn't follow that all values of θ_o are significant.

The sketch of Figure A1 is similar to that for the actual DF formation reaction where m_3 represents the DF-molecule and m_4 the D-atom. Because of the differences in mass, u_4 is always greater than u_3 and, for the energy range of interest, $u_4 > u_{cm}$ and $u_3 < u_{cm}$. The terminus of u_3 can lie anywhere on a circle of radius u_3. It can be seen from the figure that u_{3L} intersects the circle of $R = u_3$ at two points. This means that there are two values of θ_o for each value of θ except for the value of θ where u_{3L} is tangent to the circle of constant u_3. It is also

clear from the figure that there are two values of u_{3L} for each value of θ corresponding to the two possible values of θ_o. The terminus of u_4 lies somewhere on a circle of radius u_4. However, since the momenta of m_3 and m_4 must be equal in the center-of-mass frame, specifying the center-of-mass scattering angle of one of them specifies the other. Also note that, since $u_4 > u_{cm}$, there is a unique value of u_{4L} for any given value of θ.

It can be shown that the solution of the vector diagram is given by

$$u_{3L} = k_o\, u_{1L} \cos\theta_o \pm \sqrt{u_{1L}^2(k_1 - k_o^2 \sin^2\theta_o) + k_2} \qquad (6)$$

where

$$k_o = \frac{m_1}{m_1 + m_2}$$

$$k_1 = \frac{m_1\, m_2\, m_4}{m_3(m_1 + m_2)(m_3 + m_4)}$$

$$k_2 = \frac{2m_4}{m_3(m_3 + m_4)}\, \varepsilon_i$$

A completely analagous expression can be written for u_{4L} by simply interchanging m_3 and m_4.

This expression was evaluated for the $F + D_2 \rightarrow DF^* + D$ reaction using the data given in the table and the results are presented in graphical form.

The first set (Figures A2-A4) gives the laboratory velocity of the DF-molecule as a function of laboratory observation angle for F-atom velocities of 2, 5, and 8 km/sec, respectively. It can be seen that the DF-molecule always emerges forward and that the maximum scattering angle decreases with increasing F-atom velocity. Another point to note is that the velocity difference between DF-molecules in adjacent excited

states becomes relatively smaller as u_F increases. Finally, note that there are scattering angles that are accessible only to molecules in the ground vibrational state (e.g., the region between 35 and 40° in Figure 2).

Figures A5, A6 and A7 give the D-atom velocity as a function of observation angle for the same values of u_F as above. As mentioned earlier, $u_D > u_F$; hence, scattering of D-atoms into all laboratory angles is energetically possible. At a given observation angle and F-atom velocity, the difference in velocity between D-atoms for adjacent excited states is relatively larger than the difference in the velocities of the corresponding DF molecules. Experimentally this means that it is generally easier to differentiate between D-atoms corresponding to adjacent levels of excitation than is the case for measurement of the DF-molecules.

Figures A8 through A12 give the DF-molecule velocity as a function of F-atom velocity for fixed angles of observation. For small angles, products from both forward and backward scattering in the center-of-mass system are observed. As the angle increases, the forward and backward scattered components converge and finally close. This corresponds to the point where the u_{3L} vector becomes tangent to the circle of constant u_3 as shown in Figure A1.

Similar data for observation of the D-atom at the indicated angles are presented in Figures A13 through A17. Again the single-valued nature of this aspect of the reaction is seen.

An important experimental consideration can be deduced from an examination of Figures A8 through A17. At a given angle of observation the final velocity of either reaction product is dependent upon both the internal state of vibrational excitation and the kinetic energy of the incident F-atom. If the incident F-atom beam pulse has a finite velocity spread, as is almost always the case, a corresponding spread in the velocity of products in a given vibrational state results. If the incident beam velocity range is sufficiently large, products with two or more different states of internal excitation can achieve the same laboratory velocity. In order to avoid this situation the energy spread of the incident beam must be limited. Figure A18 illustrates this point.

Here we have plotted the relative velocity spread in the incident beam pulse ($\Delta u_F/u_F$) as a function of the mean incident velocity of the F-atom pulse that just results in velocity separation of products in adjacent vibrational states, specifically the v = 0 and v = 1 states for $\theta = 0$. Stated more succinctly, we require that the spread in F-atom velocities be limited to the point where $u_{DF}(v = 0) > u_{DF}(v = 1)$ and $u_D(v = 0) > u_D(v = 1)$. It is obvious that the experimental measurement of the DF-molecule as opposed to the D-atom places much more stringent requirements on the allowable velocity spread of the F-atom beam.

CONSTANTS FOR THE $F + D_2 \rightarrow DF + D$ REACTION

$Q = 32$ K cal/mole $= 2.22 \times 10^{-12}$ Ergs

	$\epsilon_{DF}(v = i)$		
V	Wave Numbers	Ergs	ϵ_i (Ergs)
0	0	0	2.223×10^{-12}
1	2906.8	$.5773 \times 10^{-12}$	1.646×10^{-12}
2	5722.3	1.136×10^{-12}	1.087×10^{-12}
3	8448.7	1.678×10^{-12}	$.545 \times 10^{-12}$
4	11088.2	2.202×10^{-12}	$.021 \times 10^{-12}$

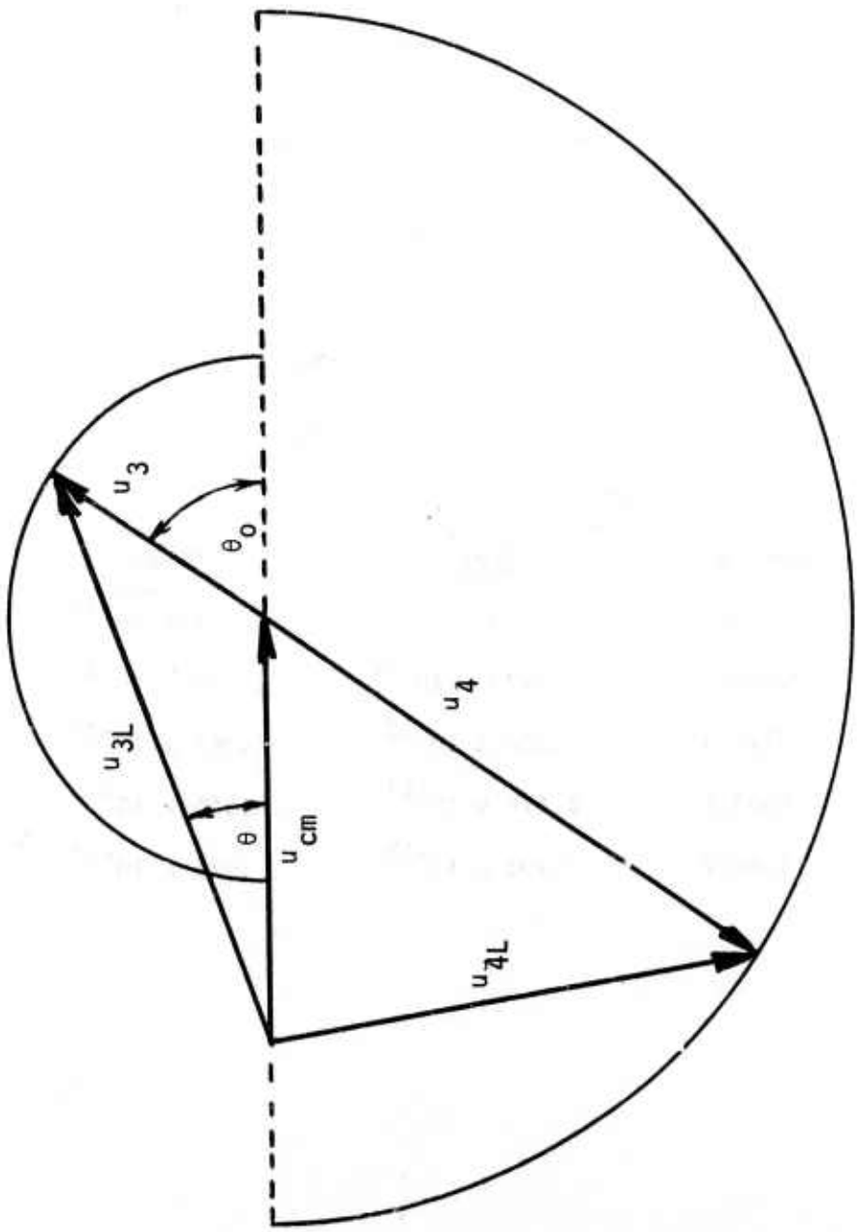

Figure A1. Vector diagram relating center-of-mass velocities to laboratory velocities.

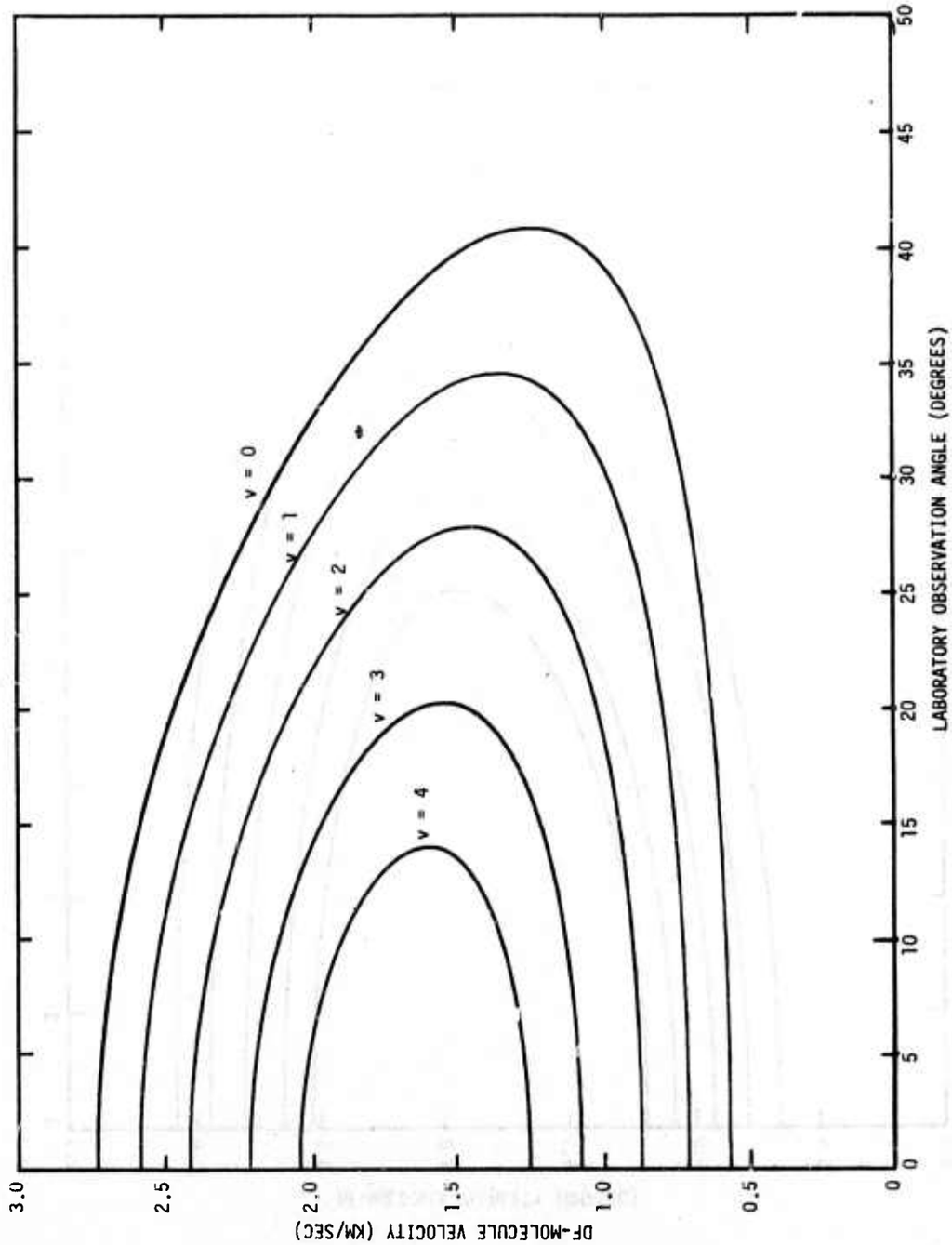

Figure A2. Laboratory velocity of the DF-molecule as a function of laboratory scattering angle for the reaction $F + D_2 \rightarrow DF + D$ at $u_F = 2$ km/sec.

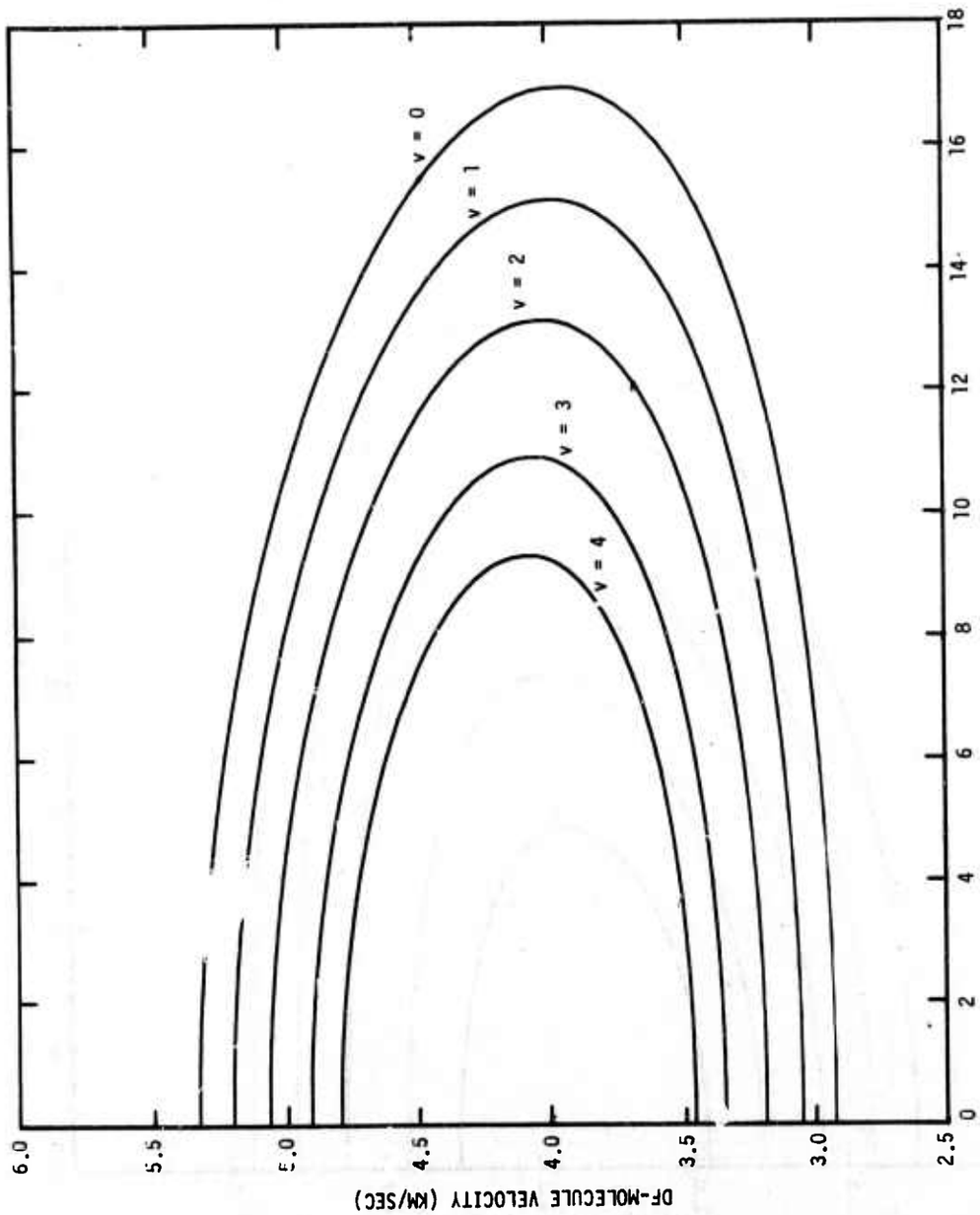

Figure A3. Laboratory velocity of the DF-molecule as a function of laboratory scattering angle for the reaction $F + D_2 \rightarrow DF + D$ at $u_F = 5$ km/sec.

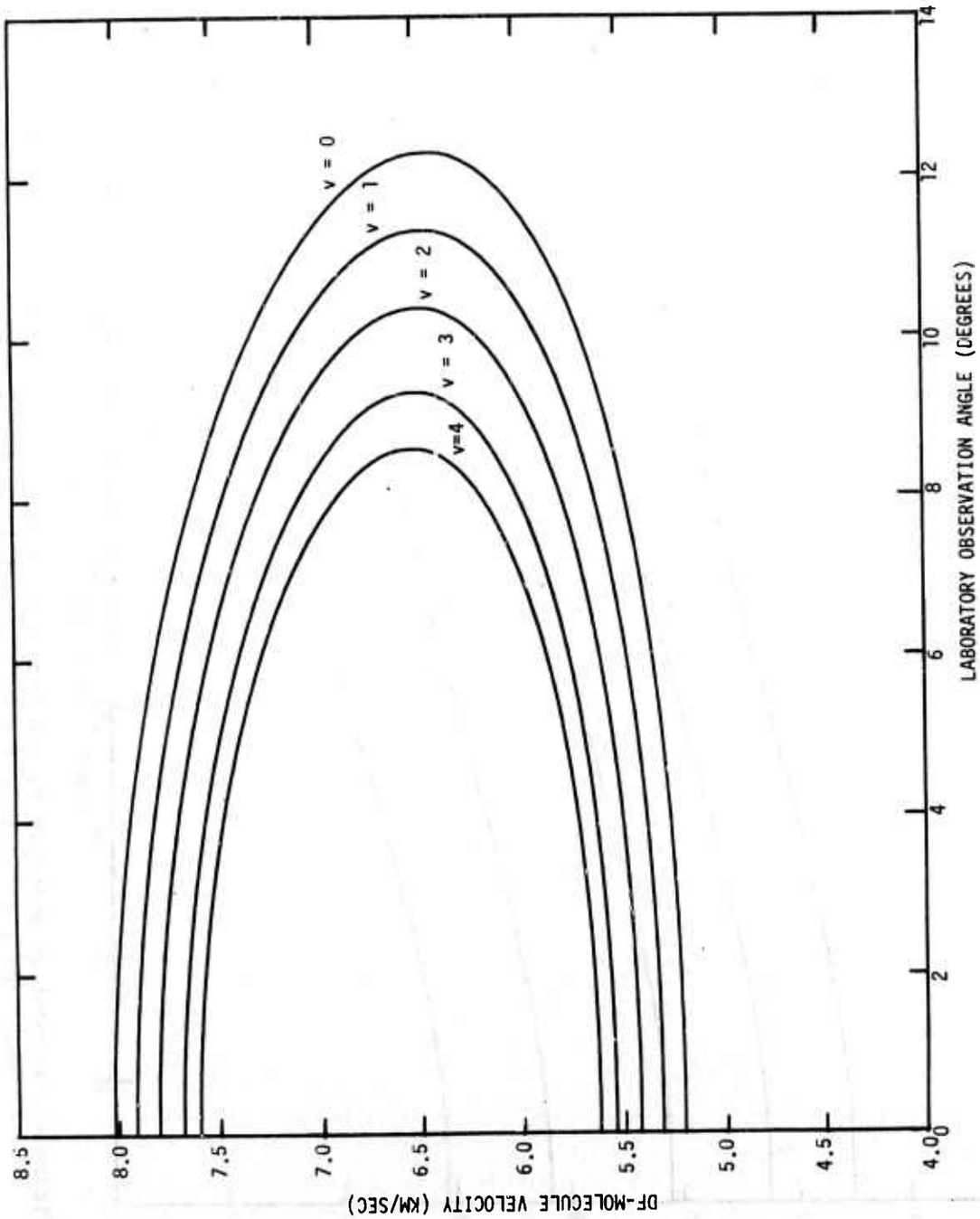

Figure A4. Laboratory velocity of the DF-molecule as a function of laboratory scattering angle for the reaction $F + D_2 \rightarrow DF + D$ at $u_F = 8$ km/sec.

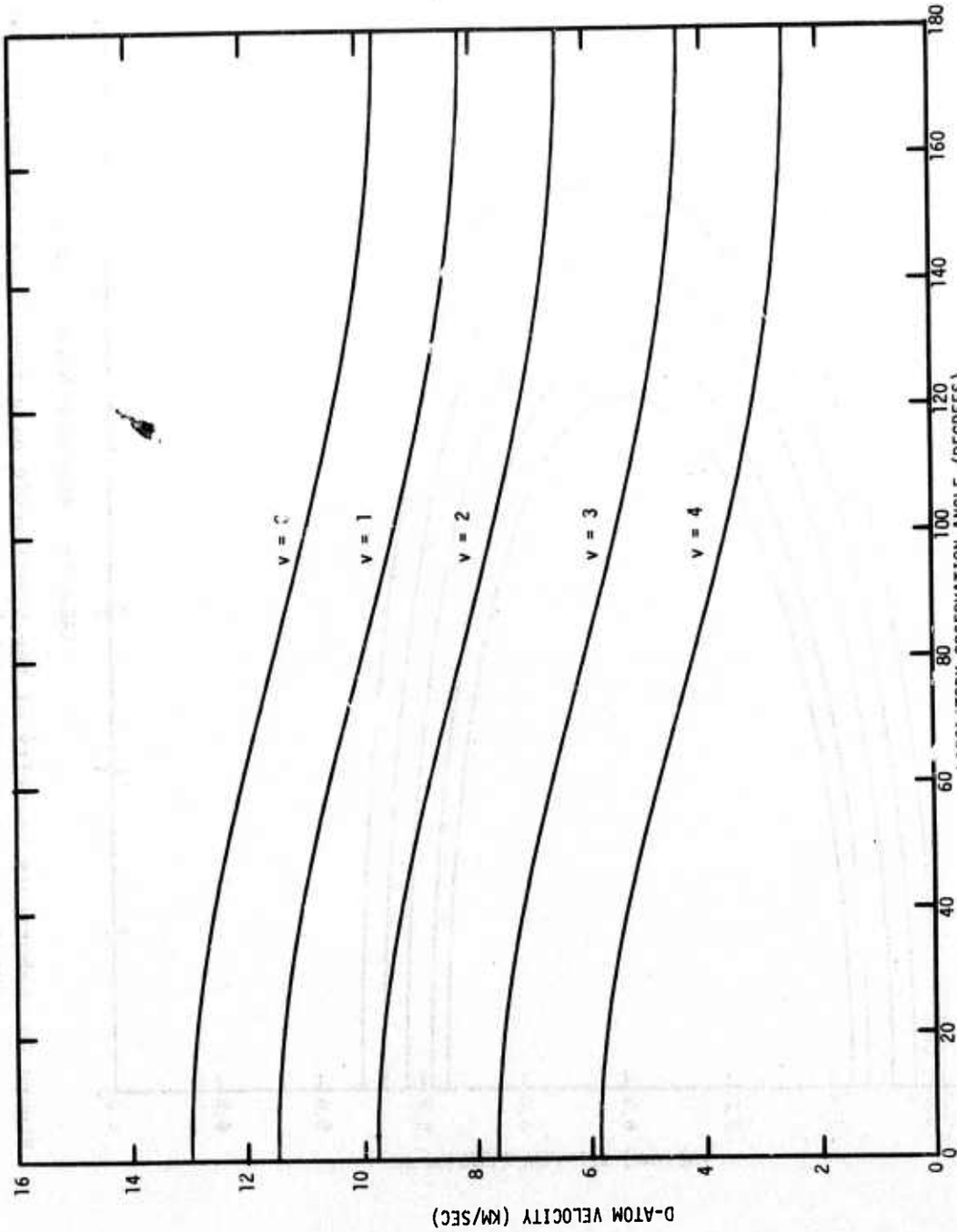

Figure A5. Laboratory velocity of the D-atom as a function of laboratory scattering angle for the reaction $F + D_2 \rightarrow DF + D$ at $v_F = 2$ km/sec.

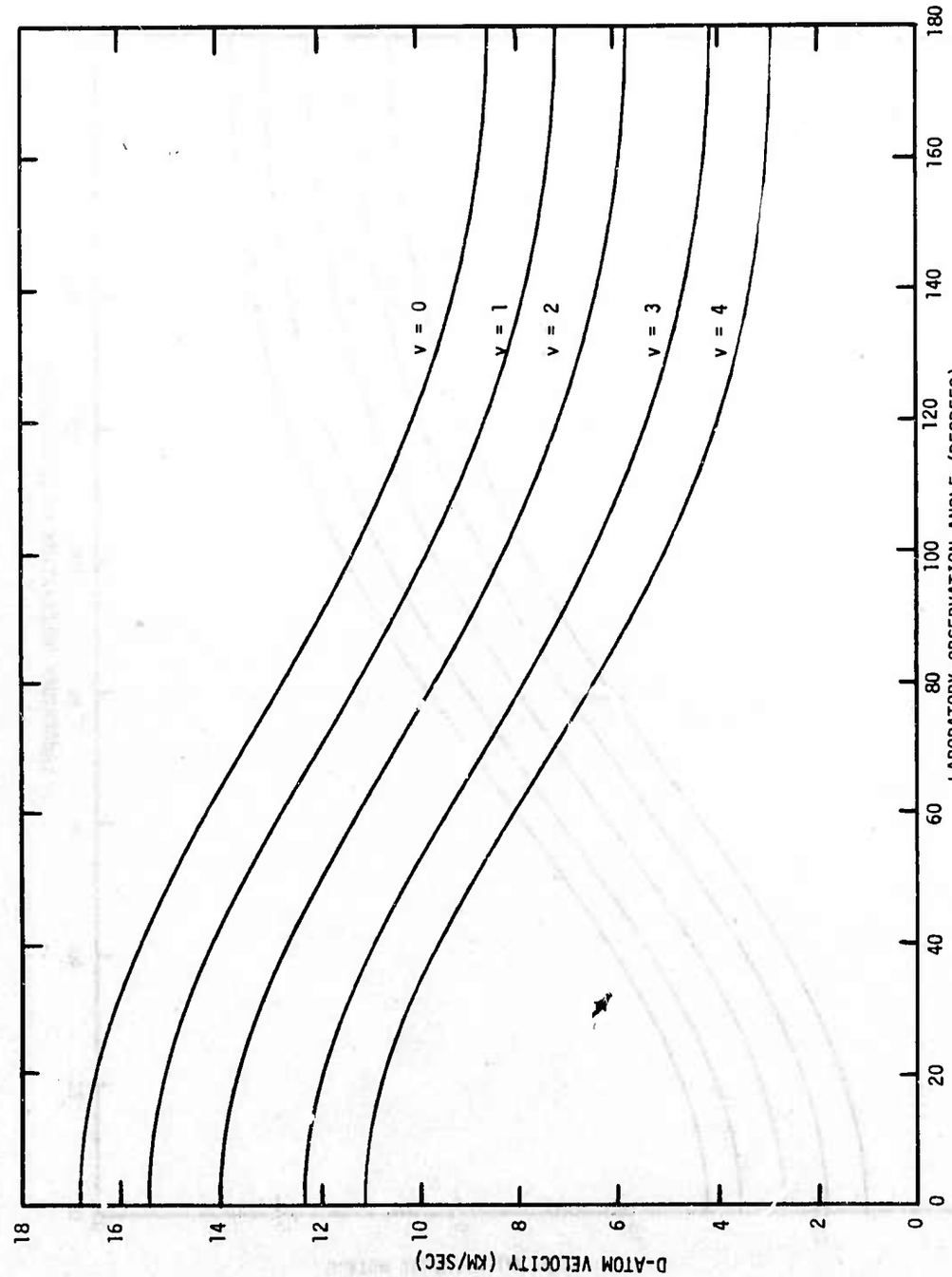

Figure A6. Laboratory velocity of the D-atom as a function of laboratory scattering angle for the reaction $F + D_2 \rightarrow DF + D$ at $u_F = 5$ km/sec.

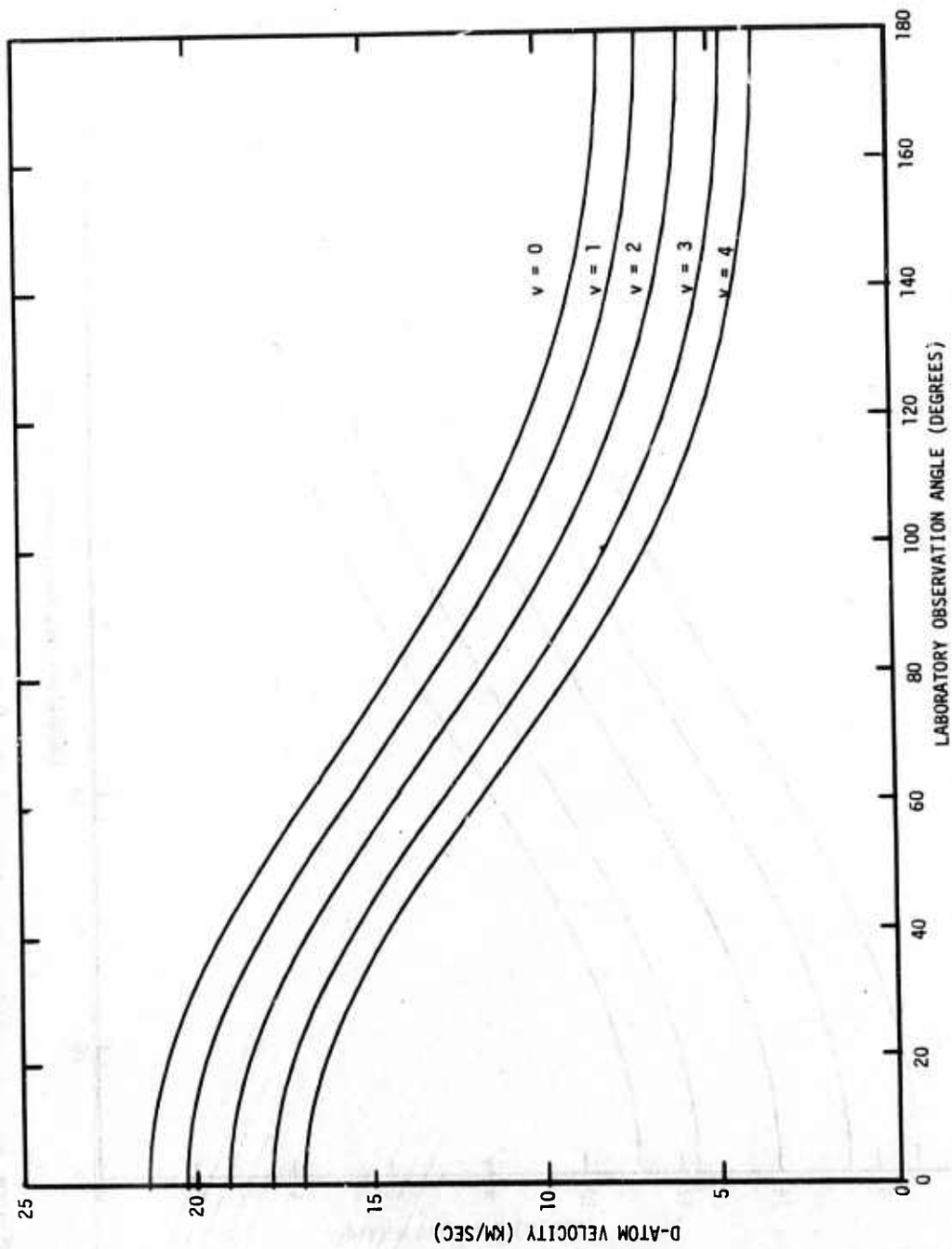

Figure A7. Laboratory velocity of the D-atom as a function of laboratory scattering angle for the reaction $F + D_2 \rightarrow DF + D$ at $u_F = 8$ km/sec.

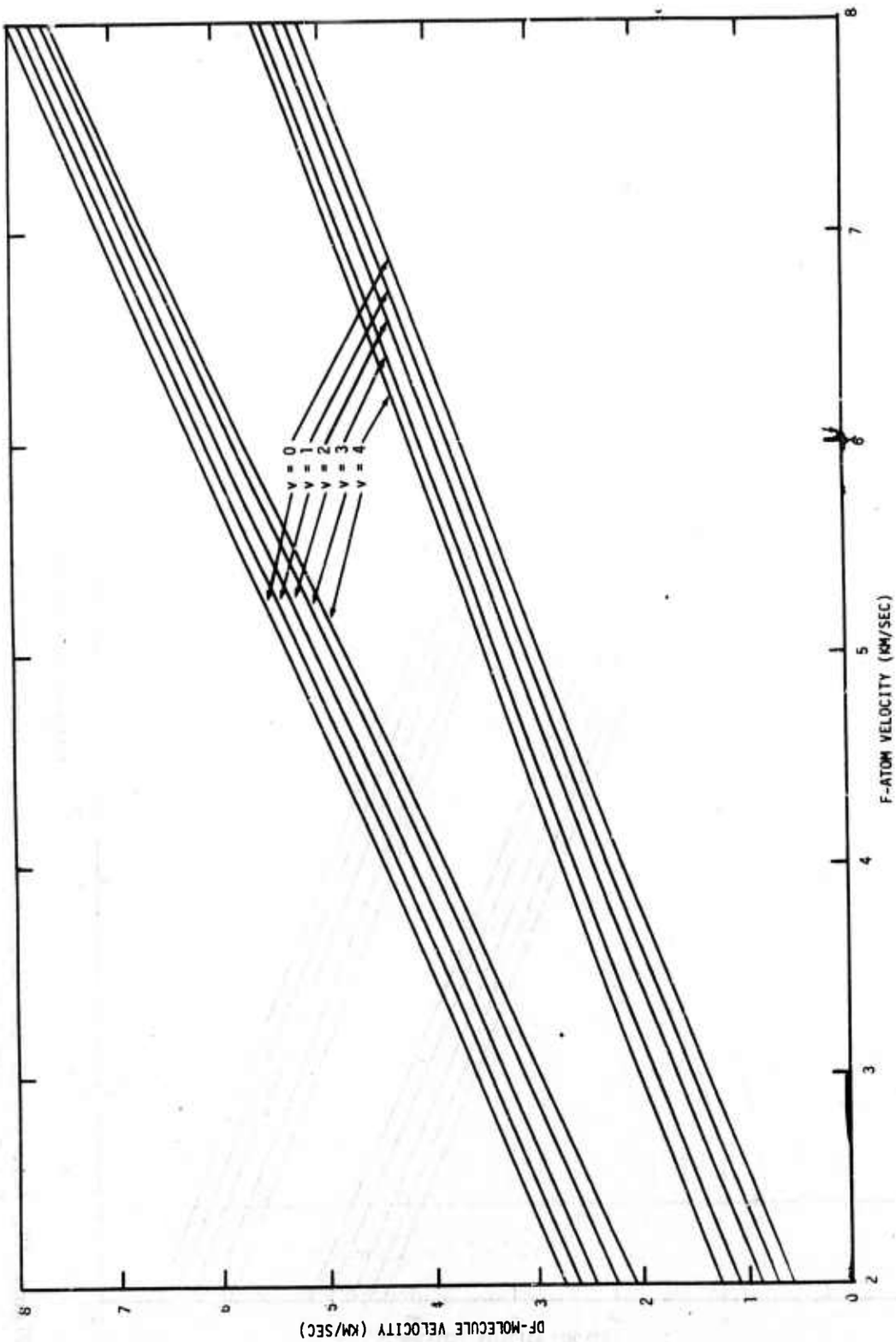

Figure A8. Velocity of the DF-molecule as a function of F-atom velocity at $\theta = 0°$ for the reaction $F + D_2 \rightarrow DF^* + D$..

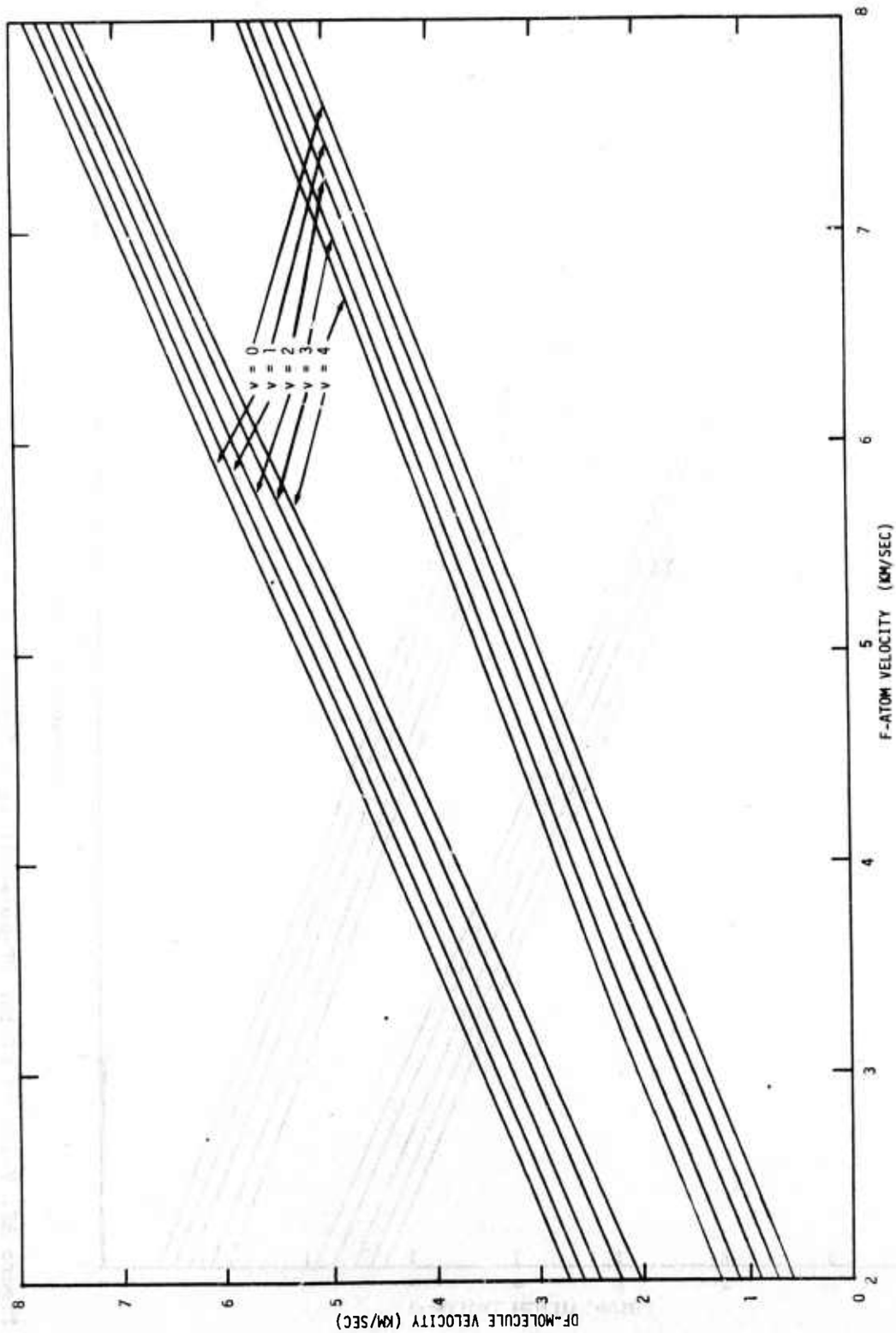

Figure A9. Velocity of the DF-molecule as a function of F-atom velocity at $\theta = 9°$ for the reaction $F + D_2 \rightarrow DF^* + D$.

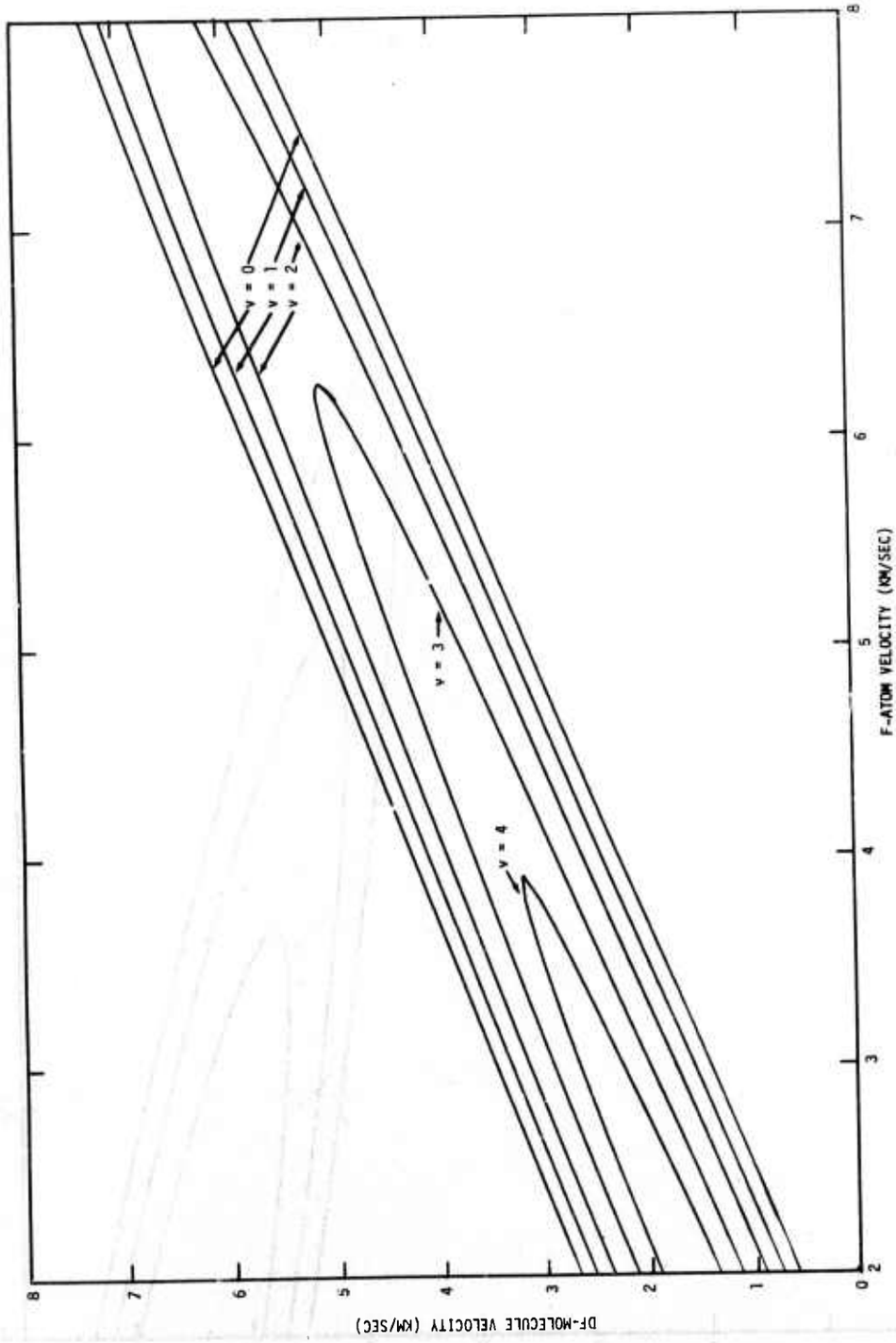

Figure A10. Velocity of the DF-molecule as a function of F-atom velocity at $\theta = 10^{\circ}$ for the reaction $F + D_2 \rightarrow DF^* + D$.

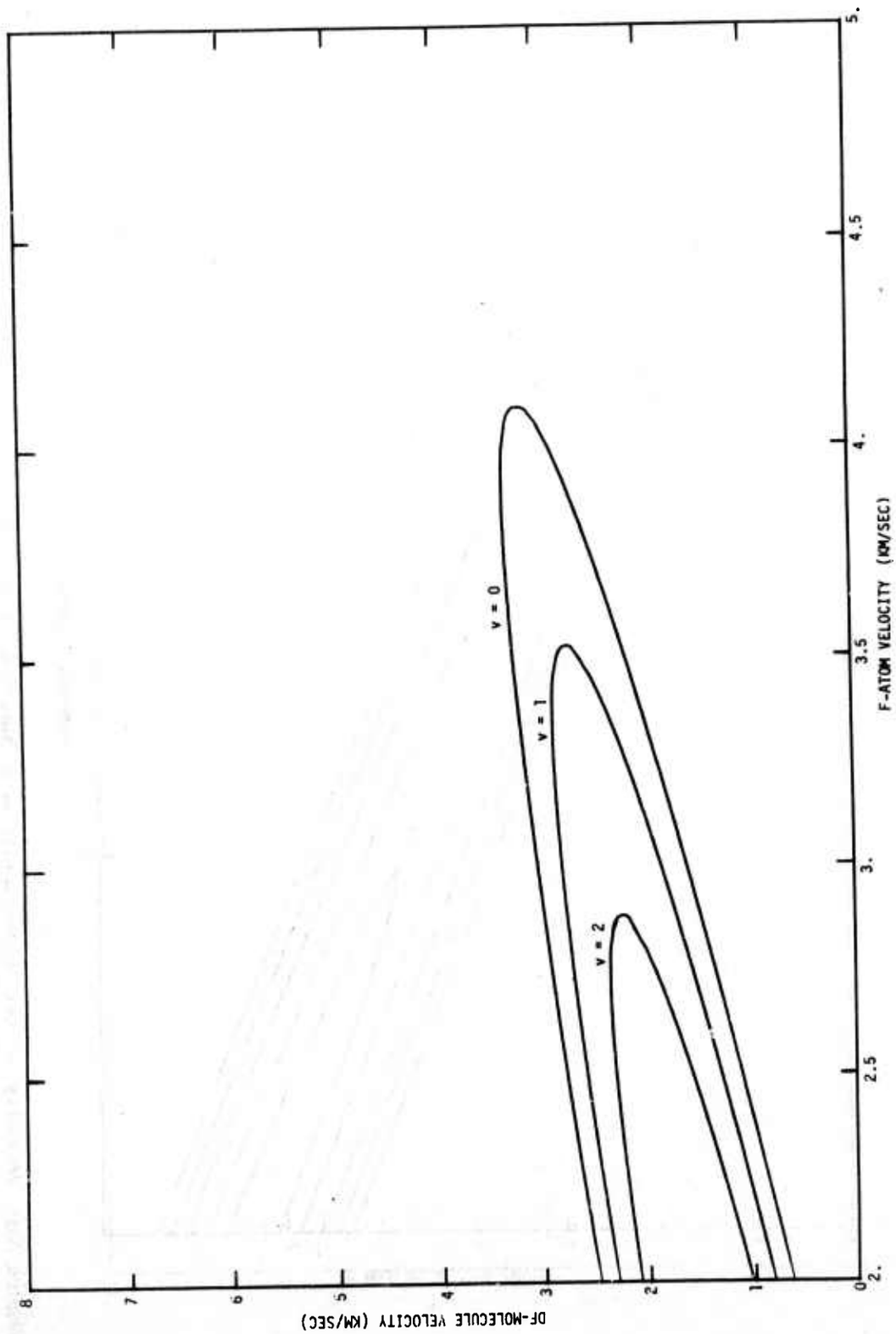

Figure All. Velocity of the DF-molecule as a function of F-atom velocity at $\theta = 20^{\circ}$ for the reaction $F + D_2 \rightarrow DF^* + D$.

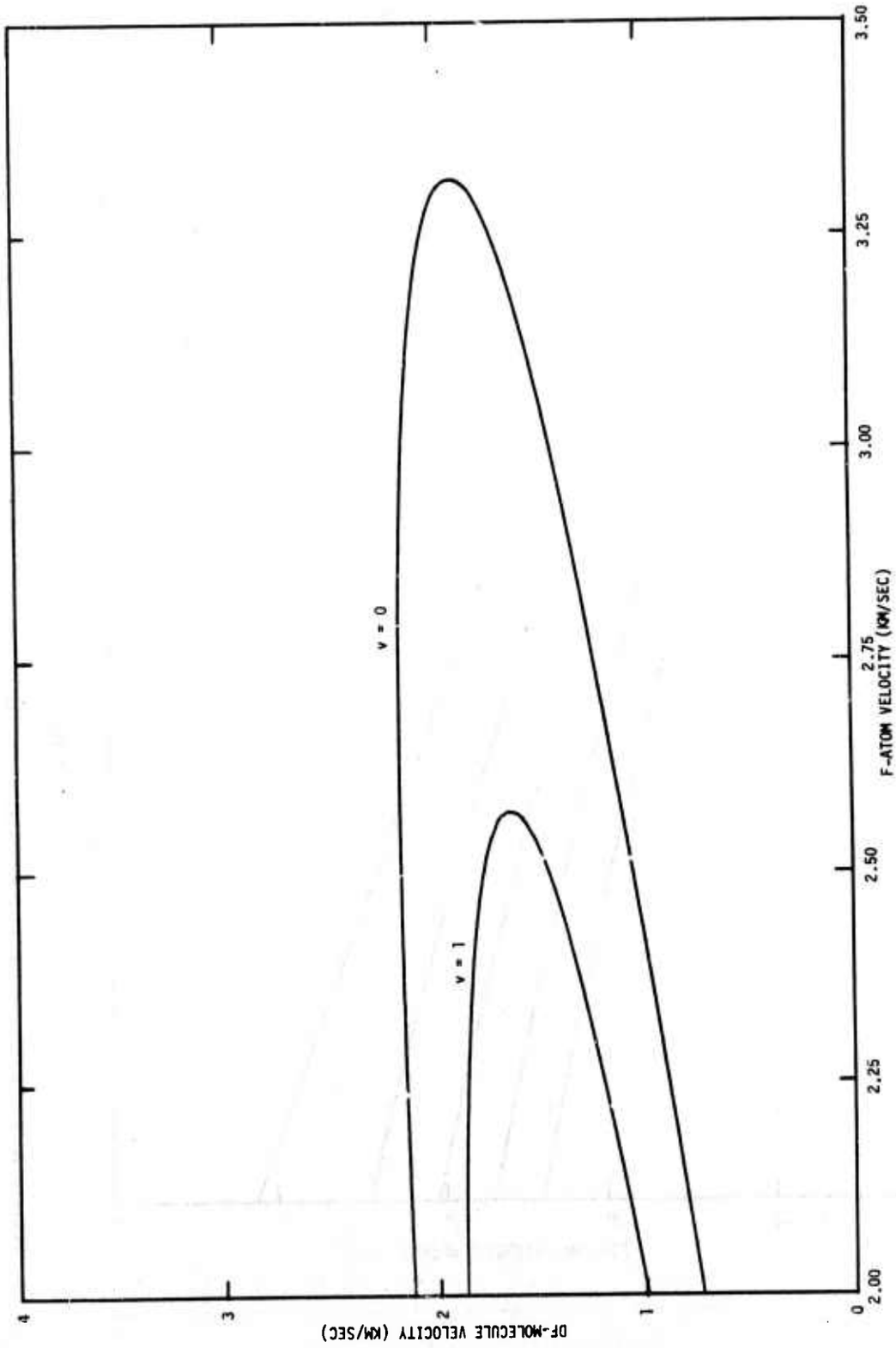

Figure A12. Velocity of the DF-molecule as a function of F-atom velocity at $\theta = 30°$ for the reaction $F + D_2 \rightarrow DF^* + D$.

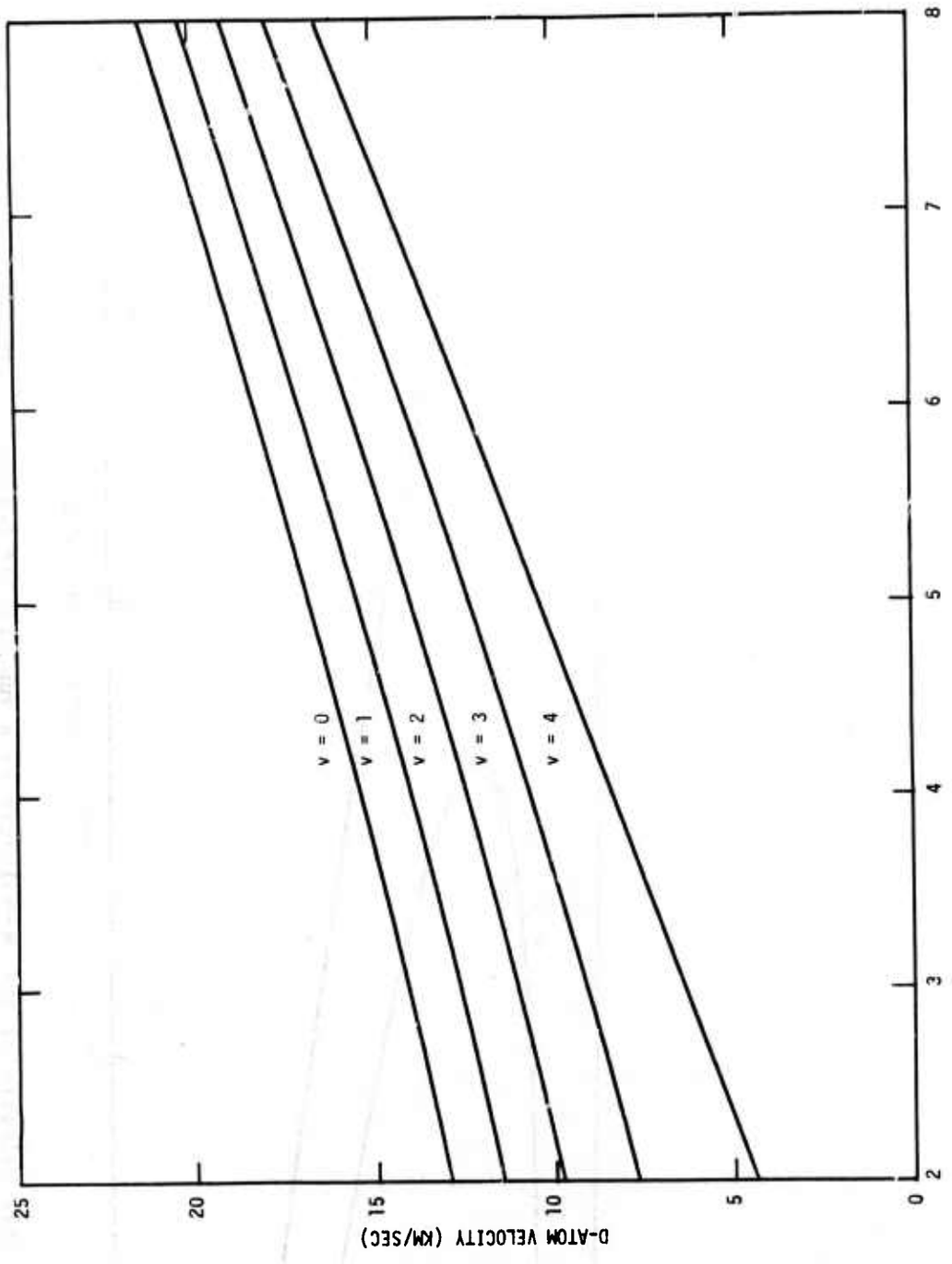

Figure A13. Velocity of the D-atom as a function of F-atom velocity at $\theta = 0°$ for the reaction $F + D_2 \rightarrow DF^* + D$.

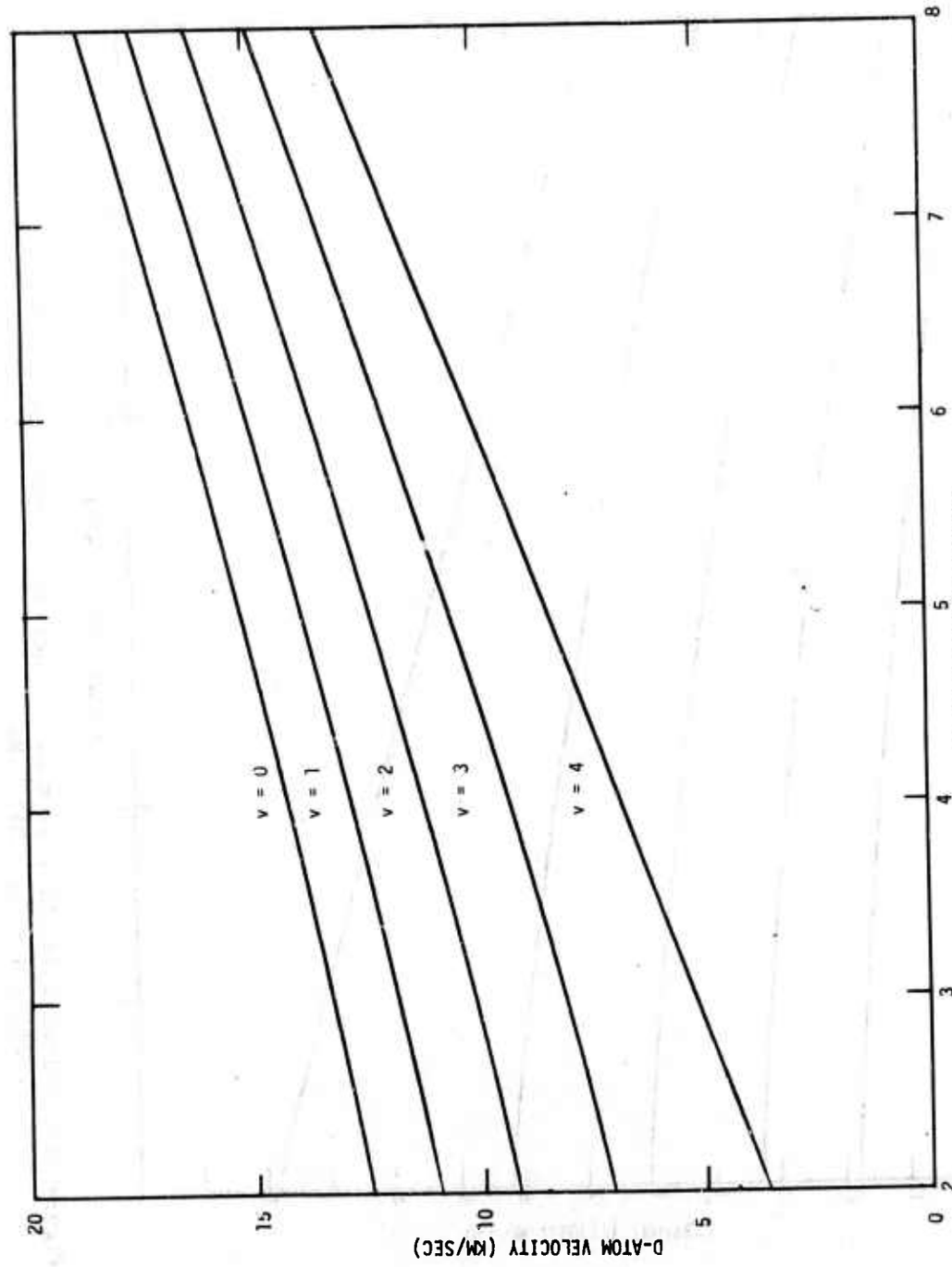

Figure A14. Velocity of the D-atom as a function of F-atom velocity at $\theta = 45°$ for the reaction $F + D_2 \rightarrow DF^* + D$.

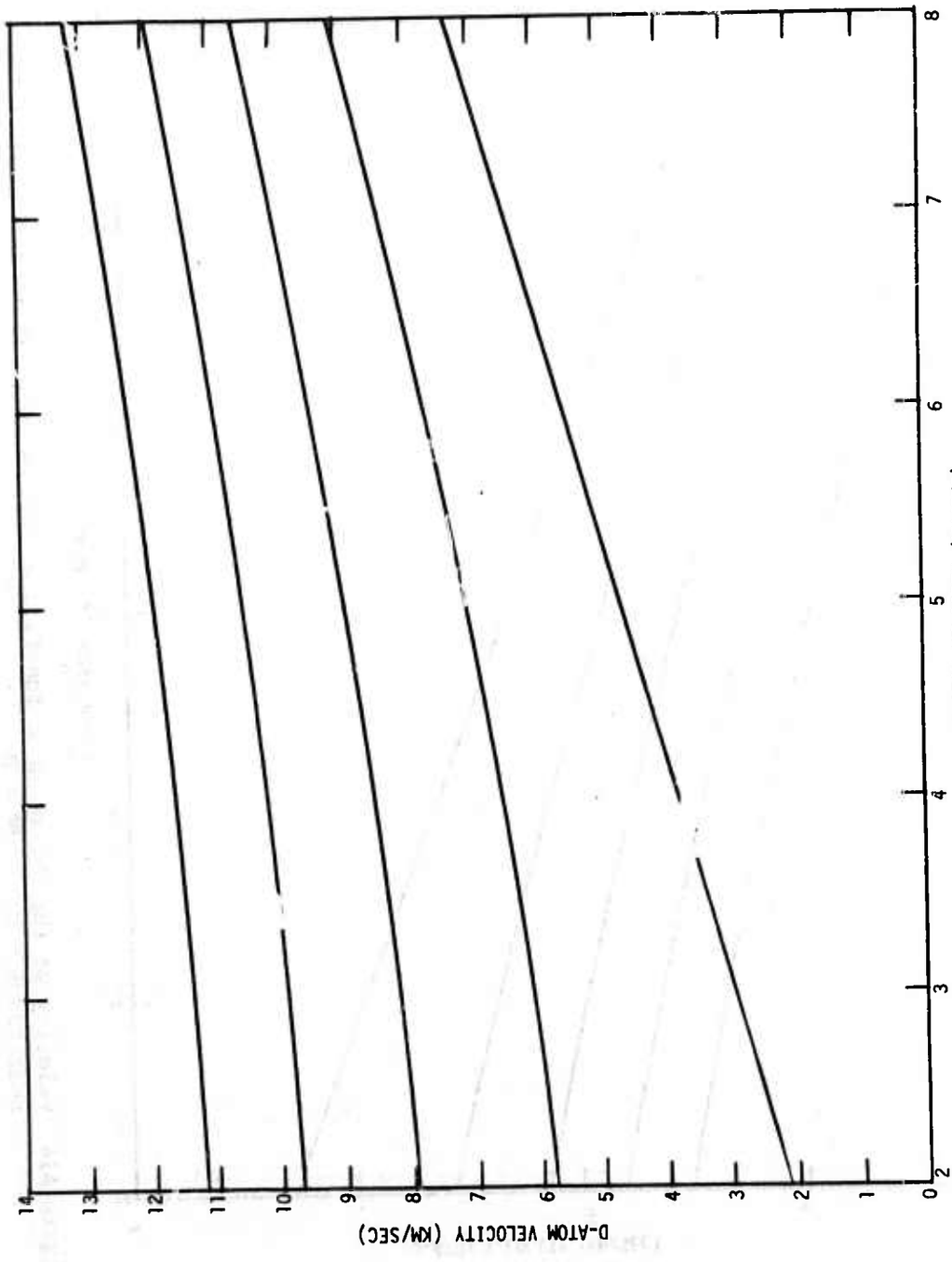

Figure A15. Velocity of the D-atom as a function of F-atom velocity at $\theta = 90°$ for the reaction $F + D_2 \rightarrow DF^* + D$.

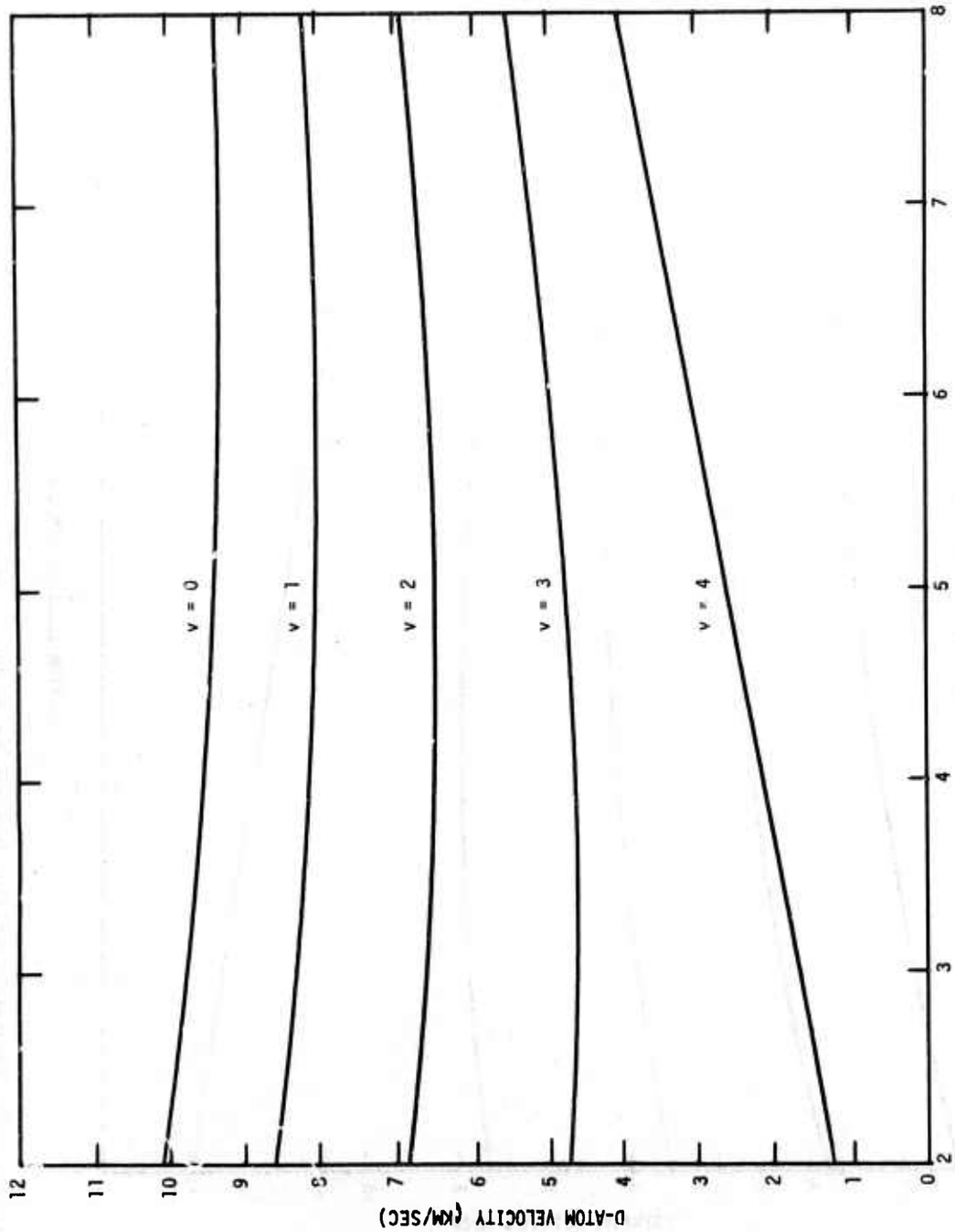

Figure A16. Velocity of the D-atom as a function of F-atom velocity at $\theta = 135°$ for the reaction $F + D_2 \rightarrow DF^* + D$.

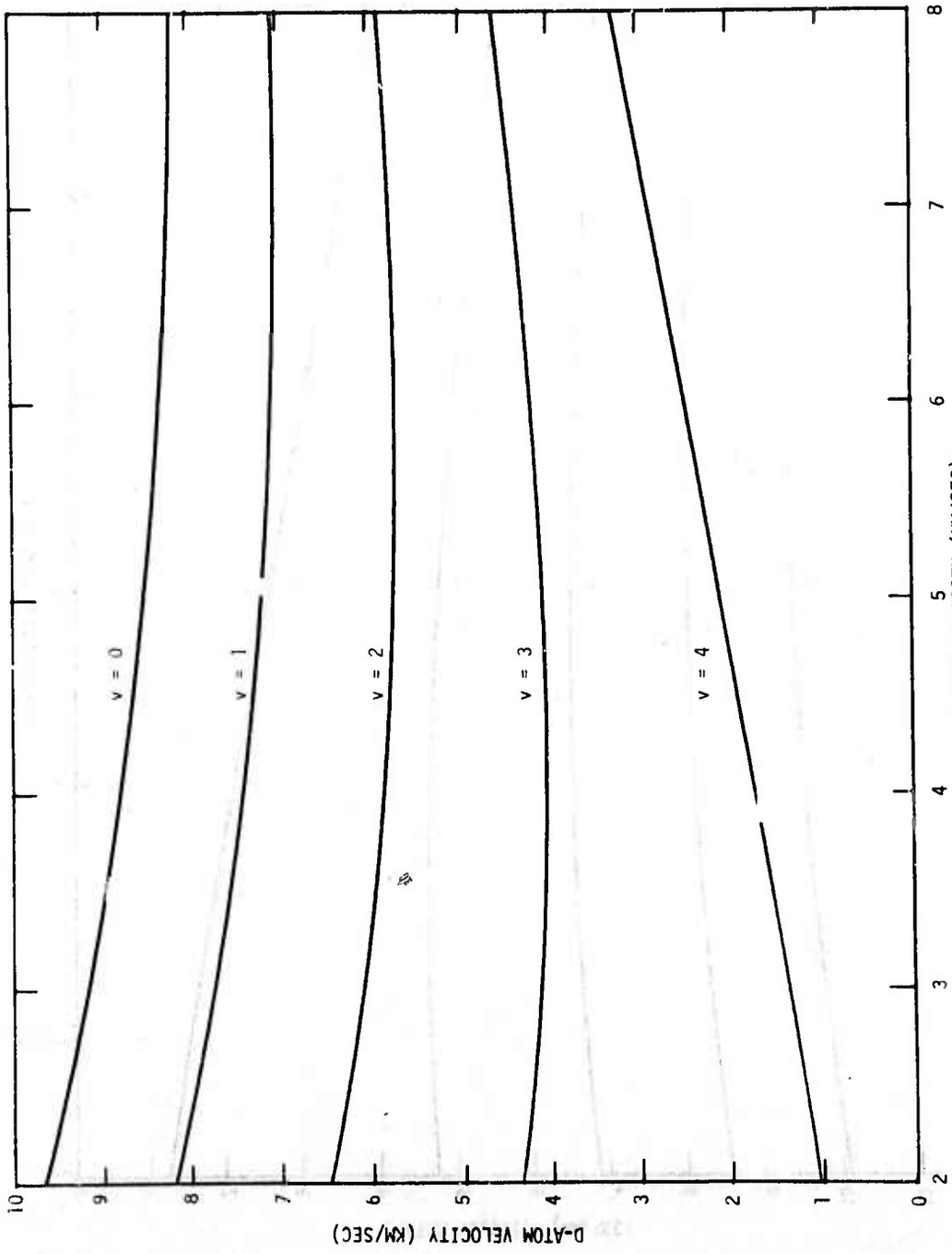

Figure A17. Velocity of the D-atom as a function of F-atom velocity at $\theta = 180°$ for the reaction $F + D_2 \rightarrow DF^* + D$.

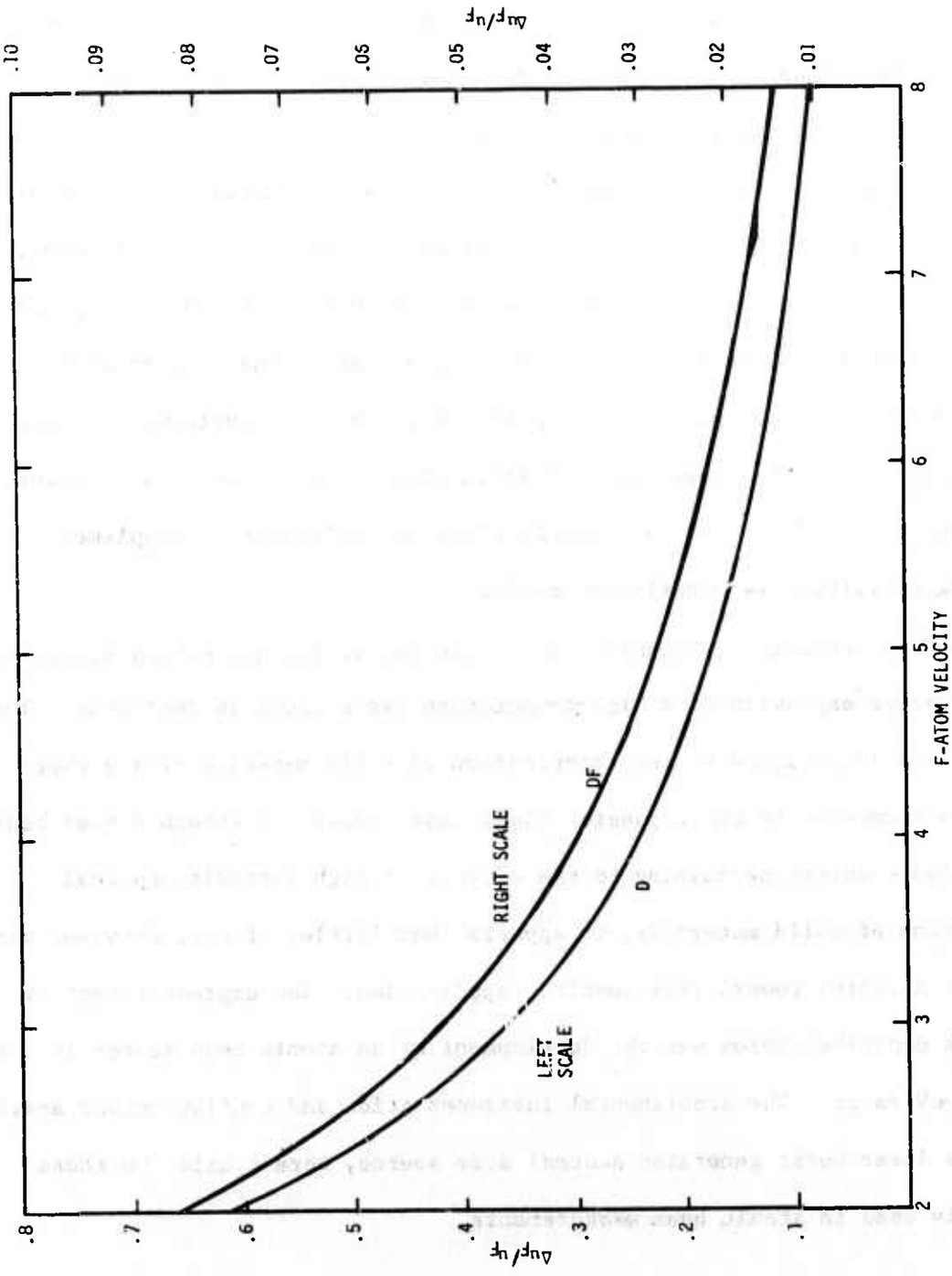

Figure A18. Maximum permissible velocity spread in the incident F-atom beam pulse as a function of u_F that results in velocity separation of DF-molecules in the v = 0 and v = 1 states and in velocity separation of D-atoms corresponding to the v = 0 and v = 1 states for $\theta = 0°$.

1.1 INTRODUCTION

Atomic and molecular beams have been widely used in recent years to study in detail the physics (and chemistry) of atomic collisions at low energies. A number of beam generation techniques have been developed for this purpose. Review articles on the subject of beam sources (e.g., see Anderson, Andres, and Fenn[1]) indicate that the achievable beam intensity tends to decline with decreasing beam energy leading to a situation of "intensity limited" experiments at low energies. Moreover, a gap exists in the 1 to 10-eV range where it is particularly difficult to obtain intense beams. The problem of intensity has been at least partially compensated for by the development of sophisticated atom detection apparatus and noise suppression techniques; however, a more intense source of moderate energy atoms and molecules to complement existing facilities is clearly desirable.

In this appendix, a technique for producing an intense pulsed atomic beam by the vacuum expansion of a high-temperature vapor cloud is described. The vapor cloud is produced by the vaporization of solid material with a short duration (compared to the expansion time) laser pulse. Although a vast body of knowledge exists pertaining to the effects of high-intensity optical irradiation of solid materials, it appears that little, if any, previous work has been directed toward this specific application. The express intent of the work described below was the development of an atomic beam source in the 1 to 10-eV range. The experimental instrumentation and configuration, apart from the laser burst generated neutral atom source, were similar to those routinely used in atomic beam measurements.

2.2 EXPERIMENTAL APPARATUS AND PROCEDURES

2.2.1 Apparatus

The experimental arrangement is shown schematically in Figure B1. The Q-switched ruby laser was capable of delivering up to 3 joules per pulse in about 75 nsec. However, the rod was of relatively poor quality and the beam exhibited considerable divergence. To limit the divergence the beam was collimated to 0.475 cm diameter by an aperture external to the laser cavity. Collimation limited the energy to about 1/2 joule per pulse. The collimated beam was brought through a quartz window in the vacuum wall and focused on the target by a 125-mm focal length lens. The lens-to-target distance was externally adjustable permitting the intensity of the laser light at the target surface to be varied at will. In specifying the energy density at the target surface, both the lens and laser beam were assumed to be perfect. This leads to an expression for the energy density at the target as a function of target-to-lens distance ℓ given by $\Sigma(\ell) = \Sigma_o [f/(f - \ell)]^2$ where f is the lens focal length, and Σ_o is the energy density at the lens.

Laser targets were clamped on the end of a vertically mounted rod located such that the laser beam axis and an axis defined by the center line of the downstream instrumentation intersected at the target surface. The rod extended through the vacuum wall and could be translated in the vertical direction and rotated about the vertical axis. In the arrangement shown, the target surface was inclined at a nominal 45° to the laser beam axis. Alternatively, the laser beam was directed down the axis of the downstream instrumentation as shown by the dashed lines in Figure B1. In this case, the target surface was

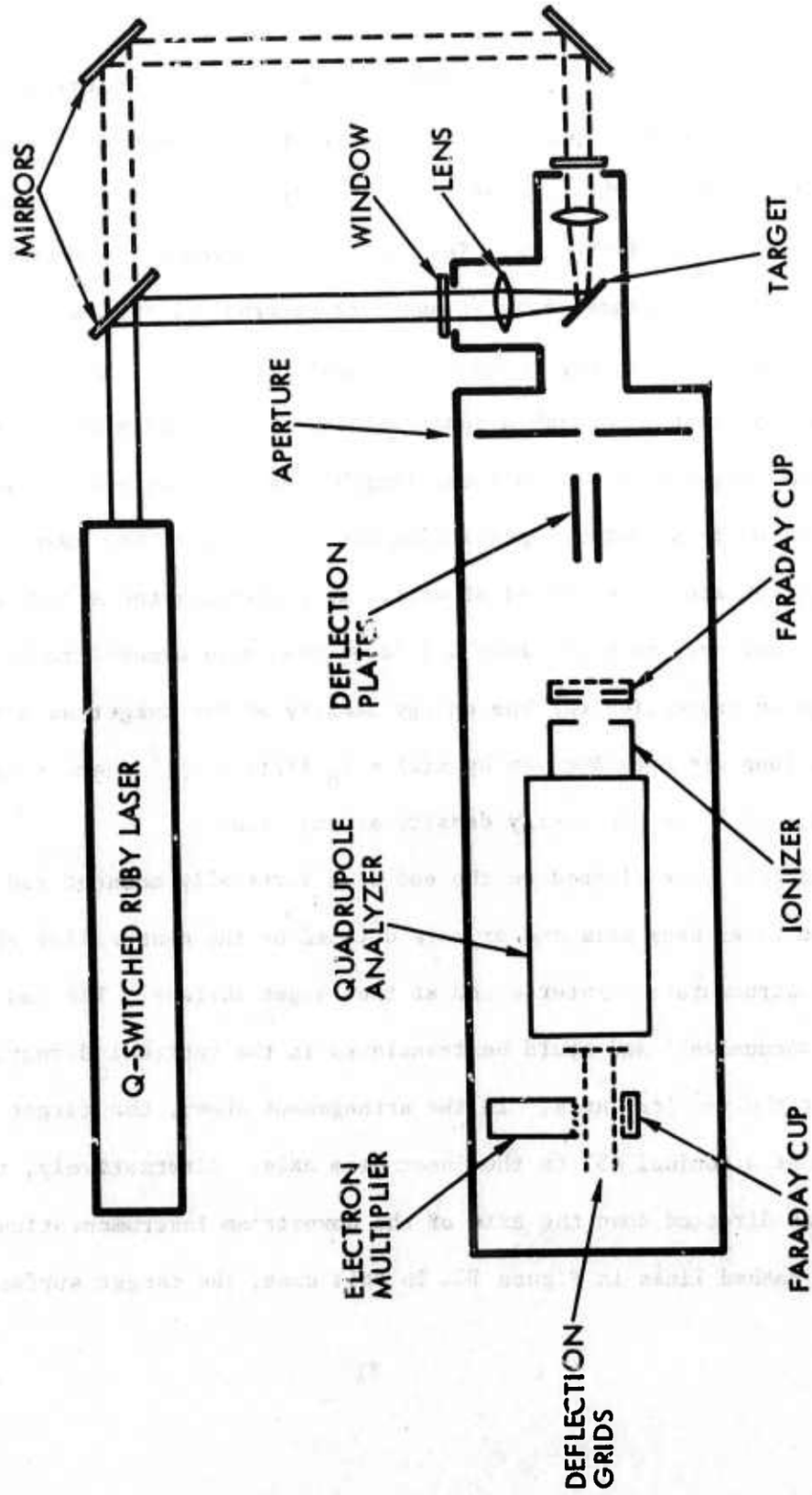

Figure B1. Schematic of the Experimental Configuration.

set perpendicular to the laser beam.

A collimating aperture located downstream from the laser target limited the expanding vapor to the axial region of the diagnostic apparatus. This was followed by a pair of electrostatic deflection plates for sweeping ions and electrons from the vapor cloud. An annular Faraday cup located at the entrance of the ionizer was used to confirm the removal of ions from the burst.

The remaining neutral fraction of the vapor cloud was analyzed and detected by means of an assembly consisting of an electron impact ionizer, an RF quadrupole mass filter, and an electron multiplier ion detector. The ionizer and quadrupole were commercial units obtained from Extranuclear Laboratories, Inc. (Ionizer - high efficiency Type II, Quadrupole - Model No. 324-9 used with either the Extranuclear C or E high-Q head). The ion detector was an EMI 11-stage venitian blind electron multiplier tube (EMT) with beryllium-copper dynodes. The tube had an active area about 2.5 cm square. It was normally operated with anode at ground potential and dynode No. 1 at -2 kV. In order to obtain a measure of the EMT detection efficiency, an arrangement whereby ions from the quadrupole analyzer (QPA) could be deflected by means of electrically biased planar grids either to the EMT or to a Faraday cup on the opposite side of the atomic beam axis was used. In order to make the "footprint" of the ion beam small compared to the active area of the EMT, ions from the QPA were accelerated an additional several hundred volts by means of a biased grid mounted perpendicular to the QPA axis before entering the deflection region.

The experimental volume was evacuated by a 6-inch oil diffusion pump equipped with a water-cooled baffle. The system included a liquid nitrogen

cold trap, but it was not used routinely. Ambient pressure in the untrapped system would reach 3×10^{-7} Torr after extended pumping. Normally, however, the experiments were run with a background pressure of about 10^{-6} Torr.

2.2.2 Experimental Procedures

The first step in a data acquisition cycle was calibration and optimization of the mass spectrometer response using the background gas as a source. The resolution was adjusted to about one amu (i.e., adjacent peaks in the background gas spectrum were completely separated) in the mass range of interest by operating the QPA in the sweep mode and observing the spectrum on an oscilloscope. The ionizer was operated with the ionizing region at 50 volts positive with respect to ground to minimize QPA transmission differences between the thermal energy background molecules and the high-energy atoms from the burst.

Data were recorded by photographing the display on a Tektronix 555 dual-beam oscilloscope. The output signal from either the EMT or the downstream Faraday cup was displayed on one of the traces while the signal from the upstream Faraday cup or the signal from a photo diode used to monitor the pulse was displayed on the other. It was found that the laser pulse was quite reproducible and it was monitored only occasionally. A delaying circuit keyed by the manual switch used to dump the laser capacitor bank generated a trigger pulse to start the oscilloscope sweep a few tens of microseconds before the Q-switched pulse occured. In some cases the Q-switch pulse was added to one of the oscilloscope traces to provide a zero time marker, but more often than not, a small concurrent noise pulse served the same purpose.

Whenever any significant changes were made in the experimental set up, a series of tests were undertaken to ensure that the observed signal from the mass spectrometer was, in fact, due to the detection of neutral atoms generated by laser bombardment. These included varying the ionizer emission current, the quadrupole mass setting, bias voltage on the ion deflection plates, etc.

3.3 EXPERIMENTAL RESULTS

Some of the significant findings of this set of experiments are best described as qualitative in nature. Moreover, even the quantitative results given below were obtained within a limited range of experimental parameters. Thus, the results by no means represent an optimization of the technique, but are simply illustrative of what was obtained for the stated conditions.

3.3.1 Qualitative Observations

It was found that important factors in the generation of a neutral atom pulse are the target geometry and form. It was originally assumed that a neutral beam could be produced by irradiating a solid block of material. It was recognized that, in order to impart high velocity to the expanding vapor cloud, it would be necessary to creat a high temperature gas with a correspondingly high degree of ionization. However, it was argued that the ions and electrons could be stripped from the cloud leaving only the neutral fraction. For some materials this proved to be the case, but for low ionization potential materials (e.g., aluminum) the cloud was almost completely ionized. Qualitatively, it appeared that the irradiation of a solid block of material resulted in raising the temperature of a thin layer of material to

very high temperatures. Supplementary experiments on the characteristics of the ion burst (to be reported separately) indicated that the laser irradiation produced a hot plasma with an initial Maxwellian distribution of velocities. Ion temperatures in the 30 to 50 eV-range were observed routinely.

The fact that only a relatively small amount of material was involved was confirmed by the use of thin film targets. It was found that repeated shots were required to penetrate a thin film even though the energy per pulse was more than adequate to completely evaporate all of the material in the laser beam spot. It appears that evaporation at the surface begins almost immediately and a vapor cloud forms in front of the target surface. The observations are consistent with a model that invokes efficient absorbtion of laser light by the vapor cloud, but inefficient transmission of energy across the vapor-solid interface, leading to the aforementioned high-temperature plasma.

This interpretation led to the use of thin targets bonded to optically transparent substrates. The laser beam was directed through the supporting glass and focused on the "rear" side of the film (i.e., the side in contact with the substrate). In this arrangement, the hot plasma produced by laser irradiation is physically constrained from expanding and heat is more efficiently conducted from the plasma to the remaining solid material. As material is ingested into the confined gas cloud, the temperature drops. This process continues until the solid barrier is breached, releasing the gas cloud. There is some evidence that the film may rupture (the film at the edge of the hole is often lifted from the substrate) but the net result is the same: a "moderate" temperature gas involving almost all of the film material in the laser beam is released and expands into the vacuum.

The advantage of the thin film target configuration was shown by tests on uranium targets using the geometry shown in Figure B1. Consecutive tests were run on a solid uranium target and thin (nominally one micron) uranium films vapor deposited on glass microscope slides. The thin film was bombarded from both the front (free surface) and rear (metal-glass interface) sides. It was found that the maximum neutral atom flux obtained with the rear film bombardment geometry exceeded that of the solid target by about a factor of ten and that of the front film bombardment by about a factor of four. The rear film geometry had the added virtue that noise (due principally to ion leakage and photoelectrons produced by scattered laser light) was drastically reduced. Similar tests on thin aluminum films versus thick targets were even more dramatic in the sense that the neutral atom signal could not even be extracted from the noise when a solid target was used. The use of thin aluminum films gave results comparable to those obtained with uranium.

Another qualitative observation is that the neutral atom flux had directional characteristics. For the geometry shown in Figure B1, the target surface is inclined at a nominal 45° to both the laser beam axis and the axis defined by the atom detection apparatus. Changing the angle by as little as 5° caused detectable differences in the atom flux. The flux obtained in the arrangement where the thin film target was placed perpendicular to both axes (i.e., the laser beam was pointed down the axis of the mass spectrometer) was greater than that in the 45° geometry by a factor of between two and five.

The intensity of the atom pulse also depends upon target material and structure. Vapor deposited metal films generally gave clean, reproducible results. A series of tests on fluorine-rich compounds gave less consistent

results. The compound targets were prepared by dusting powders (5 to 10 micron average particle size) on a thin layer of uncured epoxy resin painted on a glass slide. Excess powder was brushed off. The best results were obtained when particles covered about one-half of the surface. Some of the substances used were BiF_3, CrF_3, LiF, HgF_2, Hg_2F_2, and Teflon (in sheet form). Some of these substances were apparently susceptible to water vapor absorption as they changed color with exposure to air. (The presence of a large HF pulse observed with some of these substances was attributed to water vapor contamination). The best results were obtained with BiF_3, a white powder.

The results obtained with Teflon indicate that the laser bombardment technique may be used for the production of certain kinds of molecular beams. It was found that a CF molecule flux comparable in magnitude to the most intense atom pulses was obtained with the Teflon targets. Teflon was peculiar in the sense that it did not give rise to high intensity ion pulses when used in solid form.

3.3.2 Quantitative Results

The signal from the EMT gives a measure of the ion current from the electron impact ionizer as a function of time referenced from the laser burst. The transit time from target to ionizer specifies the neutral atom velocity. The electrical potentials in the ionizer, QPA, and detection region are known; hence it is a straightforward matter to determine the ion current as a function of the energy of the neutral atoms. Typical results are shown in Figure B2 for aluminum, uranium, and fluorine atom bursts. For the cases illustrated, the target to ionizer distance was 60 cm. The uranium and aluminum targets were

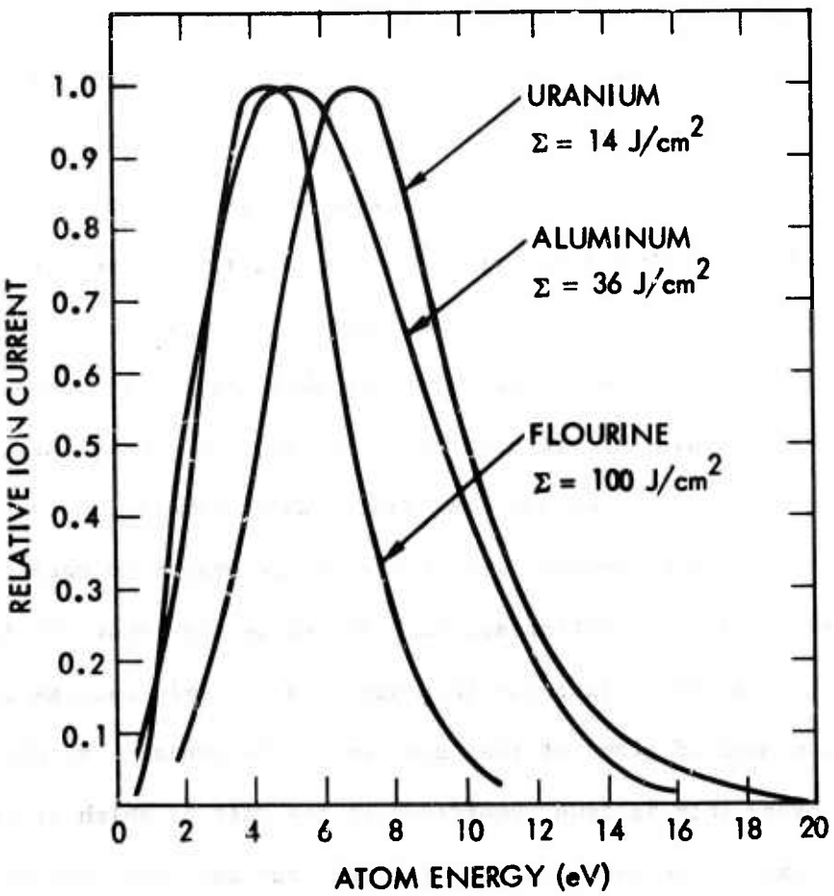

Figure B2. Relative ion current as a function of atom energy for aluminum, uranium, and fluorine bursts. The total energy in the laser pulse was fixed at ∿0.4 joules in all cases. The energy density at the target is specified for each of the materials.

both 1-micron thick films vapor deposited on microscope slides. The laser beam was incident on the rear side of the film (i.e., through the glass) in the 45° geometry. The fluorine beam pulse was obtained from the irradiation of a thin film of BiF_3 made by the method described above. For the case shown, the BiF_3 target was bombarded on the rear side with the laser beam axis coincident with the axis of the diagnostic equipment. Presumably, the fluorine burst contained bismuth atoms, but no attempt was made to detect them. Their presence would not affect the fluorine atom measurements because of the selectivity of the QPA.

Since the conversion from ion current to absolute flux is non-trivial (particularly for the U atoms), only relative currents are shown in Figure B2. The principal point to these curves is that they show the energy range over which easily detectable signals are obtained under typical conditions.

The absolute value of the energy dependent flux of fluorine atoms has been estimated by using the residual gas in the vacuum system to obtain a crude calibration of the overall detection system. It can be seen that the instantaneous ion current from the ionizer due to a particular atomic species is proportional to the number of atoms of that species in the ionizing volume at that time. To first order this is true regardless of the rate at which atoms enter and leave the volume. Examination of the residual gas spectrum indicated that roughly one-half of the total ion current was due to H_2O in the untrapped system. To the extent that the ionization and detection efficiencies for all of the residual gases are the same, the relative ion current gives the partial pressure of the several background gases. To show that this assumption is not grossly in error, the cold trap was filled which resulted in a total pressure drop of about one-third (as indicated by an ionization gauge) and a reduction

in the H_2O ion current of about 50%. This observation is consistent with an upper limit to the partial pressure of H_2O of two-thirds of the total. As an additional test, the system pressure was increased by a factor of ten with neon. To a good approximation the ratio of neon ion current to H_2O ion current was twenty indicating that the detection efficiencies for neon and H_2O are comparable. It is not unreasonable to expect that the detection efficiency for fluorine atoms would be comparable also.

These tests gave a calibration factor of 1.9 amperes/Torr for residual H_2O. Under identical conditions of resolution, ionizer emission current, etc. the fluorine atom signal shown in Figure B2 was recorded. Using the unmodified H_2O calibration factor, the maximum current of 6×10^{-6} amperes corresponds to a partial pressure of about 3×10^{-6} Torr and a number density $n_F = 10^{11}$ F atoms/cm^3. Since the mean free path is several meters at this pressure, the fluorine beam is clearly collisionless.

These values represent lower limits because the ionizing volume accessible to ambient H_2O molecules was about five times greater than the volume to which flowing F atoms were restricted due to a collimating aperture at the entrance to the ionizer. It is not likely that the ionizing efficiency is uniform throughout the physical volume of the ionizing region; hence, the correction factor should not be as large as the ratio of volumes. In the presentation of results that follows, the apparent number density has been rather arbitrarily multiplied by a factor of two. This represents a best guess at the true value. Considering the crudity of the overall calibration procedure, the uncertainty in absolute values could easily be as much as a factor of five.

Given n_F as a function of E from the procedure outlined above, the flux of F atoms for any value of E is given by $J = n_F v$ atoms/cm^2/sec where $v = \sqrt{2E/m}$. This representation of the results is shown in Figure B3. Note that the flux is given in absolute terms as observed at a distance of 60 cm from the laser target.

Another representation of the results gives the energy spectrum of the expanding vapor cloud. This is derived as follows: the number of atoms dN passing through a plane of unit area at a distance x from the source in a time interval dt is given by $dN = Jdt$. But

$$t = \frac{x}{v} = \frac{x}{\sqrt{2E/m}} \tag{1}$$

It follows that

$$dt = -\frac{1}{2}\sqrt{mx^2/2E^3}\, dE \tag{2}$$

Eliminating dt gives

$$\frac{dN}{dE} = -\frac{J}{2}\sqrt{mx^2/2E^3} \tag{3}$$

By making the appropriate substitutions, this simplifies to

$$F(E) = \left|\frac{dN}{dE}\right| = \frac{n_F x}{2E} \quad \text{atoms/cm}^2\text{/eV} \tag{4}$$

Plotting this quantity as a function of E gives the result shown in Figure B4. for the same fluorine burst shown in Figures B2 and B3. The magnitude is for an aperture of 1 cm^2 at a distance of 60 cm from the source. The number of atoms per laser burst contained in a given energy band can be determined by the use of Figure B4. For example, the number of atoms with energies between 4.5 and

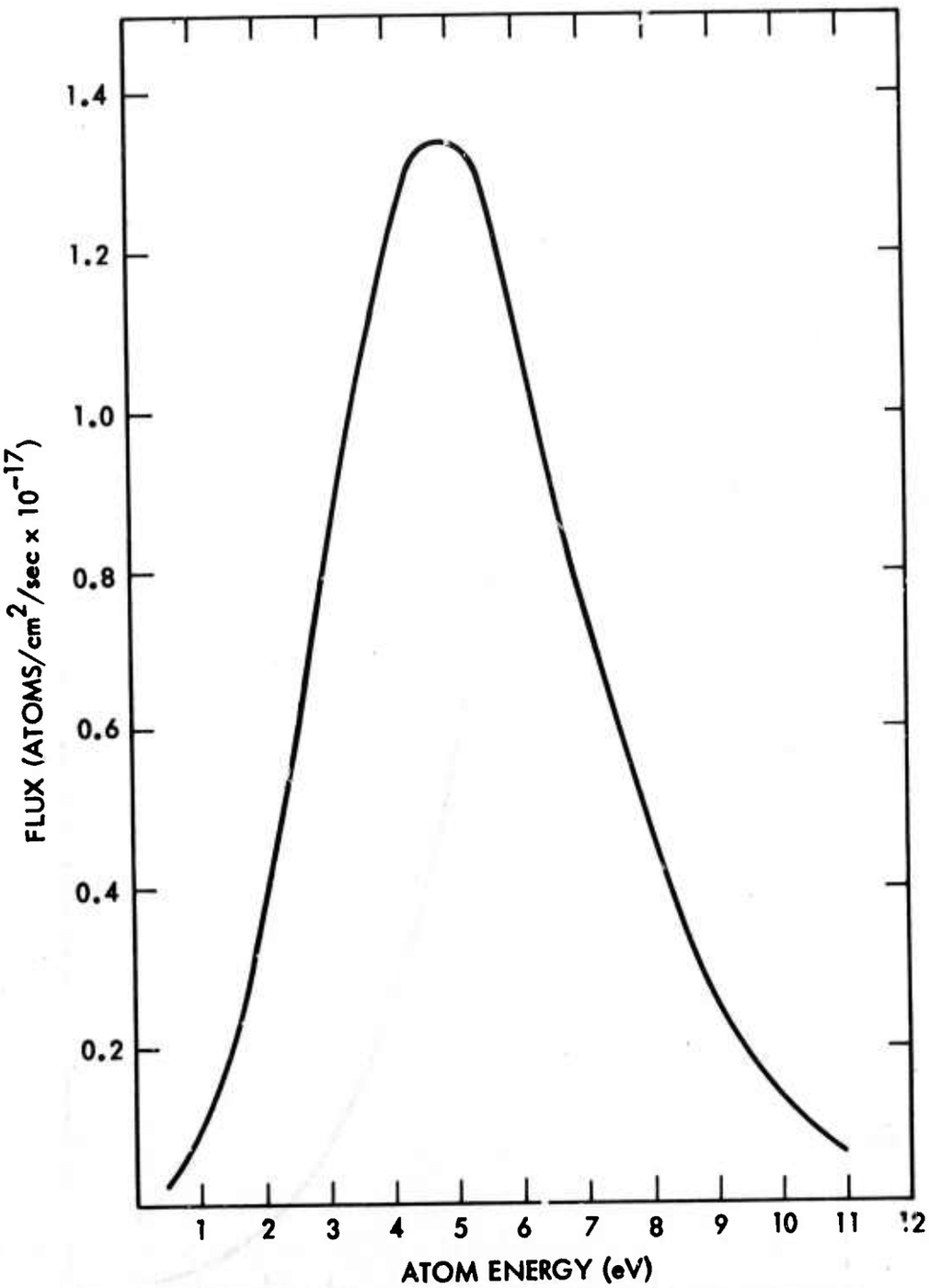

Figure B3. The absolute flux of fluorine atoms as a function of atom energy at a distance of 60 cm from the laser target. The laser energy density was approximately 100 joules/cm^2 at the target surface.

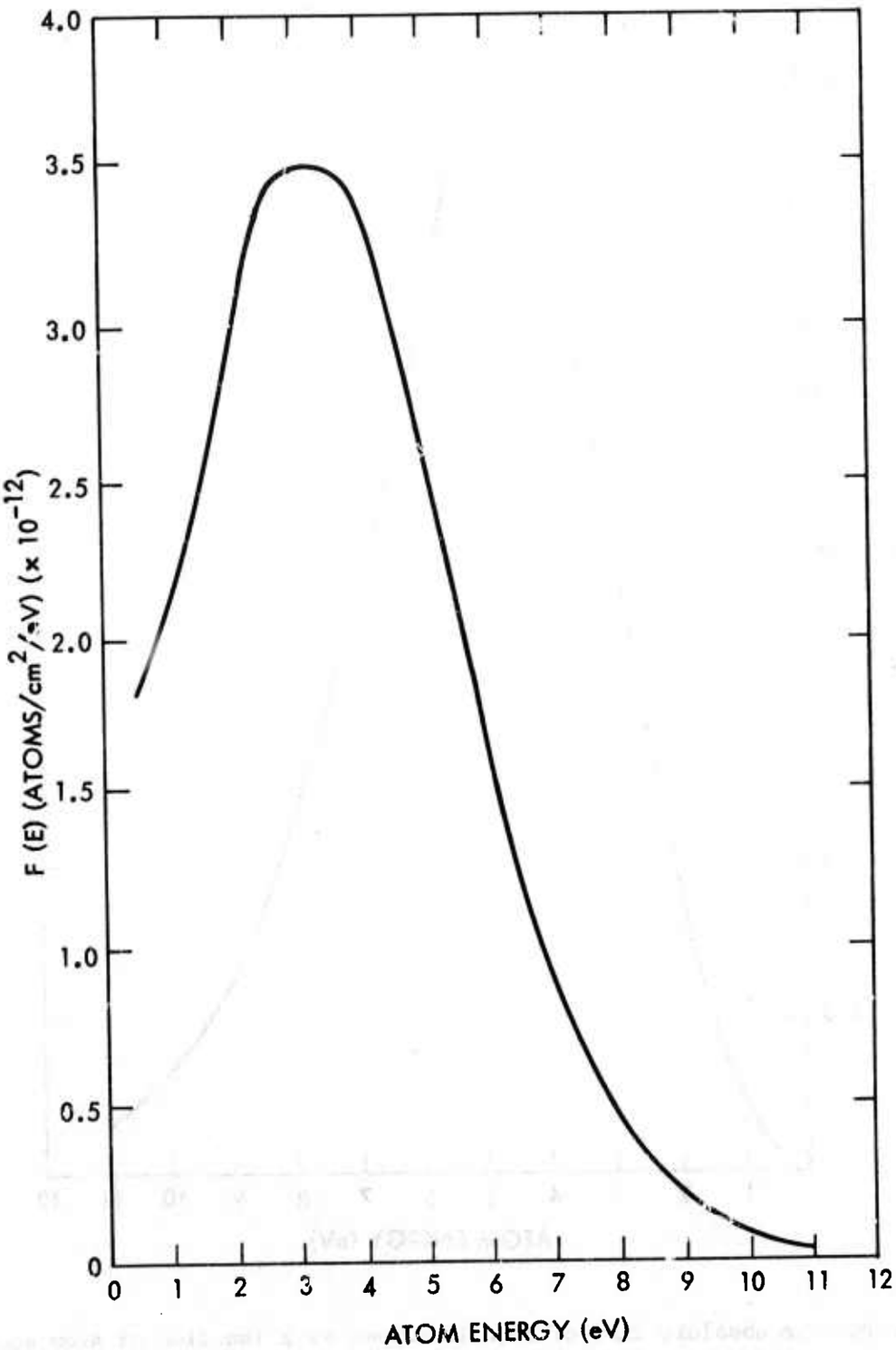

Figure B4. The energy spectrum of fluorine atoms in a burst as observed at a point on an axis normal to the target surface.

5.5 eV ($\Delta E/E = 0.20$) is about 2.5×10^{12} atoms/burst. For $\Delta E/E = 0.1$ at E = 5 eV, the number is halved. By the same token, the total number of atoms contained in the burst in the 1 to 10 eV range is on the order of 2×10^{13} atoms/cm^2.

As mentioned earlier, the kinetic energy of atoms in the pulse can be adjusted by varying the energy density of laser light at the target surface. This effect is shown in Figure B5 where the kinetic energy of aluminum atoms at the peak of the ion current pulse is plotted as a function of laser energy density. The laser energy was fixed at ~0.4 joules/pulse and the energy density was varied by changing the lens-to-target spacing. The target was a 0.5 micron thick vapor deposited aluminum film. As shown by the graph, the atom energy measured at the peak increases with approximately the square root of the energy density in this region. The increase in energy does not proceed without limit, however, because the formation of ions becomes the dominant process. The number of atoms per pulse actually passes through a maximum in the energy density range shown in Figure B5. Furthermore, the efficiency of utilization of the laser energy reaches a maximum in this region as shown in Figure B6 for the same data presented in Figure B5. As implied, the total kinetic energy of the atom pulse is the sum of the kinetic energies of the individual atoms making up the total pulse. As before, the measurements are referenced to a detector 60 cm from the laser impact site. The implications of these observations are that the laser energy is dissipated by conduction and radiation at low energy densities and by the formation of energetic ions at high energy densities.

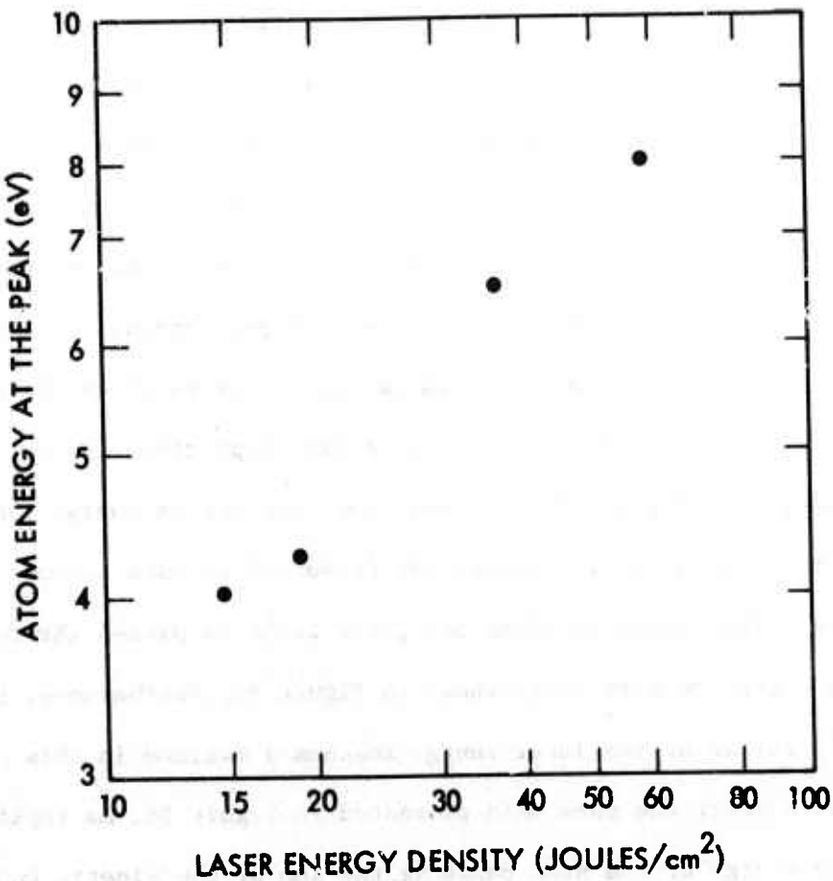

Figure B5. Atom energy as a function of laser beam energy density. The atom energy plotted corresponds to the peak of the distribution. The target was a 1/2 micron thick aluminum film.

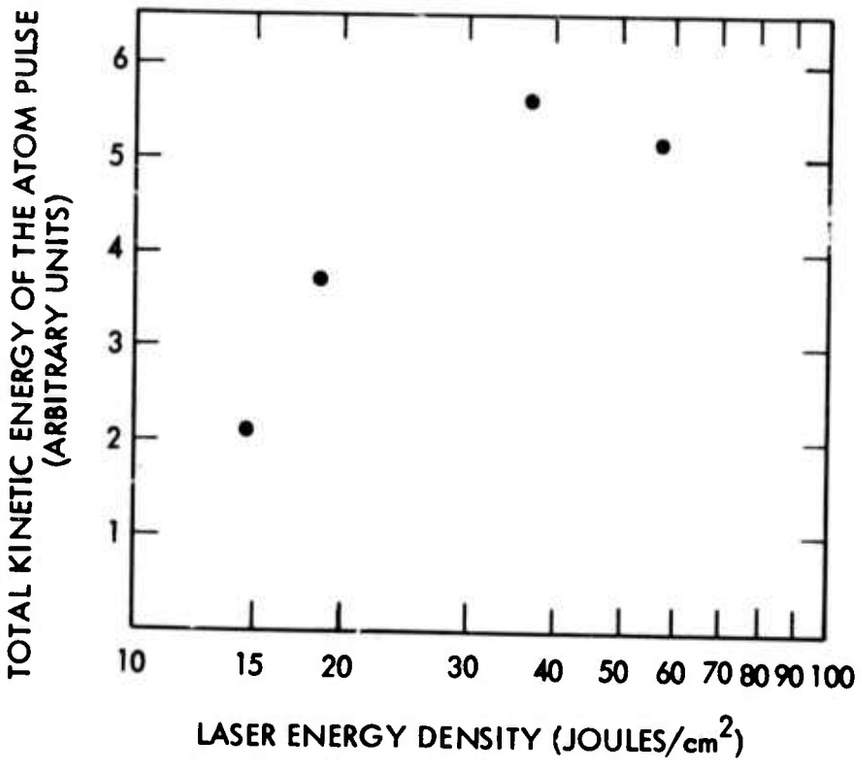

Figure B6. Total kinetic energy content of the atom pulse as a function of laser beam energy density.

4.4 DISCUSSION AND COMPARISON WITH OTHER NEUTRAL BEAM SOURCES

Direct comparison of the results given above with those obtained with more "conventional" approaches is complicated by the pulsed nature of the laser generated beam. As will be noted from the brief summary that follows, the most commonly used atomic beam sources are basically steady state.

At low energies, effusive sources are widely used. Conceptually, an effusive source is a pressurized vessel with a small exit aperture or slit through which the gas escapes into a high vacuum region. Effusive sources are most commonly used with gaseous species, but may also be used with normally solid or liquid substances by heating the material to the point where its vapor pressure is sufficiently high. A condition for effusive flow is that the molecular mean free path in the reservoir must be large compared to the size of the exit aperture. In most applications the effusing gas is collimated by an aperture located at some distance from the exit aperture. Collimation serves the dual roles of defining the beam and limiting gas flow into the experimental region.

According to Anderson *et al.*,[1] the chief limitation to the intensity of molecular beams from effusive sources is the pumping required to handle the gas load in the expansion region. They indicate that a pumping speed of 10^5 litres/sec is required to maintain a pressure of 10^{-4} Torr in the expansion volume for an effusive source capable of delivering a flux of 10^{16} molecules/cm^2/sec at a distance of 1 meter from the source. For equilibrium conditions, a Maxwellian distribution of velocities exists in the reservoir. Because of the selectivity of the exit aperture, the mean energy in the expanded beam is

3kT/2. Practical reservoir temperatures are limited to a few thousand degrees Kelvin with the result that useful beam intensities can be achieved only for energies less than 1/2 electron volt.

A variation of the simple effusive source utilizes an array of small channels to "focus" the expanding gas into narrow beam. According to Anderson *et al*.[1] multichannel arrays reduce pumping requirements for low beam intensities but this advantage is lost at beam intensities approaching the 10^{16} molecules/cm^2/sec level.

Another variation of the effusive source is the supersonic nozzle which is characterized by a higher reservoir pressure than the simple effusive source. In beam applications, the familiar expansion nozzle is replaced by a skimmer. It's function is much the same as that of the exit aperture in the effusive source. In contrast to the effusive source where the angular distribution of molecular flow is spherical, the flow downstream from the skimmer is ellipsoidal. Thus for the same gas throughput, the axial density is higher resulting in a net decrease in the pumping speed required for a given beam intensity. Compared to the effusive source, the velocity distribution is narrower in a supersonic nozzle. Anderson, Andres, and Fenn[2] state that 11% of the total flux is within 5% of the mean molecular velocity for an effusive beam while 47% of the molecules lie within 5% of the mean for a Mach 10 nozzle. They further state that useful energies on the order of 1 eV can be achieved by this method.

Higher energy atomic beams may be produced by passing ion beams through charge exchange cells where the charge on some fraction of the incident ions is neutralized by charge transfer collisions with the ambient gas in the cell. In principle, ion beams of virtually any atomic or molecular species can be

produced by one means or another and transported to the entrance of the charge exchange cell. The intensity of the ion beam, however, may vary widely depending upon the atomic species in question and the means by which it is ionized. In any case, an upper limit to the beam intensity at a given energy is imposed by space charge considerations. A high degree of energy selectivity may be obtained with the parent ion beam. If, however, the monoenergetic character of the beam is to be retained through the charge exchange process, a minimum condition is that the charge exchange cross section must be large compared to the momentum transfer cross section. This is usually the case at low energy only for "resonant" charge transfer which occurs between like atomic species or for atomic species with nearly equal ionization potentials.

As one example of the characteristics of atomic beams produced by ion charge exchange, Utterback and Miller[3] produced an N_2 molecular beam in the energy range 5 to 1000 eV with an intensity ranging from 10^8 molecules per second at "low energy" to 10^{10} at "high energy." Judging from the dimensions of their apparatus, these values correspond to fluxes of 10^9 to 10^{11} molecules/cm^2/sec. At a mean energy of 34 eV, the energy spread was ±0.5 eV (as determined from the half width of a differentiated stopping potential curve).

In addition to those described above, a variety of other techniques (e.g., shock tube driven nozzle beams, arc heated high-temperature nozzles, mechanical accelerators) have been developed and used in certain applications.

The energy region where maximum beam intensities are reached with the laser bombardment technique lies in the gap between thermal and charge exchange beams. Instantaneous beam intensities are at least as great if not significantly greater than can be achieved by other means.

The pulsed nature of the beam has both advantages and disadvantages. In many cases current due to ionized background gas is the principal source of noise in atomic beam measurements. A large increase in the signal-to-noise ratio from a steady state beam may be obtained by mechanically chopping the incident beam at a fixed frequency and using synchronous detection of the modulated beam. The situation for the pulsed beam is similar. Since the pulse is of relatively short duration, slowly varying noise sources may be suppressed by using a narrow bandpass filter on the ion detector. The principal disadvantage of the pulsed character of the beam is the practical one of optimizing the mass spectrometer response in the absence of a steady state or regularly repetitive source.

The wide range of atom energies contained in a single burst may be an advantage or disadvantage depending upon the particular application. For experiments where the observable quantity manifests itself almost immediately following an interaction (e.g., excitation of short-lived optical states) or where the product of an interaction retains a memory of the energy of the initial collision (e.g., elastic scattering) the energy dependence of the particular interaction may be observed in a single burst. In other cases (e.g., highly exothermic chemical reactions), the energy spread can be a distinct disadvantage. In principle, a mechanical velocity filter synchronized with the firing of the laser could be used to limit the energy spread. However, the short duration of the atom pulse imposes rather severe speed requirements on the filter.

The laser generated pulsed atomic beam technique appears to be applicable to a wide variety of atomic and molecular species. Although the results reported above emphasized atomic species, beam intensities of comparable magnitudes have been observed for several molecular species. The principal requirement is that the bond strength of the desired molecule be great enough to avoid excessive dissociation at elevated temperatures.

A final precautionary point concerns the internal energy state of the atoms or molecules. Because of the high temperatures involved, atoms or molecules may be formed in excited states. Short lived states pose no particular problems, but metastable states with half lives comparable to or longer than the atom time of flight to the experimental region could influence the experiment. No attempt to assess the internal state of excitation of beam atoms was made in these experiments.

The laser bombardment technique described above provides a means of producing intense atomic and molecular beams in an energy range not easily reached by other methods. The key to effective utilization of the laser energy is the thin film target geometry. The technique is applicable to a wide range of atomic and molecular species. The pulsed nature of the beam allows the use of simple time-of-flight techniques to determine the energy spectrum of the expanding vapor cloud. Because of these characteristics, the technique should prove to be useful in a variety of experiments on atomic collision interactions.

REFERENCES

1. J. B. Anderson, R. P. Andres, and J. B. Fenn, Advances in Atomic and Molecular Physics, Vol. 1, Edited by D. R. Bates (Academic Press, New York, London, 1965).

2. J. B. Anderson, R. P. Andres, and J. B. Fenn, Advances in Chemical Physics, Vol. X, Edited by John Ross (Interscience Publishers, New York, London, Sydney, 1966).

3. N. G. Utterback and G. H. Miller, Rev. Sci. Instru. 32, 1101 (1961).